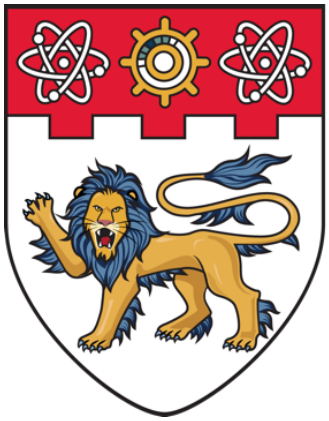
PERFORMANCE ENHANCEMENT OF THE MEMBRANE DISTILLATION PROCESS VIA MEMBRANE SURFACE MODIFICATION FOR SURFACTANT-CONTAINING FEED WATER



NANYANG TECHNOLOGICAL UNIVERSITY

SINGAPORE

PERFORMANCE ENHANCEMENT OF THE MEMBRANE DISTILLATION PROCESS VIA MEMBRANE SURFACE MODIFICATION FOR SURFACTANT-CONTAINING FEED WATER

NICK CHEW GUAN PIN
Interdisciplinary Graduate School
Nanyang Environment and Water Research Institute
Singapore Membrane Technology Centre

2018

NICK CHEW GUAN PIN 2018

PERFORMANCE ENHANCEMENT OF THE MEMBRANE DISTILLATION PROCESS VIA MEMBRANE SURFACE MODIFICATION FOR SURFACTANT-CONTAINING FEED WATER

NICK CHEW GUAN PIN

NICK CHEW GUAN PIN

Interdisciplinary Graduate School
Nanyang Environment and Water Research Institute
Singapore Membrane Technology Centre

A thesis submitted to the Nanyang Technological University in partial fulfilment of the requirement for the degree of
Doctor of Philosophy

2018

ACKNOWLEDGEMENTS

This thesis would not have been possible without the guidance and help of many individuals who contributed and extended their most valuable assistance in one way or another.

First and foremost, I would like to express my deepest appreciation and gratification towards my project supervisors, Prof. Rong Wang and Dr. Chandresh Malde, for their exemplary guidance and enthusiastic encouragement throughout this research journey. They served as a great resource and have always been positive role models. Their willingness to share their wealth of knowledge and experience in and beyond the field of membranes has been very much appreciated. They have shown me, by their example, what a good scientist (and person) should be.

Profound gratitude is also due to research fellows, Dr. Shanshan Zhao, Dr. Chun Heng Loh and Dr. Kunli Goh, for their wonderful collaborations. Without their dedication, knowledge, contributions, insights, and advices, this study would not have been as successful as it has been. Notably, their critique of the methods and practices used in my research has improved the quality of my work tremendously.

This project would have been impossible without the financial support of the Interdisciplinary Graduate School Research Scholarship or the Johnson Matthey Public Limited Company. I would also like to acknowledge funding support from the Singapore Economic Development Board to the Singapore Membrane Technology Centre. I am ever so grateful to the Singapore Membrane Technology Centre and the Nanyang Environment and Water Research Institute for providing me with a safe working environment equipped

This page is intentionally left blank

with state-of-the-art research facilities.

I would like to take this opportunity to give my heartfelt thanks to Visiting Professor, Prof. William B. Krantz, for his beneficial workshops on oral communication and research writing skills. He has definitely made me a more confident and better speaker. As my teacher and mentor, he has taught me more than I could ever give him credit for here.

I am deeply grateful to the staff from the Nanyang Environment and Water Research Institute for their kind assistance in administrative matters. They include Ms. Hera Catharina Adam, Ms. Zan Chin Chin Ong, Ms. Wai Yee Chan, and Mr. Zheng Xin Joseph Kwan. Without their help, I would not have been able to carry out my daily routine so efficiently and without much hassle.

Nobody has been more important to me in the pursuit of this doctorate than the members of my family. I thank them for their understanding, patience, tremendous support, and unconditional love throughout this challenging period. Most importantly, I wish to thank my partner and our dog, who provided me with unending inspiration. I would also like to apologize to anyone I had inadvertently left out in my acknowledgements.

NICK CHEW

This page is intentionally left blank

LIST OF PUBLICATIONS

- ***Journals:***

1. **Chew, N.G.P.**, S. Zhao, C. Malde, R. Wang, Polyvinylidene fluoride membrane modification via oxidant-induced dopamine polymerization for sustainable direct-contact membrane distillation, **J. Membr. Sci.** 563 (2018) 31–42.

2. **Chew, N.G.P.**, S. Zhao, C. Malde, R. Wang, Superoleophobic surface modification for robust membrane distillation performance, **J. Membr. Sci.** 541 (2017) 162–173.

3. **Chew, N.G.P.**, S. Zhao, C.H. Loh, N. Permogorov, R. Wang, Surfactant effects on water recovery from produced water via direct-contact membrane distillation, **J. Membr. Sci.** 528 (2017) 126–134.

4. **Chew, N.G.P.**, S. Zhao, R. Wang, Recent advances in membrane development for treating surfactant- and oil-containing feed streams via membrane distillation, Manuscript in preparation.

5. **Chew, N.G.P.**, Y. Zhang, K.L. Goh, R. Wang, Hierarchically-structured Janus membrane surfaces for enhanced membrane distillation performance, Manuscript in preparation.

6. Tan, Y.Z., L. Han, **N.G.P. Chew**, W.H. Chow, R. Wang, J.W. Chew, Membrane distillation hybridized with a thermoelectric heat pump for energy-efficient water treatment and space cooling, **Appl. Energy** 231 (2018) 1079–1088.

7. Xu, Y., Y. Lin, **N.G.P. Chew**, C. Malde, R. Wang, Biocatalytic PVDF composite hollow fiber membranes for CO_2 removal in gas-liquid membrane contactor, **J. Membr. Sci.** 572 (2019) 532–544.

- ***Conference Proceedings:***

1. **Chew, N.G.P.**, S. Zhao, C. Malde, R. Wang, Novel modification method for membranes used in membrane distillation, **11th International Desalination Workshop**, Singapore, 12th – 13th July 2018 (Oral Presentation).

2. **Chew, N.G.P.**, S. Zhao, C. Malde, R. Wang, PVDF membrane modification via oxidant-induced dopamine polymerization for extend applications of membrane distillation, **Johnson Matthey Academic Conference 2018**, Loughborough, UK, 10th – 11th April 2018 (Oral Presentation).

3. **Chew, N.G.P.**, S. Zhao, C. Malde, R. Wang, Superoleophobic surface modification for robust membrane distillation performance, **11th International Congress on Membranes and Membrane Processes**, San Francisco, CA, USA, 29th July – 4th August 2017 (Oral Presentation).

4. **Chew, N.G.P.**, S. Zhao, C. Malde, R. Wang, Superoleophobic surface modification for robust membrane distillation performance, **Engineering with Membranes Conference 2017**, Singapore, 26th – 28th April 2017 (Poster Presentation), **Best Poster Award**.

5. **Chew, N.G.P.**, S. Zhao, C.H. Loh, N. Permogorov, R. Wang, Surfactant effects on water recovery from produced water via direct-contact membrane distillation,

Johnson Matthey Academic Conference 2016, Loughborough, UK, 12th – 13th April 2016 (Poster Presentation).

This page is intentionally left blank

TABLE OF CONTENTS

ACKNOWLEDGEMENTS i

LIST OF PUBLICATIONS v

TABLE OF CONTENTS ix

LIST OF TABLES xii

LIST OF FIGURES xiii

LIST OF ABBREVIATIONS xvii

SUMMARY xxi

Chapter 1 Introduction 1

1.1. Background 1

1.2. Problem statement 5

1.3. Research objectives 8

1.4. Thesis outline 9

Chapter 2 Literature Review 11

2.1. MD requirements and configurations 11

2.2. Studied MD applications and challenges for practical implementation 15

2.2.1. Seawater desalination 16

2.2.2. Food industry 16

2.2.3. Textile industry 17

2.2.4. Chemical industry 18

2.2.5. Petrochemical industry 20

2.2.6. Pharmaceutical industry 21

2.3. Fouling and wetting control strategies in MD 22

2.3.1. Types of fouling in MD 24

2.3.1.1 Inorganic fouling 24

2.3.1.2 Organic fouling 24

2.3.1.3 Biological fouling 25

2.3.2. Fouling and wetting control strategies 26

2.3.2.1. Pretreatment 26

2.3.2.2. Membrane flushing 28

2.3.2.3. Gas bubbling 28

2.3.2.4. Temperature and flow reversal 30

2.3.2.5. Development of novel membranes with fouling- and wetting-resistant properties 30
2.3.2.5.1 Homogenous hydrophobic membrane 31
2.3.2.5.2. Superhydrophobic surface 32
2.3.2.5.3. Composite dual-layer membrane 33
2.3.2.5.4 Triple-layer membrane 36
2.3.2.5.5 Omniphobic membrane 37

Chapter 3 Materials and Methods 39
3.1. Materials and chemicals 39
3.2. Membrane characterization tests 41
3.3. Preparation and characterization of surfactant solutions and surfactant-stabilized O/W emulsions 44
3.4. DCMD performance tests 45

Chapter 4 Surfactant Effects on Water Recovery from Produced Water via Direct-contact Membrane Distillation 47
4.1. Introduction 47
4.2. Results and discussion 48
4.2.1. Oil droplet sizes and zeta potentials of surfactant-stabilized O/W emulsions. 48
4.2.2. Effects of surfactant types 50
4.2.3. Effects of the presence of oil 57
4.2.4. Effects of different surfactant-stabilized petroleum emulsions 59
4.2.5. Effects of oil concentration 61
4.2.6. Effects of oil types 62
4.2.7. Confirmation of surfactant penetration into membrane pores and membrane fouling 63
4.3. Conclusions 65

Chapter 5 Superoleophobic Surface Modification for Robust Membrane Distillation Performance 67
5.1. Introduction 67
5.2. Experimental 68
5.2.1. Fabrication of composite PVDF hollow fiber membrane 68
5.3. Results and discussion 70
5.3.1. Membrane surface characterizations 70
5.3.2. Deposition of PDA/PEI on the PVDF-P membrane surface 72

5.3.3. Wetting properties of the pristine and modified membranes 77
5.3.4. Membrane performance in DCMD tests 78
5.3.4.1. Saline feeds with four types of surfactant 78
5.3.4.2. Surfactant-stabilized petroleum-in-water emulsions 83
5.3.5. Comparisons to other MD membranes 86
5.4. Conclusions 88

Chapter 6 Polyvinylidene Fluoride Membrane Modification via Oxidant-induced Dopamine Polymerization for Sustainable Direct-contact Membrane Distillation 89
6.1. Introduction 89
6.2. Experimental 90
6.2.1. Fabrication of composite PVDF membrane 90
6.2.2. Raw seawater 91
6.3. Results and discussion 92
6.3.1. Observations of membrane surface morphology 92
6.3.2. Characterizations of membrane surface chemistry 95
6.3.3. Underwater oil-membrane interactions 98
6.3.4. Membrane performance in DCMD tests 100
6.3.4.1. Saline feeds with anionic, cationic, and non-ionic surfactants 100
6.3.4.2. Surfactant-stabilized petroleum-in-water emulsion 107
6.3.4.3. Raw seawater 108
6.4. Conclusions 110

Chapter 7 Conclusions and Recommendations 113
7.1. Overall conclusions 113
7.2. Recommendations for future research 115

References 119

LIST OF TABLES

Table 3-1. Properties of oils used in this study. 40
Table 3-2. Properties of surfactants used in this study. 40
Table 3-3. PVDF membrane properties. 40
Table 4-1. Number average mean droplet size, span of distribution, and zeta potential of the surfactant-stabilized O/W emulsions. 49
Table 4-2. Wetting time, final permeate conductivity, and contact angle of surfactant-fouled membranes in DCMD using feed with different surfactants. 52
Table 5-1. Surface roughness parameters and water contact angles of the pristine PVDF and PVDF-P membranes. 71
Table 5-2. The elemental compositions (in atomic percentage) of the inner (IS) and outer (OS) surfaces of the pristine PVDF and PVDF-P membranes. 75
Table 5-3. Comparison of performances among various MD membranes. 87
Table 6-1. Main compositions of the seawater used in this study. 92
Table 6-2. Surface roughness parameters and water contact angles of the pristine PVDF and 6h-mPVDF membranes. 94
Table 6-3. Elemental compositions (in atomic percentage) of the outer (OS) and inner (IS) surfaces of the pristine PVDF and 6h-mPVDF membranes. 97

LIST OF FIGURES

Fig. 1-1. Expected growth in total primary energy demand by 2035. Adapted from World Energy Outlook 2013 [1]. 2
Fig. 1-2. Schematic illustrating different sources of produced water [4]. 2
Fig. 1-3. Management strategies for produced water [2]. 3
Fig. 1-4. State-of-the-art produced water treatment techniques. 4
Fig. 1-5. The concept of the direct-contact membrane distillation process. 5
Fig. 2-1. Different types of MD configuration. 14
Fig. 2-2. Fouling- and wetting-resistant properties of different novel membranes in low surface tension feed solutions [145]. 38
Fig. 4-1. Oil droplet size distributions of different O/W emulsions. 49
Fig. 4-2. Effects of 3.5 wt% NaCl solution on permeate flux (filled symbols) and conductivity (hollow symbols). Feed volumetric flow rate (Q_f) = 0.7 L min^{-1}; Permeate volumetric flow rate ($Q_{p)}$ = 0.25 L min^{-1}; Feed temperature (T_f) = 333 K; Permeate temperature (T_p) = 293 K. 50
Fig. 4-3. Effects of surfactant types (same molar concentration) on permeate flux (filled symbols) and conductivity (hollow symbols). Q_f = 0.7 L min^{-1}; Q_p = 0.25 L min^{-1}; T_f = 333 K; T_p = 293 K. 52
Fig. 4-4. Hypothetical illustration of the adsorption of surfactant unimers on the PVDF membrane surface. 53
Fig. 4-5. Effects of surfactant types (same mass concentration) on permeate flux (filled symbols) and conductivity (hollow symbols). Q_f = 0.7 L min^{-1}; Q_p = 0.25 L min^{-1}; T_f = 333 K; T_p = 293 K. 57
Fig. 4-6. Effects of the presence of oils on permeate flux (filled symbols) and conductivity (hollow symbols). Tween® 20 concentration was 50 mg L^{-1}. Tween® 20-stabilized petroleum emulsion was prepared using 50 mg L^{-1} of Tween® 20 and 950 mg L^{-1} of petroleum. Q_f = 0.7 L min^{-1}; Q_p = 0.25 L min^{-1}; T_f = 333 K; T_p = 293 K. 58
Fig. 4-7. Effects of different surfactant-stabilized petroleum emulsions on permeate flux (filled symbols) and conductivity (hollow symbols). Q_f = 0.7 L min^{-1}; Q_p = 0.25 L min^{-1}; T_f = 333 K; T_p = 293 K. 59
Fig. 4-8. Proposed interactions of (a) Span® 20-stabilized, (b) Tween® 20-stabilized, and (c) SDS-stabilized emulsions with the PVDF membrane surface. 60

Fig. 4-9. Effects of oil concentration on permeate flux (filled symbols) and conductivity (hollow symbols). Q_f = 0.7 L min^{-1}; Q_p = 0.25 L min^{-1}; T_f = 333 K; T_p = 293 K. 62
Fig. 4-10. Effects of oil types on permeate flux (filled symbols) and conductivity (hollow symbols). Q_f = 0.7 L min^{-1}; Q_p = 0.25 L min^{-1}; T_f = 333 K; T_p = 293 K. 63
Fig. 4-11. FTIR spectra of the pristine and wetted PVDF membranes. Transmittance normalized against CF peak. (a) Span® 20 experiments, (b) Tween® 20 experiments, (c) SDS experiments. 64
Fig. 4-12. FESEM images of (a) pristine PVDF membrane and membranes fouled by (b) 50 mg L^{-1} Span® 20, (c) 50 mg L^{-1} Tween® 20, (d) 50 mg L^{-1} SDS, (e) 500 mg L^{-1} Tween® 20/Petroleum Emulsion, (f) 500 mg L^{-1} Span® 20/Petroleum Emulsion, (g) 500 mg L^{-1} SDS/Petroleum Emulsion, and (h) 500 mg L^{-1} Tween® 20/VPO Emulsion. 65
Fig. 5-1. Schematic of co-deposition of PDA/PEI on the outer surface of a PVDF membrane and its application in water recovery from oil-in-water emulsions via DCMD. 69
Fig. 5-2. FESEM images of the outer surface morphologies of the pristine PVDF (a1 and a2), PVDF-P (b1 and b2), and ultrasonicated PVDF-P (c1 and c2) membranes; FESEM images of the cross-section morphologies of the pristine PVDF (a3), PVDF-P (b3), and ultrasonicated PVDF-P (c3) membranes..... 71
Fig. 5-3. Pore size distributions of the (a) pristine PVDF and (b) PVDF-P membranes. . 72
Fig. 5-4. ATR-FTIR spectra of the outer surfaces of the pristine PVDF and PVDF-P membranes. Transmittance was normalized against the CF peak. 73
Fig. 5-5. (a) XPS survey scan spectra of the inner (IS) and outer (OS) surfaces of the pristine PVDF and PVDF-P membranes. Deconvolution of (b) C 1s, (c) N 1s, and (d) O 1s spectra of the outer surface of the PVDF-P membrane. 74
Fig. 5-6. Proposed polydopamine reaction mechanisms with polyethylenimine. 76
Fig. 5-7. Surface zeta potentials of the pristine PVDF and PVDF-P membranes as a function of pH. 1 mM NaCl was used as the electrolyte solution. 77
Fig. 5-8. Captured images of the underwater interactions between oil droplets tethered via a needle and the pristine PVDF (a1-a3) and PVDF-P (b1-b3) membrane surfaces. . 78
Fig. 5-9. DCMD performances of the pristine PVDF and PVDF-P membranes by feeding 3.5 wt% NaCl. Feed volumetric flow rate (Q_f) = 0.7 L min^{-1}; Permeate volumetric flow rate (Q_p) = 0.25 L min^{-1}; Feed temperature (T_f) = 333 K; Permeate temperature (T_p) = 293 K. 79

Fig. 5-10. DCMD performances of the pristine PVDF and PVDF-P membranes by feeding 50 mg L^{-1} of (a) Span® 20, (b) Tween® 20, (c) SDS, and (d) DTAB in 3.5 wt% NaCl. For the SDS experiment, PVDF-P membrane was flushed with Milli-Q® water when flux reached the lowest point. For each experiment, the feed tank was periodically refilled with overflow from the permeate reservoir to maintain the feed concentration. Q_f = 0.7 L min^{-1}; Q_p = 0.25 L min^{-1}; T_f = 333 K; T_p = 293 K. 83
Fig. 5-11. DCMD performances of the pristine PVDF and PVDF-P membranes by feeding 500 mg L^{-1} of DTAB-stabilized petroleum-in-water emulsion. Fresh emulsions were prepared every 24h for the PVDF-P experiment. Q_f = 0.7 L min^{-1}; Q_p = 0.25 L min^{-1}; T_f = 333 K; T_p = 293 K. 85
Fig. 5-12. Schematic of interaction of DTAB-stabilized O/W emulsion with the pristine PVDF and PVDF-P membranes. 85
Fig. 6-1. Schematic of oxidant-induced deposition of PDA on the outer and inner surfaces of a PVDF hollow fiber membrane. 91
Fig. 6-2. FESEM images of the outer surface morphologies of the pristine PVDF (a1 and a2), 2h-mPVDF (b1 and b2), 6h-mPVDF (c1 and c2), and ultrasonicated 6h-mPVDF (d1 and d2) membranes. FESEM images of the cross-section morphologies of the pristine PVDF (a3), 2h-mPVDF (b3), 6h-mPVDF (c3), and ultrasonicated 6h-mPVDF (d3) membranes. 93
Fig. 6-3. Pore size distributions of the (i) pristine PVDF and (ii) 6h-mPVDF membranes. 94
Fig. 6-4. ATR-FTIR spectra of the outer surfaces of the pristine PVDF, 2h-mPVDF, and 6h-mPVDF membranes. Transmittance was normalized against the CF peak. 95
Fig. 6-5. (a) XPS survey scan spectra of the outer (OS) and inner (IS) surfaces of the pristine PVDF and 6h-mPVDF membranes. Deconvolution spectra of (b) C 1s, (c) N 1s, and (d) O 1s on the outer surface of the 6h-mPVDF membrane (the inner surface coating time is 1 h). 97
Fig. 6-6. Surface zeta potentials of the pristine PVDF and 6h-mPVDF membranes as a function of pH. 1 mM NaCl was used as the background electrolyte solution. 98
Fig. 6-7. Captured images of the underwater interactions between petroleum droplets tethered via a needle and the pristine PVDF (a1-a3) and 6h-mPVDF (b1-b3) membrane surfaces. 100
Fig. 6-8. DCMD performances of the pristine PVDF, PDA/PEI, 2h-mPVDF-O and 2h-mPVDF membranes by feeding 3.5 wt% NaCl. Feed volumetric flow rate (Q_f) = 0.7

L min^{-1}; Permeate volumetric flow rate (Q_p) = 0.25 L min^{-1}; Feed temperature (T_f) = 333 K; Permeate temperature (T_p) = 293 K. 101
Fig. 6-9. Schematic diagram of proposed mechanisms for flux enhancement through oxidant-induced surface modification. 102
Fig. 6-10. DCMD performances of the pristine PVDF, PDA/PEI, and 6h-mPVDF membranes by feeding 50 mg L^{-1} of SDS in 3.5 wt% NaCl. For each experiment, the feed tank was periodically refilled with overflow from the permeate reservoir to maintain the feed concentration. Q_f = 0.7 L min^{-1}; Q_p = 0.25 L min^{-1}; T_f = 333 K; T_p = 293 K. 104
Fig. 6-11. DCMD performances of the pristine PVDF, PDA/PEI, and 6h-mPVDF membranes by feeding 50 mg L^{-1} of DTAB in 3.5 wt% NaCl. For each experiment, the feed tank was periodically refilled with overflow from the permeate reservoir to maintain the feed concentration. Q_f = 0.7 L min^{-1}; Q_p = 0.25 L min^{-1}; T_f = 333 K; T_p = 293 K. 105
Fig. 6-12. DCMD performances of the pristine PVDF, PDA/PEI, and 6h-mPVDF membranes by feeding 50 mg L^{-1} of Tween® 20 in 3.5 wt% NaCl. For each experiment, the feed tank was periodically refilled with overflow from the permeate reservoir to maintain the feed concentration. Q_f = 0.7 L min^{-1}; Q_p = 0.25 L min^{-1}; T_f = 333 K; T_p = 293 K. 106
Fig. 6-13. DCMD performances of the pristine PVDF, PDA/PEI, and 6h-mPVDF membranes by feeding 500 mg L^{-1} of Tween® 20-stabilized petroleum-in-water emulsion. Fresh emulsions were prepared daily for the respective experiments. Q_f = 0.7 L min^{-1}; Q_p = 0.25 L min^{-1}; T_f = 333 K; T_p = 293 K. 108
Fig. 6-14. DCMD performances of the pristine PVDF and mPVDF membranes by feeding seawater. For each experiment, the feed tank was periodically refilled with overflow from the permeate reservoir to maintain the feed concentration. Q_f = 0.7 L min^{-1}; Q_p = 0.25 L min^{-1}; T_f = 333 K; T_p = 293 K. 110

LIST OF ABBREVIATIONS

Abbreviation	Description
AFM	Atomic force microscope
AGMD	Air gap membrane distillation
ATR-FTIR	Fourier transform infrared spectroscope via attenuated total reflectance
BP	Bucky papers
CMC	Critical micelle concentration
CNIM	Carbon nanotubes immobilized membrane
CNTs	Carbon nanotubes
CO_2	Carbon dioxide
DA	Dopamine hydrochloride
DCMD	Direct-contact membrane distillation
DLVO	Derjaguin Landau Verwey Overbeek
DTAB	Dodecyltrimethylammonium bromide
EfOM	Effluent organic matter
FESEM	Field emission scanning electron microscope
FO	Forward osmosis
FO-MD	Forward osmosis membrane distillation
HCl	Hydrochloric acid
HLB	Hydrophilic-lipophilic balance
LEP	Liquid entry pressure
LTH	Low temperature hydrothermal
MD	Membrane distillation
MDBR	Membrane distillation bioreactor
MF	Microfiltration

NaCl	Sodium chloride
NaOH	Sodium hydroxide
NF	Nanofiltration
NOM	Natural organic matter
OMW	Olive mill wastewater
O/W	Oil-in-water
PACl	Poly-aluminum chloride
PDA	Polydopamine
PE	Polyethylene
PEG	Polyethylene glycol
PEI	Polyethylenimine
PP	Polypropylene
PS	Polystyrene
PTFE	Polytetrafluoroethylene
PVA	Polyvinyl alcohol
PVDF	Polyvinylidene fluoride
RCW	Recirculating cooling water
RO	Reverse osmosis
SC	Solar collectors
SDS	Sodium dodecyl sulfate
SGMD	Sweeping gas membrane distillation
SGSP	Salinity gradient solar ponds
SMMs	Surface-modifying macromolecules
TCA	1,1,1-trichloroethane
TCM	Traditional Chinese medicine
TDS	Total dissolved solids

TFC	Thin film composite
TiO_2	Titanium dioxide
TOC	Total organic compound
TP	Total phosphorous
Tris	Tris(hydroxymethyl)aminomethane
TS	Total solids
UF	Ultrafiltration
UV	Ultraviolet
VMD	Vacuum membrane distillation
VOCs	Volatile organic compounds
VPO	Vacuum pump oil
XPS	X-ray photoelectron spectroscope

This page is intentionally left blank

SUMMARY

With its many advantages, direct-contact membrane distillation (DCMD) appears to hold potential for the recovery of high quality water from different industrial effluents. Porous hydrophobic polyvinylidene fluoride (PVDF) membranes have been extensively used in DCMD operations. However, these PVDF membranes are vulnerable to membrane fouling and pore wetting in low surface tension feeds, restricting its application for water recovery from challenging industrial wastewaters. The mechanisms involved are not fully understood due to a lack of study on the interaction between different low surface tension contaminants and the membrane surface in the DCMD domain. To address these challenges, this work aims at developing a fundamental understanding of the relationship between surfactant-stabilized oil-in-water (O/W) emulsions and a PVDF membrane surface in DCMD operations. The results reveal that surfactant concentration and hydrophobicity had an influence on membrane fouling and wetting behaviors of these emulsions. Notably, surfactants with a lower hydrophilic-lipophilic balance value could make the PVDF membrane surface less hydrophobic and cause less severe fouling by restraining the adsorption of oil droplets on the membrane surface. These findings suggest that membrane surface modification is required to achieve fouling- and wetting-resistant properties for robust long-term applications.

Inspired by mussels' byssus with remarkable adhesive power that is neither degraded nor deformed in the marine environment, dopamine coating has emerged as an option for membrane surface modification. In this work, two composite hollow fiber membranes were fabricated, one by single-step co-deposition of polydopamine (PDA)/polyethylenimine and the other via accelerated oxidant-induced PDA deposition onto the surface of a commercial hydrophobic PVDF substrate. The successful deposition was verified using different characterization techniques. These composite membranes

exhibited Janus wettability with its modified surface being underwater superoleophobic for preventing organics adhesion while insuring that unmodified pores beneath the surface remained hydrophobic for vapor transport. The anti-fouling and anti-wetting properties of both modified membranes were investigated via bench-scale DCMD experiments by feeding a series of low surface tension solutions. In comparison to the pristine PVDF membrane, the modified membranes demonstrated excellent fouling- and wetting-resistant properties in different surfactant solutions as well as O/W emulsions. This was ascribed to the formation of an interfacial hydration layer and deposition of functional groups within the membranes' rough hierarchical structures. The PDA-decorated membrane was also used for seawater desalination, during which it maintained a stable flux and high salt rejection rate. Furthermore, the PDA-decorated membrane presented a flux enhancement of up to 70% over the pristine PVDF membrane in 3.5 wt% NaCl solution at 333 K. This study demonstrates the potential of both modified membranes for extended DCMD applications such as water recovery from industrial wastewater containing low surface tension substances.

Chapter 1 Introduction

1.1. Background

The importance of oil and gas in today's context cannot be overstated as they continue to account for nearly 78% of the world's total energy consumption as shown in Fig. 1-1 [1]. With many production activities, a substantial volume of produced water is generated annually within the oil and gas industry, making it one of the most water-intensive industries. Produced water is essentially wastewater co-produced in a production well along with the oil and/or gas phase(s) as illustrated in Fig. 1-2 [2]. This trapped water is brought up to the surface during oil and gas extraction operations. It is commonly known as the largest waste stream from the oil and gas refineries as it contains a variety of pollutants, namely: (i) dissolved and dispersed oils and greases; (ii) production solids; (iii) dissolved gases; (iv) soluble and insoluble organics; (v) production chemicals; (vi) inorganics and (vii) dissolved formation minerals [3]. These constituents of produced water are highly dependent on the geological locations as well as formation processes. Managing produced water has become a consequential part of the sustainable development of the oil and gas industry due to stringent environmental legislations, severe strain on water resources, and escalating costs of wastewater disposal [3].

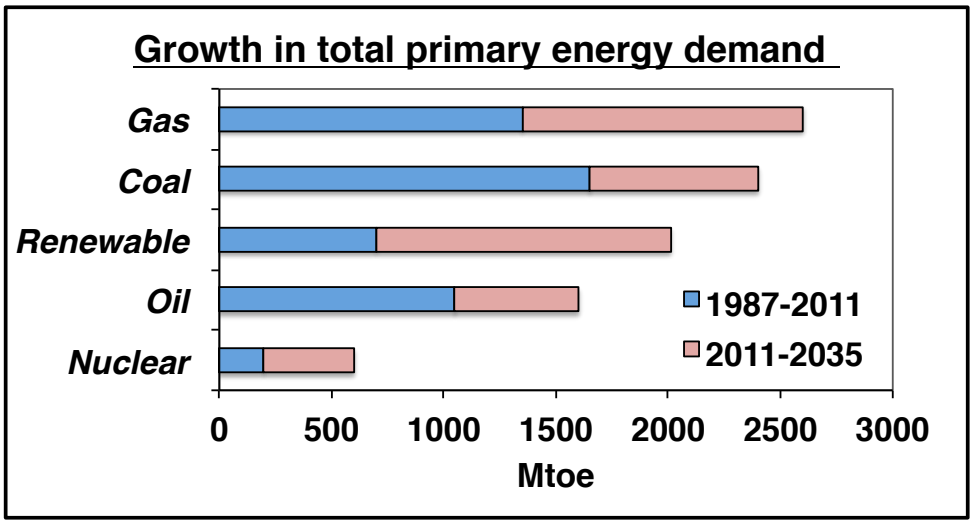


Fig. 1-1. Expected growth in total primary energy demand by 2035. Adapted from World Energy Outlook 2013 [1].

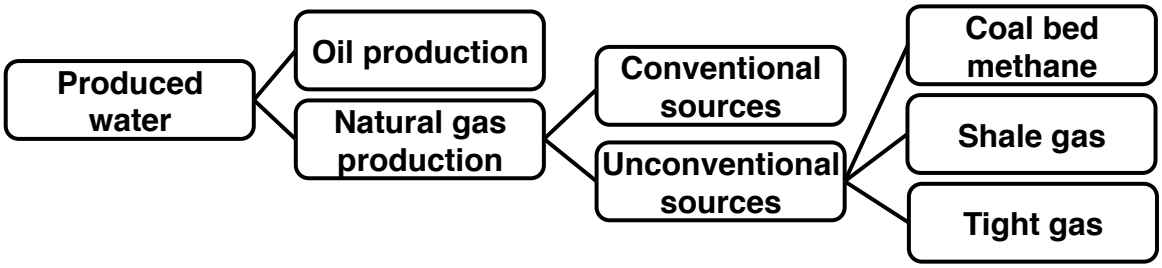


Fig. 1-2. Schematic illustrating different sources of produced water [4].

Generally, several options are available for produced water management as depicted in Fig. 1-3: (i) injection of the produced water into the same formation process or another suitable formation; (ii) discharge back into the environment after treatment; (iii) reuse in oil and gas field operations after treatment; and (iv) beneficial reuse for consumption or agricultural purposes after treatment [5]. Amongst these management methods, the reuse of produced water is a growing trend as it provides a potential profit stream [6]. To tap on this potential, produced water has to be first treated to remove main constituents such as oils and greases, production chemicals (surfactants), and production solids (salts). The treatment techniques for produced water can be broadly classified into the physical, chemical, and biological methods as illustrated in Fig. 1-4. However, conventional treatment methods often have several intrinsic disadvantages, including low removal efficiencies of oil droplets with diameters less than 20 μm, low water recovery,

high operating costs as well as the possibility of corrosion and recontamination [7]. The rapid development of membrane technologies offers attractive solutions to produced water treatment. Over the past few decades, membrane processes such as microfiltration (MF) [8-10], ultrafiltration (UF) [11-13], nanofiltration (NF) [14-16], reverse osmosis (RO) [17, 18], and forward osmosis (FO) [19] have been applied for produced water treatment. These membrane technologies have been preferred over conventional methods due to their high oil removal efficiencies, small footprint, as well as easy operation and maintenance. While some of these processes can be combined to achieve high removal efficiencies, high operating costs remain a major concern. Another grand challenge is membrane fouling caused by oil droplets and soluble organics.

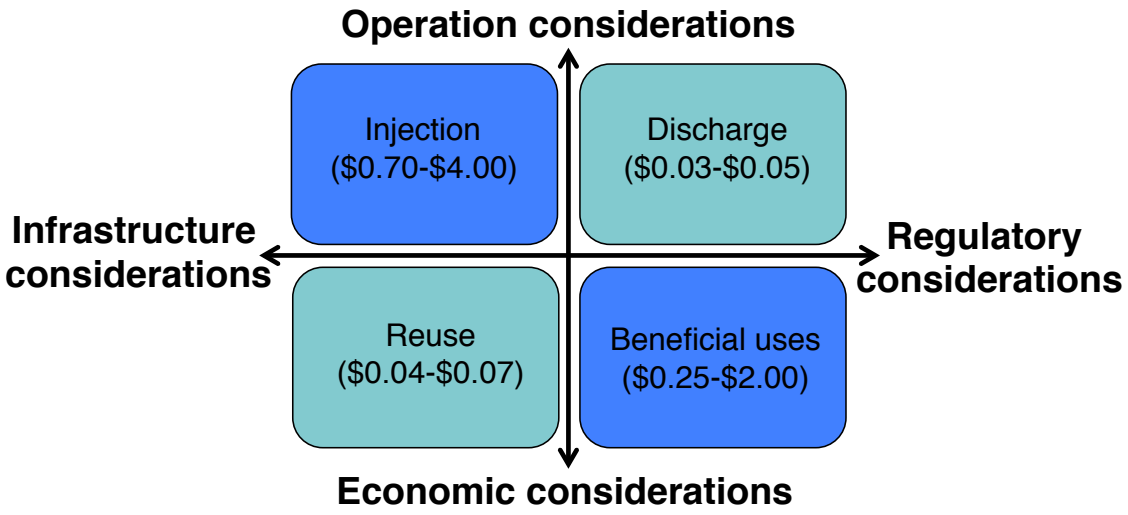


Fig. 1-3. Management strategies for produced water [2].

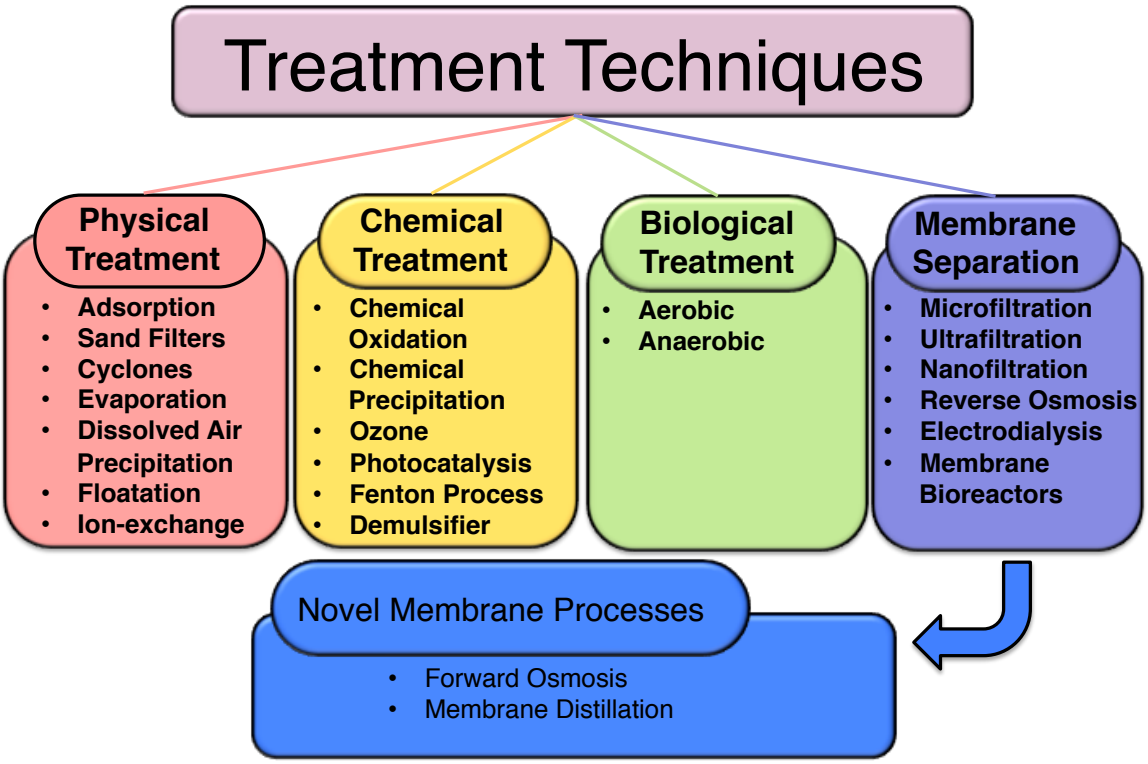


Fig. 1-4. State-of-the-art produced water treatment techniques.

Membrane distillation (MD) is an emerging thermally driven separation process using a hydrophobic porous membrane as a selective barrier against liquid transport. In the MD process, the transport of water vapor molecules through the membrane pores is driven by the partial vapor pressure difference resulting from the temperature difference between the hot feed and the cold permeate [20-22]. Highly purified distillate is produced when the vapor molecules condense on the cold permeate side, while most of the nonvolatile species are rejected. MD has a couple of distinct advantages over other pressure-driven membrane processes that include its ability to treat wastewater with high salinity and utilize low-grade thermal energy, which is an abundant available source of emission-free power in the oil and gas industry [23-30]. From the economic perspective, MD's small footprint and low operating cost render it a leading candidate for small-scale and off-grid applications for water recovery from produced water [31]. Among four different types of configuration, the direct-contact membrane distillation (DCMD) is widely studied due to its simple operation mode as illustrated in Fig. 1-5 [32].

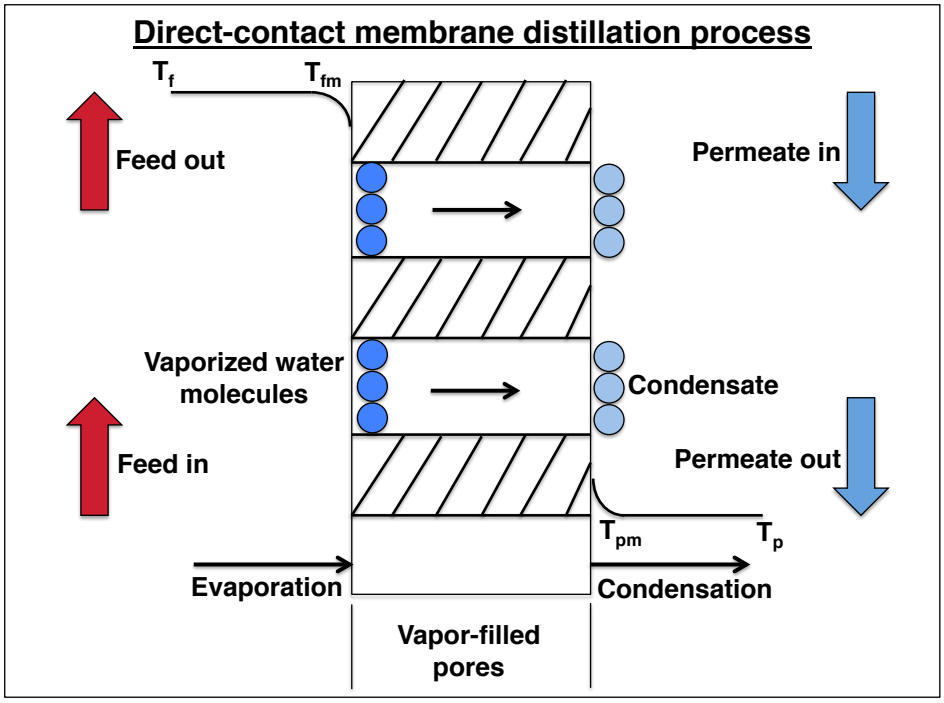


Fig. 1-5. The concept of the direct-contact membrane distillation process.

1.2. Problem statement

In the MD process, the porous hydrophobic membrane is a crucial element for efficient vapor transport and preventing liquid permeation from the saline feed to the distillate. Hence, conventional MD membranes are typically fabricated from hydrophobic polymeric materials that include polypropylene (PP), polyvinylidene fluoride (PVDF), and polytetrafluoroethylene (PTFE). Specifically, PVDF is one of the most extensively used polymeric materials for MD operations ascribing to its excellent thermal stability, chemical stability, and mechanical strength. These membranes have shown stable performances for treating relatively clean feeds that contain mostly salt. However, they are vulnerable to membrane fouling and pore wetting when used to treat challenging feeds that contain hydrophobic (e.g. oil) and/or amphiphilic (e.g. surfactants) pollutants. Adsorption of these substances on the membrane surface can lower the pore liquid entry pressure (LEP) or cause pore blockage, which compromises on the recovery rate and distillate quality [33].

Over the past decade, numerous studies have been conducted on the application of MD for the treatment of oily wastewater and produced water [5, 34-38]. The influences of pretreatment, operating conditions, and novel membrane surface modifications have been intensively studied. In most of these works, different pretreatment techniques were used to remove oil before the MD stage. Therefore, the true potential of MD in the treatment of produced water has not been explored. In particular, very limited amount of work has been reported on the influences of surfactants on membrane fouling and pore wetting. Only with an in-depth understanding of the relationship between different types of foulant and the membrane surface, robust MD membranes with fouling- and wetting-resistant properties can then be developed. This could potentially extend the applications of the MD process to treating oil-in-water (O/W) emulsions such as produced water as well as surfactant-containing wastewaters from the textile, food, paint, polymer, cosmetic, and pharmaceutical industries, to name a few [39-49].

Minimizing pore wetting and fouling of PVDF membranes concurrently have proven to be challenging. A wide range of surface modification methods has been adopted to achieve this goal. Hierarchical re-entrant structures, coupled with low surface energy, can improve the anti-wetting properties of omniphobic membranes as they represent a significant energetic barrier that has to be overcome in order to transit from the metastable Cassie-Baxter state to the fully wetted Wenzel state [50-54]. The other approach to mitigate fouling and wetting involves creating a superhydrophilic skin layer on the top of a hydrophobic or omniphobic substrate [37, 55-57]. This forms a hydration layer surrounding the superhydrophilic skin and renders the membrane surface superoleophobic under water. Besides that, incorporation of low surface energy functional groups into the hydrophilic matrix can further facilitate the detachment of hydrophobic

foulants such as oil [58]. It is evident from these studies that strides have been made in improving the anti-fouling and anti-wetting properties of MD membranes. Yet, most of these surface modification techniques are often too complex for practical applications. Therefore, developing a facile technique to engineer robust MD membranes that can handle wastewaters containing low surface tension pollutants is of high priority.

Moreover, to make MD membranes commercially viable, membranes with high vapor permeability have to be developed [59]. This can be achieved through altering vapor-membrane interaction, which is one of the major physicochemical factors determining permeability [60, 61]. Apart from that, striking a balance between high mass transfer and low heat loss is also vital in enhancing vapor permeation flux in MD operations [62]. In line with this, much effort has been focused on performing surface modification on commercially available polymeric substrates to attempt to enhance flux, which includes the immobilization of carbon nanotubes (CNT) in membrane pores [59, 60, 63-67]. CNT's excellent thermal conductivity reduces the effect of temperature polarization, which in turn brings about an increase in vapor driving force across the membrane. In addition, CNT's remarkable sorption and desorption capacity contribute favorably to water-membrane interactions. Faster removal of water vapor from the membrane pores is also possible via CNT's atomic-scale smooth surface. Similar concepts have been proposed through incorporating nanodiamond and graphene oxide within the membrane matrix [68, 69]. Besides that, reducing vapor transport distance while maintaining the membrane thickness can facilitate mass transport across the membrane [62]. These works have contributed tremendously to developing MD membranes with enhanced flux, but the performances of these membranes in saline feeds containing low surface tension pollutants are found to be undesirable. To put it succinctly,

while interest in MD has increased significantly in recent years, the lack of robust membranes has contributed to its low acceptance for large-scale industrial applications.

1.3. Research objectives

The general objective of this study is to enhance the performance of the MD process for surfactant-containing feed water via surface modification. The specific directives include:

- The fundamental understanding of the composition of real produced water solutions that can be used for MD and the types of foulant that are present;

- Establishing an in-depth understanding of the interaction of different surfactant-stabilized O/W emulsions with membrane chemistry and surface structures;

- Conducting a comprehensive study on the issues of membrane fouling and pore wetting via bench-scale DCMD experiments by feeding a series of low surface tension saline wastewater;

- Tailoring and architecting of commercial hydrophobic PVDF hollow fiber membranes via a facile and accelerated approach to develop robust membranes with fouling- and wetting-resistant properties;

- Corroboration of surface chemistry and hierarchical structure of the modified PVDF membranes via characterization tests; and

- Drawing comparisons to latest studies available in the literature in an attempt to benchmark the performances of the modified membranes and determine the relevance of these studies from a broader perspective.

1.4. Thesis outline

This thesis encompasses seven chapters, which are highlighted as follows:

Chapter 1: Introduction – A brief background on MD, its existing challenges, and research objectives are summarized in this chapter.

Chapter 2: Literature review – This is a critical review of the available literature on the advantages and disadvantages of different MD configurations, different applications of MD, as well as fouling and wetting control strategies in MD to better appreciate the different topics covered in this thesis.

Chapter 3: Materials and methods – This chapter covers in detail the materials, chemicals, and methodologies used in this Ph.D. study.

Chapter 4: Surfactant effects on water recovery from produced water via direct-contact membrane distillation – This chapter is the first attempt to understand the roles of surfactants and oils in water recovery from produced water via DCMD by elucidating the fouling and wetting mechanisms observed on a commercial hydrophobic PVDF hollow fiber membrane. A comprehensive study is performed with different types of oil and surfactant via a bench-scale DCMD experimental rig. With this foundation, robust MD membranes with fouling- and wetting-resistant properties are developed as demonstrated in Chapters 5 and 6.

Chapter 5: Superoleophobic surface modification for robust membrane distillation performance – This is the first report on single-step co-deposition of polydopamine (PDA) and polyethylenimine (PEI) on the outer surface of a hydrophobic PVDF hollow fiber substrate that can be used for low surface tension feeds via DCMD. An interfacial hydration layer that is formed within the modified layer, coupled with the presence of protonated amine-functional groups, can effectively prevent membrane fouling and pore wetting in the presence of low surface tension contaminants.

Chapter 6: Polyvinylidene fluoride membrane modification via oxidant-induced dopamine polymerization for sustainable direct-contact membrane distillation – The previous surface modification technique discussed in Chapter 5 is facile but time-consuming. Hence, the focus is shifted towards developing an accelerated technique to engineer robust membrane surfaces for extended applications of DCMD. Through the use of an oxidant, a composite hollow fiber membrane with sandwich structure is developed within a few hours. Its underwater superoleophobicity can effectively prevent organics adhesion. Notably, this novel membrane presents a flux enhancement of up to 70%.

Chapter 7: Conclusions and recommendations – Empirical evidences from Chapters 4, 5, and 6 are summarized here. Recommendations for future work are elaborated in this chapter.

Chapter 2 Literature Review

This review will focus on better understanding the advantages and disadvantages of different MD configurations. Besides that, the types of feed suitable for treatment/separation via the MD process will be explored, which involves the interaction of the feed (i.e. composition) with the membrane chemistry and surface structures. Furthermore, prior studies on the types of fouling that are likely to occur in different MD processes will be discussed. This knowledge is paramount since contrary to expectations, the occurrence of fouling can lead to pore wetting. With this foundation, prior studies on membrane surface modification are then summarized. This review will end with a critique of the state-of-the-art.

2.1. MD requirements and configurations

MD is a continuous thermal-driven desalination process based on the vapor-liquid equilibrium [32, 70, 71]. In this process, water vapor molecules from the warm saline feed transport through a porous hydrophobic membrane and condense into highly purified distillate on the cold permeate side, driven by the water vapor pressure difference associated with the temperature gradient across the membrane. MD has been proposed as a promising candidate for water recovery from highly saline feeds over conventional pressure-driven membrane processes due to its merits of low sensitivity to feed salinity, moderate operating conditions, and ability to utilize low-grade thermal energy that is abundantly available within many industries [53, 72, 73].

While the technology is promising, some of MD's drawbacks have limited its use in large-scale industrial applications. There is no specifically designed membrane

available for MD processes. Currently, the membranes used for MD processes are originally fabricated for the MF or UF process but have been utilized for various MD applications due to their hydrophobicity and appropriate pore sizes. On the other hand, the novel MD membranes fabricated thus far have issues with unstable and low permeate flux due to both the concentration and temperature polarization phenomena. In most MD cases, heat transfer is the rate-limiting step. Therefore, it is paramount to reduce heat loss during conduction across the membrane matrix and vapor-filled pores. Apart from that, membrane fouling and pore wetting are also tough tackling issues of the MD process.

As such, MD membranes must be anti-wetting and anti-fouling. Some of the common polymeric materials used are PTFE, PP, and PVDF. These materials are hydrophobic in nature, which is a key requirement for MD membranes. An excellent MD membrane should possess several characteristics in order to fulfill the earlier promises of the MD technology. When designing a MD membrane, it is paramount to take into account mass and heat transfer since both operate in tandem during the MD process. A MD membrane should have a narrow pore size distribution and an optimal pore size ranging between 0.1 μm and 1 μm [74]. While a larger pore size is desired to achieve higher permeate fluxes, a smaller pore size can reduce the possibility of liquid penetration that ultimately leads to pore wetting. Hence, an optimal pore size should be determined for different types of feed solution and operating condition.

In addition, MD membrane should have a high porosity, preferably between 30% and 85%, in order to achieve higher permeate fluxes since higher porosity provides a larger evaporation surface area [74]. The thermal conductivity of high porosity membranes is low since the conductive heat transfer coefficient of the vapor molecules is significantly lower than the polymer used. The optimal thickness of a single layer MD

membrane should range between 30 μm and 60 μm [74] while the thickness of a dual layer hydrophobic/hydrophilic composite membrane can have a hydrophobic layer that is as thin as 5 μm [75]. In general, the permeate flux is reduced as the membrane becomes thicker because there is an additional resistance to mass transfer but on the other hand, a thicker membrane can reduce conductive heat loss. In order to strike a balance between the impacts of mass transfer and heat transfer resistances, different membrane thicknesses have to be carefully studied.

It is understood that the MD membrane does not interfere with the vapor-liquid equilibrium but instead acts only as a support for its interfaces [74]. The MD membrane should display good thermal stability and excellent chemical resistance to a variety of feed solutions and at least one layer of the MD membrane should be hydrophobic in order to prevent pore wetting. It is paramount to prevent pore wetting as it has adverse effects on the quality of the distillate, which remains one of the major obstacles impeding the wider application of MD [76, 77]. Furthermore, the MD membrane should have high LEP, which is dependent on the maximum pore size and the membrane hydrophobicity.

Fig. 2-1 shows the four main configurations for MD, namely direct-contact membrane distillation (DCMD), vacuum membrane distillation (VMD), sweeping gas membrane distillation (SGMD), and air gap membrane distillation (AGMD), which involve coupled mass and heat transfer phenomena.

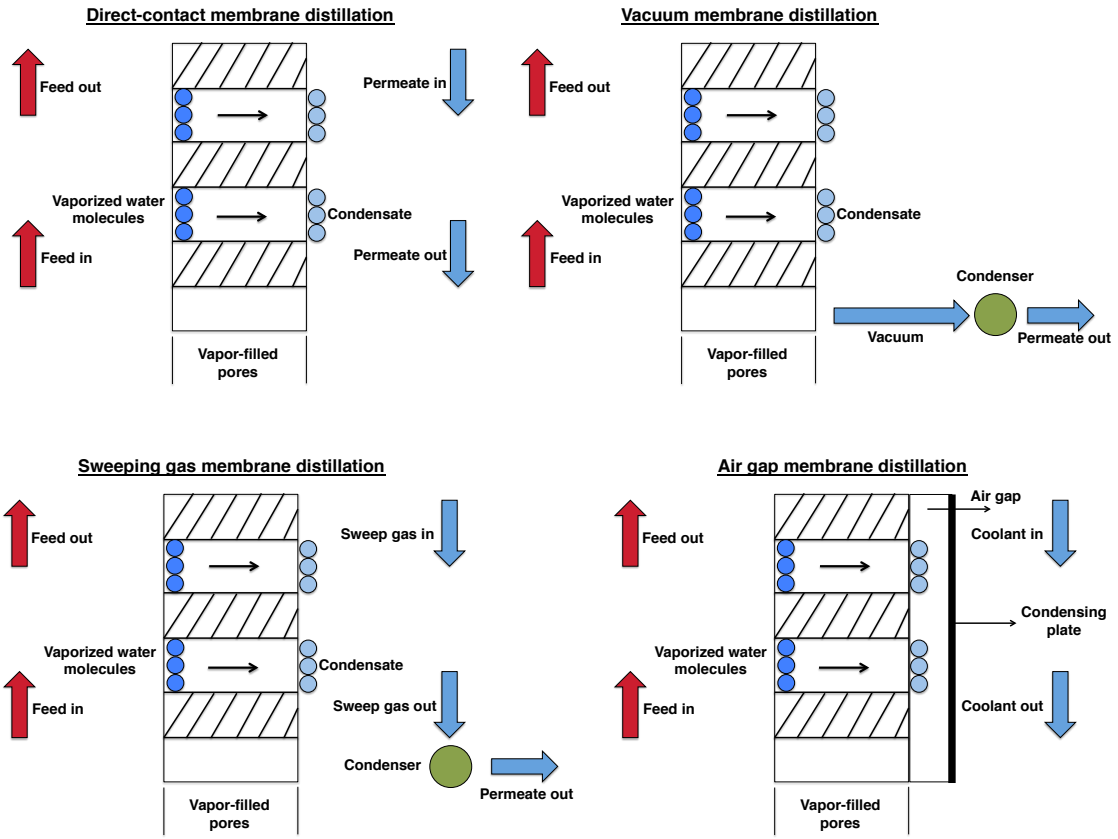


Fig. 2-1. Different types of MD configuration.

In DCMD, an aqueous solution that is colder than the feed is in direct contact with the permeate side of the membrane. Condensation takes place on the cold liquid-vapor interface inside the membrane module and does not require the use of external condensers. Its main drawback is the massive loss of heat through conduction across the membrane, which explains the system's low thermal efficiency.

Vacuum is applied on the permeate side of the membrane by a vacuum pump, which consumes energy, in the VMD configuration. Due to its complexity, the operation and maintenance of the system requires highly skilled workers. The applied pressure is lower than the saturation pressure of the volatile molecules in the feed and condensation takes place outside of the membrane module. As such, the mass transfer resistance and conductive heat loss are negligible in this type of configuration. Thus, VMD has the potential to achieve much higher flux than DCMD. On the other hand, in the SGMD

configuration, cold inert gas sweeps the permeate side of the membrane carrying vapor molecules. Similar to VMD, condensation takes place outside of the membrane module. SGMD enhances mass transfer efficiency and reduces heat loss but requires a much larger condenser than VMD due to the large amount of sweeping gas and vapor. It is the least studied configuration in MD.

In AGMD, a stagnant air gap is interposed between the membrane and the condensation surface. The evaporated volatile molecules cross both the membrane pores and air gap to condense over the cold surface inside the membrane module. There is reduced heat loss but an additional resistance to mass and heat transfer is formed due to the air gap thus resulting in lower permeate fluxes.

Most of the papers published in journals have focused on the DCMD configuration, which contributes to more than 60% of the papers published, because of its simple operation mode. In view of that, the DCMD configuration will be adopted to which all details given in this thesis refer. That being said, each configuration has its own advantages and limitations depending on the type of application.

2.2. Studied MD applications and challenges for practical implementation

MD is an attractive option for saline and wastewater treatment as well as for the concentration of solutions that are sensitive to heat, such as juices and dairy products. It can also be applied to the pharmaceutical industry for the concentration of blood and protein solutions. MD has many possible applications but is particularly attractive for the oil and gas industry due to the availability of low-grade thermal energy in this industry.

2.2.1. Seawater desalination

Saline water desalination is the most studied MD application by researchers since in theory, the complete rejection of non-volatile solutes is possible. Alternatively, for sparsely populated areas without access to fresh water supplies, MD can serve as small-scale and stand-alone units. Li and Sirkar employed the VMD configuration, where the feed temperature and flow velocity were varied, for desalination [78]. The performance of cross flow and parallel flow hollow fiber modules were investigated. The conclusion was that the former could achieve a significantly higher brine heat transfer coefficient. Water vapor fluxes as high as 71 kg m^{-2} h^{-1} were achieved by increasing the pore size and applying a more open coating.

However, without the availability of low-grade waste heat or renewable energy sources to heat the feed solution, the energy requirement becomes a major stumbling block. Amongst the first to couple solar energy with MD, Hogan et al. studied on the feasibility of solar-heat MD in arid/rural areas [79]. The pilot plant demonstrated the good compatibility of solar energy and MD and could possibly provide clean drinking water to these regions. More recently, Mericq et al. investigated on the utilization of solar energy in the form of salinity gradient solar ponds (SGSP) and solar collectors (SC) [80]. The immersion of the membrane module directly in an SGSP suffered the undesirable effects of the concentration and temperature polarization phenomena. In comparison, the use of SC produced fluxes as high as 140 L m^{-2} h^{-1}.

2.2.2. Food industry

In the food industry, dewatering is a crucial stage in the processing of fruit juices and milk as it makes the concentrates more resistant to microbial attack and chemical deterioration [81]. This in turn greatly enhances the taste, flavor, and color. Kimura and

Nakao used PTFE membranes for the concentration of mandarin orange juice, milk, sugar, and gelatin [82]. For the case of the mandarin orange juice, a comparison between the MD and RO processes were made. It was observed that an increase in feed concentration led to a higher flux in the MD process, as compared to the RO process. However, lower fluxes were observed in the concentration of milk, sugar, and gelatin where there was increased mass transfer resistance imposed by the viscous feed solution.

Calabro et al. studied on the suitability of MD in the concentration of orange juice [83]. They described the transport phenomena and formulated heat and mass transfer balances. By varying the operating conditions, they were able to conclude that MD is a concentration technique with potential and can be applied to other citrus juices. Subsequently, there have been more publications on the application of MD in the food industry. For example, Nene et al. demonstrated the concentration of sugar syrup while Christensen et al. performed MD on whey protein and achieved a concentration of at least 34% of the total dissolved solids [84, 85].

As early as the 1980s, researchers such as Chlubek and Tomaszewska have already begun studying on the feasibility of the MD process in the field of dairy processing [86]. In spite of that, there have been very few publications until recently [87, 88]. However, one possible drawback of the application of MD in the food industry is that the requirement to heat the feed solution to maintain the vapor pressure difference can lead to a serious loss of organic volatiles [89].

2.2.3. Textile industry

MD can also be applied in the textile industry as demonstrated by Calabro et al. [90]. Through the MD process, lesser amount of raw dye and water would be required

because of the high concentration level of dye recovered and the excellent quality of the distillate collected. Not only will the cost of textile wastewater treatment be cheaper, there will also be lesser pollution. More recently, Criscuoli et al. used VMD for the concentration of different dye solutions and understood the relationship between the different operating parameters and flux [91]. Interestingly, apart from fouling, they observed swelling of the membrane due to an interaction between the dye and the polymeric membrane.

2.2.4. Chemical industry

Over the years, MD has proven its worth in the chemical industry and there have been an increasing number of publications in this area. Tomaszewska was one of the pioneers to perform the concentration of the solution obtained after extraction of phosphogypsum with sulfuric acid by using PTFE membranes, which maintained its hydrophobicity even after 100 h of operation but experienced some damages due to its low mechanical strength [92]. The removal of carcinogenic VOCs from industrial wastewater is essential to protecting public health and the environment from these adverse effects. Wu et al. used PVDF membranes for the removal of benzene/toluene from wastewater [93]. A 99% removal of benzene/toluene was achieved at feed temperature 323 K and feed flow rate of 0.001 m^3 h^{-1}. A key finding was that the liquid phase and membranes imposed resistances to the mass transport of both benzene and toluene. Similarly, Wu et al. removed 1,1,1-trichloroethane (TCA), which is known to be carcinogenic, from wastewater using PVDF hollow fiber membranes [94]. They observed up to 97% removal of TCA at a feed temperature of 323 K and feed flow rate of 0.001 m^3 h^{-1}.

Glycerol, which is typically a by-product of bioethanol production, can be

converted into value-added chemicals. Shirzazi et al. were the first to apply MD for the separation of glycerol-water solutions, which can be found in many industrial wastewater effluents [95]. They used the Taguchi model to predict the best experimental conditions and observed some interactions between these conditions and the various operating variables. The data obtained concluded that the two most influential factors were the feed temperature and the sweeping gas flow rate. Madhumala et al. recovered hydrochloric acid (HCl) from a chloralkali industrial effluent and dehydrated glycerol-water mixture using PTFE and polystyrene (PS) membranes, respectively [96]. They suggested that MD is an economically viable and environmentally friendly technology.

MD has proved to be promising in the biofuel industry for bioethanol processing as well. Banat and Simandl used PVDF membranes for the separation of ethanol from aqueous streams and discovered that feed temperature played the most significant role in the resulting flux [97]. The exponential relationship between the vapor pressure and temperature meant that any fluctuations of the latter would have a significant impact on the driving force across the membrane. Gryta developed a bioreactor integrated with a MD unit and made a comparison with one without the MD unit [98]. The former was able to achieve better efficiency and productivity by selectively removing the volatile fermentation products from the broth. The CO_2 bubbles formed in the fermenting broth enhanced the turbulence in the boundary layer, which in turn improved on the mass transfer of ethanol across the PP membranes. Lewandowicz et al. utilized the MD technique for the recovery of ethanol [99]. The MD technique presented several benefits, which include an increase in ethanol production, more complete fermentation of sugars, lower osmotic pressure entering the fermentation broth, lower formation of the by-product glycerol, and sustainable increase in the numbers of yeast cells. However, high concentrations of volatile compounds might lead to low selectivity and pore wetting.

2.2.5. Petrochemical industry

In the petrochemical industry, the production of polyolefins requires important chemicals such as ethylene and propylene [100]. The large-scale separation of the olefin from the corresponding paraffin is a crucial step in the manufacture of the above-mentioned olefins [101]. Wastewater from the petrochemical industry may contain highly toxic species such as phenolic compounds or aromatic amines, which are inhibitory to biomass at high concentrations. More importantly, petrochemical wastewater often contains large quantities of oil. On the other hand, produced water from the hydraulic fracturing process contains dispersed oils, suspended particles, chemicals, and saline water [38].

So far, there have been a handful of literature reporting on the applicability of MD for the treatment and reuse of petrochemical wastewater and produced water. Khaing et al. investigated on the applicability of a novel submerged membrane distillation bioreactor (MDBR) for the reclamation of petrochemical wastewater [102]. The MDBR system was able to maintain a stable flux of 5.5–8.6 L m^{-2} h^{-1} for more than a month without membrane cleaning. The permeate quality met the requirements of NEWater albeit with a slightly higher total organic carbon (TOC) content. It was discovered that the inorganic fouling of the MD membranes was the predominant cause of flux decay, which could be recovered through chemical cleaning.

Singh and Sirkar used commercially available PTFE membranes for the treatment of produced water obtained from the steam assisted gravity drainage process in a DCMD setup [36]. It could achieve water vapor flux that was of one magnitude higher than the RO process. One other advantage MD has over RO is the ability of the former to utilize waste heat. Furthermore, the permeate produced was of good quality and posed no

problem to subsequent steam generation. On the other hand, Alkhudhiri et al. treated produced water from the Arabian Gulf with PTFE flat sheet membranes and concluded that the AGMD configuration can be a cost effective process [5]. It was observed that an increase in both the temperature and flow rate of the feed led to an improved permeate flux. One important discovery was that there was no direct relationship between energy consumption and membrane pore size.

Zuo and Wang studied the relationship between the discharge of coastal petrochemical industries and the anti-fouling/anti-wetting properties of a novel MD membrane [37]. The novel surface modification approach, which includes creating a highly hydrophilic membrane surface through polyethylene glycol (PEG) grafting and the deposition of titanium dioxide (TiO_2) nanoparticles, was able to achieve a consistent flux over one day of operation with no signs of fouling and pore wetting. Zhang et al. developed a hybrid forward osmosis-membrane distillation (FO-MD) system to treat synthetic produced water [38]. Thin film composite (TFC) membranes based on cellulose triacetate hollow fiber supports and PVDF hollow fiber membranes were employed for the FO and MD processes respectively. The hybrid system demonstrated the effective recovery of water and organic additives from the produced water for reuse.

2.2.6. Pharmaceutical industry

There have been comparatively fewer papers published in journals discussing on the feasibility of treating pharmaceutical wastewater via the MD process. Pharmaceutical wastewater often contains high concentrations of bio-resistant organic contaminants [103]. These contaminants typically include ibuprofen (an anti-inflammatory), dibucaine (a topical anesthetic), acetaminophen (an analgesic), and diphenhydramine (an anti-histamine) [63]. Ding et al. investigated on the fouling resistance of PTFE membranes in

the concentration of traditional Chinese medicine (TCM) by DCMD [104]. It was observed that the deposition of suspended particles in the TCM extract was the predominant cause of fouling, which can be controlled by increasing the feed temperature and feed velocity. Gethard and Mitra discovered that MD was an effective concentration approach [105]. Subsequently, based on their previous experimental work, Gethard et al. synthesized a carbon nanotube immobilized membrane (CNIM) for the concentration of pharmaceutical waste [63]. They reported that the introduction of carbon nanotubes (CNTs) could increase the permeate flux and enhance the concentration of pharmaceutical waste.

While promising, uncertainties in its energy consumption and economic costs remain major hurdles for large-scale MD applications. In order for MD to be a more economically viable technology, the utilization of waste heat is crucial. Fortunately, both the petrochemical and pharmaceutical industries offer a significant amount of waste heat that can be recovered to improve on the aspects of performance and profitability. However, in view of the greater potential shown in the application of the MD process for the treatment of petrochemical wastewater and produced water, it is proposed that more emphasis be placed on studying about the characteristics of produced water feed as well as its interaction with membrane chemistry and surface structures.

2.3. Fouling and wetting control strategies in MD

There have not been many intensive studies conducted on fouling and wetting in MD despite the fact that Lawson and Lloyd highlighted a couple of decades ago the importance of conducting more research in this direction [70]. As such, there is still a lack of data on the fouling and wetting phenomena as observed in MD and it remains one of the tough tackling issues faced in MD processes [106].

Fouling is an inherent phenomenon associated with membrane processes. It refers to the accumulation of unwanted deposits that are present in the stream being treated, on membrane surfaces or in membrane pores. Consequently, the microenvironment near the membrane surface reaches a non-steady state, leading to progressive pore wetting and the subsequent degradation of membrane performance such as flux decay or poor quality of the distillate collected. Gryta reported that it is very likely to witness at least a 50% reduction in the efficiency of MD processes after 50-100 h of operation due to fouling [107]. This severely impairs the productivity and daily operation of plants that employ membrane processes. However, different MD membranes are likely to encounter varying degrees of fouling depending on certain factors that include surface structures, feed composition used, operating parameters, and etc.

The flow channels of hollow fiber membranes are extremely small. As such, the accumulation of foulants will inevitably lead to situations where the increase in pressure drop allows the hydrostatic pressure to overcome the LEP [74]. This could potentially lead to pore wetting that involves penetration of the feed solution into the membrane pores, which in turn compromises the recovery rate and distillate quality. Besides that, fouling shortens the lifespan of membranes. There are four main types of fouling: (i) inorganic salt scaling caused by high concentration solutions that exceed its solubility limit; (ii) particulate and colloidal fouling; (iii) organic fouling caused by natural organic matter (NOM); and (iv) biological fouling due to the presence of microorganisms and marine macro-organisms.

Through better understanding on the interactions that exist between these foulants and the membrane surface, fouling can then be better controlled in MD processes. Many researchers have studied on the Derjaguin, Landau, Verwey, and Overbeek (DLVO)

theory, which attributed the interaction between foulants and membrane surface to the van der Waals attraction force and double-layer electrostatic repulsion force. The convention states that like charges repel each other while opposite charges attract. Therefore, in order to control fouling and wetting, an efficient method is to keep the interaction between the foulants and the membrane surface to a minimum.

2.3.1. Types of fouling in MD

2.3.1.1 Inorganic fouling

Inorganic fouling is typically caused by inorganics such as Ca^{2+}, Mg^{2+}, CO_3^{2-}, SO_4^{2-}, silica, and iron. Precipitates such as $CaCO_3$, $CaSO_4$ and $MgCO_3$ can form on the surface of membranes when the solubility limit of the above-mentioned ions is exceeded. The concentration polarization phenomenon may be responsible for bringing too much of the solutes to the membrane surface, which in turn precipitate and cause fouling. Cheng and Wiersma observed that salt scaling would diminish the membrane's hydrophobicity and lead to the subsequent wetting of the membrane pores [108].

2.3.1.2 Organic fouling

Organic fouling usually refers to the adsorption or deposition of organic waste material or decay products of biological activity within the MD system on the surface of membranes. It becomes prevalent when dealing with surface water and wastewater. In surface water, NOM is present. Humic substances, which are the predominant species of NOM, are formed through vegetative decay. These are complex and poorly defined anionic macromolecules that tend to be charged. However, Srisurichan et al. reported that fouling caused by humic acids is easier to control and manage in the MD process as compared to other membrane processes [109]. On the other hand, wastewater such as

produced water contains effluent organic matter (EfOM) that includes strong foulants such as polysaccharides, aminosugars, polyhydroxyaromatics, and proteins that can attach onto membrane surfaces [3].

2.3.1.3 Biological fouling

In the tropical region, biological fouling can become a major problem faced in MD processes. It occurs when microorganisms such as bacteria, algae, or fungi grow and attach themselves onto suitable surfaces such as MD membranes. Macro-organisms such as barnacles, mussels, polychaetes, and various species of bryozoans and hydroids play a major role in biological fouling too. To put it succinctly, biological fouling is the result of the undesirable formation of biofilms on membrane surfaces. Once it is formed, it has the potential to cause MD membranes to suffer severe loss of performance and requires the use of costly cleaning procedures to maintain output and quality. Interestingly, biological fouling usually overlaps or co-occurs with organic fouling [110, 111]. Typically, biological fouling involves fouling layers with pores or free volume less than 50 nm [112].

Gryta studied on the growth of microorganisms in different MD applications [113]. He concluded that biological fouling is less serious in MD than in other membrane processes due to factors such as feed composition and feed temperature. While the results look promising, it is worth noting that only one type of membrane was used in this study. Had a larger range of polymeric membranes been used, the observations would have been of more value. Gryta categorized fouling layers into porous and homogenous (non-porous) [107]. In the case of the porous fouling layer, flux decay is mainly attributed to the temperature polarization phenomenon while the flux decay in the latter case is predominantly caused by the increase in mass transfer resistance.

2.3.2. Fouling and wetting control strategies

2.3.2.1. Pretreatment

The pretreatment of feed solutions is one of the most common and effective methods to minimize fouling and wetting in many membrane processes and this consequently greatly enhances the permeate flux as well as its quality [114]. On the other hand, it has become common knowledge within the global membrane fraternity that poor pretreatment can possibly shorten membrane lifespan, increase operating pressure, and increase the cost of membrane cleaning.

Since MD is a type of reduced pressure distillation, El-Bourawi et al. observed that there was less likelihood of the compaction of fouling layers and feed pretreatment need not be as intensive as other pressure driven membrane processes [74]. Having said that, the need for pretreatment cannot be understated since actual feed solutions often contain a wide variety of potential foulants.

There have been many different pretreatment methods employed in MD operations and some of these include filtration, degasification, coagulation, membrane-based filtration, thermal softening, and precipitation. However, membrane-based filtration methods such as MF [115], UF [35], NF [116], and even FO [38] have been gaining increasing attention in the past decade within the MD fraternity. In a recent study conducted by El-Abbassi et al., two pretreatment processes namely coagulation/flocculation and MF were used for the treatment of olive mill wastewater (OMW) [115]. Their effects on MD performance were investigated. The latter was found to be a better pretreatment process since it was able to remove 30% of total solids (TS) as compared to the 23% of TS removed by coagulation/flocculation. Besides that, MF as a pretreatment process can achieve higher permeate flux by up to 25%.

Gryta et al. used UF as a pretreatment process prior to MD for the purification of oily wastewater [35]. PVDF UF membranes and PP MD membranes were used in this study. It was found that permeate from the UF process contained less than 5 ppm of oil while subsequent treatment by the MD process could completely remove any remaining oil pollutants.

Gryta discovered that the precipitation of protein could be limited by boiling of feed solutions followed by filtration [107]. This reduced the TOC and turbidity of the saline wastewater by 60% and 79%, respectively. In addition, a study conducted by Gryta observed that the boiling of the feed solution led to the decomposition of bicarbonates, which precipitate to form scales on the surfaces of membranes [117]. By thermally pretreating the feed, the amount of bicarbonates in the feed was reduced by 2–3 times. The thermal pretreatment method is more beneficial to waters with high hardness.

Coagulation is widely recognized as a low cost pretreatment option in membrane processes. Coagulation refers to the addition of certain chemicals that provides positive charges to neutralize the negatively charged colloidal particles. This causes the particles to come together to form much larger particles that can be more easily removed. Rapid mixing is introduced to dissolve the chemicals and distribute them evenly in the water. Wang et al. studied the effects of coagulation on MD of recirculating cooling water (RCW) [118]. It was discovered that poly-aluminum chloride (PACl) as a coagulant could reduce the amount of TOC and total phosphorous (TP) contents. The optimized PACl dosage was determined to be 15 mg L^{-1}. The coagulation process enhanced the trans-membrane flux by as much as 23%. This is caused by the formation of larger crystals on the surfaces of the membranes that could not be deposited inside the pores of these membranes and this led to reduced pore wetting.

2.3.2.2. Membrane flushing

Nghiem and Cath flushed PTFE membranes with Milli-Q® water after every 20 h of operation to mitigate the effects of scaling in a DCMD setup [119]. The experiments were performed on typical foulants such as $CaSO_4$, $CaCO_3$, and silicate. The preliminary results showed that $CaSO_4$ was the main contributor to scaling. Subsequent tests observed lesser $CaSO_4$ scaling with an increase in feed temperature and this was in good agreement with another study done by He et al. [120]. Consistent and regular membrane flushing could effectively remove nucleation sites on the surfaces of membranes and control the occurrence of scaling. This in turn led to sustainable flux during MD operation. However, this study did not properly account for the effects of flow rates and different flow regimes.

2.3.2.3. Gas bubbling

In order to remove the layers of foulants accumulated on the surfaces of membranes, there is a need to increase the shear rates at these surfaces and gas bubbling can achieve that [121, 122]. The mechanisms involved in gas bubbling have been well described in several literature and in particular by Cui et al. [123]. Cui et al. identified the following four mechanisms: (i) bubble-induced secondary flow; (ii) physical displacement of the concentration polarization layer; (iii) pressure pulsing caused by passing bubbles; and (iv) increase in superficial cross-flow velocity.

Chen et al. investigated on the benefits of incorporating gas bubbling into MD operations, which included reduced effects of the temperature polarization phenomenon and increased shear rates to delay fouling [122]. Experimental tests were carried out on commercial PVDF hollow fiber membranes in a DCMD setup and it was observed that the permeate flux enhancement ratio could reach up to 1.72 at an optimized gas flow rate.

The following operating conditions when coupled with gas bubbling were found to be able to achieve higher ratios: (i) increased feed temperature; (ii) low velocities in the feed and permeate streams; (iii) inclined membrane modules; (iv) shorter fiber lengths; and (v) low packing density. In their subsequent study, Chen et al. reported that fine bubbles (2–3 mm) with narrow size distribution are generally preferred because of their tendencies to create even flow distribution, intensifying mixing, and improving surface shear rates [21].

It is worth noting that these studies were performed on synthetic saline solutions. In reality, seawater can possibly contain complicated foulants. While the results look promising, it is hard to predict if this method will work as well in real applications. Besides that, it was observed that the flux enhancement ratio fell beyond the optimized gas flow rate due to excessive flow bypassing.

In a separate study, Ding et al. investigated on the fouling resistance through the incorporation of intermittent gas bubbling in concentrating the extract of TCM in a DCMD setup [124]. Intermittent gas bubbling was suggested instead of continuous gas bubbling. This was because the latter method reduced the interaction between the feed solution and the membrane surface while some bubbles stayed inside the membrane pores and reduced the vapor pressure difference. Both scenarios led to a decline in the flux. On the other hand, intermittent gas bubbling for durations of 1–3 min created a two-phase flow, which greatly improved the surface shear rate on the PTFE membranes and this in turn removed foulants accumulated on the surfaces of these membranes. It is important to note that to achieve the best cleaning efficiency, gas bubbling should be performed under the following conditions: (i) increased gas flow rates; (ii) increased gas bubbling duration; and (iii) decreased MD duration. As observed in the above-discussed literature, gas bubbling in the feed stream can be an effective method in removing external fouling

layers but its effectiveness in removing internal fouling layers in MD membranes has not been studied.

2.3.2.4. Temperature and flow reversal

Recently, Hickenbottom and Cath reported a novel approach to mitigate the effects of fouling and wetting in MD operations, which in turn can lead to sustainable fluxes, improved salt rejection properties, and lower chemical costs for membrane cleaning [125]. As their names suggest, the flow reversal method refers to exchanging the feed side and permeate side before scaling takes place while the temperature reversal method refers to reversing the direction of the driving force across the MD membrane. The tests results concluded that the latter method was more effective in mitigating fouling. While the results look promising, it is worth noting that this study provided no explanation on the nucleation kinetics involved as well as scale formation. Had that explanation been made available, the observations would have been of more value. Furthermore, these approaches have not been proven and tested on other feed compositions as well as foulants. Hence, there is a need for further studies to be conducted in that direction.

2.3.2.5. Development of novel membranes with fouling- and wetting-resistant properties

Over the years, researchers have proposed several types of membrane configuration for the MD process, such as the single-layer, dual-layer, and triple-layer. The dual-layer hydrophobic-hydrophilic composite MD membrane, which consists of a thin hydrophobic top layer and thick hydrophilic substrate, was patented by Cheng and Wiersma [108].

Yang et al. proposed two general strategies for surface modification [20]. The first strategy involves the introduction of materials with high hydrophobicity through coating or grafting and obtaining small maximum pore size on the membrane surface. The other alternative strategy is to create a dense hydrophilic layer on top of a hydrophobic substrate to protect the mouth of the membrane pores and make it less vulnerable to pore wetting when coming in contact with hydrophobic foulant species, which can be rather prevalent in industrial effluents such as in the case of produced water. Hydrophobic foulants that have the tendency to foul in aqueous solutions include colloids, proteins, clays, and oil droplets. To prevent membrane fouling and pore wetting, the membrane should have the desirable surface chemistry, which prefers binding to water to other materials. In other words, the surface must be superhydrophilic.

2.3.2.5.1 Homogenous hydrophobic membrane

In the early stages of MD research, the focus was on homogenous hydrophobic membranes. Drioli and Wu made a comparison between flat sheet and capillary commercial membranes fabricated from different polymeric materials such as PP and PTFE [126]. These membranes showed good performance when used to treat NaCl and sugar solutions. Similarly, Drioli et al. tested PP capillary membranes on the treatment of NaCl and glucose solutions [127]. It validated the potential of the MD process for the concentration of solutions and production of ultrapure water as the distillate. Banat and Simandl carried out trials on the performance of commercial PVDF and PTFE membranes for the treatment of synthetic seawater [77]. The following conclusions were drawn: (i) the quality of the distillate was significantly affected by pore wetting; and (ii) an increase in the concentration of the feed solution only led to a marginal decline in the flux.

In recent years, with the advancement in nanotechnology, researchers have begun to turn their attention to CNT-based membranes due to their excellent properties and fast fluid flow through their interior as observed by Dumee et al. [128]. CNT Bucky-Papers (BP) was developed for desalination. Its high contact angle (113°), high porosity (90%), and low thermal conductivity (2.7 kW $m^{-2} h^{-1}$) render the CNT BP a potential candidate for MD applications. It was reported to exhibit better performance than most polymeric membranes, with salt rejection of 99% and flux rate of 12 kg $m^{-2} h^{-1}$. The durability and hydrophobicity of the CNT BP were further enhanced in a separate work [129]. A two-step alkoxysilane treatment led to an increase in the contact angle (from 125° to 140°) and LEP (from 193 kPa to 441 kPa). Dumee et al. also demonstrated that enhanced hydrophobicity led to increased vapor permeation. This was largely attributed to the 'thin insulating air film on the surface of the membrane generated by the hydrophobic forces' [130].

2.3.2.5.2. Superhydrophobic surface

Recently, more researchers have directed their attention towards the creation of superhydrophobic and self-cleaning surfaces through increasing the surface roughness followed by the modification of these surfaces with low energy and non-polar molecules [131]. Superhydrophobic surfaces have high contact angles between 150° and 180° as well as low tilting angles of less than 10° [132].

Liao et al. invented a facile method to create superhydrophobic PVDF nanofiber membranes through surface modifications involving the use of polydopamine (PDA) for surface activation, the deposition of silver nanoparticles, and hydrophobic treatment with 1-dodecanethiol [131]. A contact angle of 153° ± 4° and LEP of 146 kPa were achieved. Razmjou et al. prepared TiO_2 nanocomposite PVDF membranes through the low

temperature hydrothermal (LTH) process [133]. The deposition of TiO_2 nanoparticles increased the surface roughness and this was followed by surface fluorosilanization to lower the surface energy. The LEP and water contact angle were 190 kPa and 163° ± 3°, respectively. Besides that, higher flux recovery was observed after chemical cleaning, which is an indication of enhancement in the anti-fouling property of the membranes.

Dong et al. fabricated superhydrophobic PVDF-PTFE electrospun nanofibrous membranes with contact angle of 152.2° and LEP of 137 kPa by varying the amount of PTFE content in the dope solution [134]. A stable flux was achieved. Zhang et al. sprayed a mixture of polydimethylsiloxane and SiO_2 nanoparticles on PVDF membranes to achieve superhydrophobicity [135]. A contact angle of 156° and LEP of 275 kPa were achieved. While the post-tested membranes showed excellent anti-fouling property, the quality of the distillate collected can be improved. Yang et al. achieved improved permeate flux via CF_4 plasma surface modification of PVDF membranes, which have a contact angle of 162.4° [136]. The larger air, membrane, and water three-phase interface contributed by the superhydrophobic surfaces elucidated the enhancement in the permeate flux.

It should be pointed out that the enhancement of hydrophobicity might not be suitable for organic fouling mitigation. When the MD process is applied to feed waters containing surface-active species, such as surfactants, the underwater oleophobicity of the membrane surface should also be taken into consideration.

2.3.2.5.3. Composite dual-layer membrane

The development of novel dual-layer hydrophobic-hydrophilic composites was due to the need for MD membranes with higher flux. This can be achieved since there

will be supposedly lesser resistance to the transport of vapor molecules as well as lower conductive heat loss. Cheng and Wiersma patented the first composite membrane [108]. Khayet et al. developed a facile approach to prepare novel porous hydrophobic-hydrophilic composite by adhering fluorinated surface-modifying macromolecules (SMMs) onto a polyetherimide (PEI) substrate [75]. The as-prepared membranes validated the benefits of a dual-layer composite and even outperformed commercial PTFE membranes. The membrane pore size was inversely correlated with the concentration of PEI in the casting solution. As such, higher flux was observed when the concentration of PEI was lower. Khayet et al. continued with their previous work by developing a novel method for determining the thickness of the hydrophobic layer of composite membranes. The thickness exhibited a directly proportional relationship with the concentration of the hydrophilic substrate in the casting solution. However, operational parameters such as the stirring rate and temperature had no effect on the thickness of the hydrophobic layer.

Bonyadi and Chung proposed a novel method for the fabrication of dual-layer hydrophobic-hydrophilic hollow fiber membranes via a co-extrusion spinning process [137]. While the use of weak coagulants such as water/methanol can achieve desirable membrane characteristics, they tend to weaken the mechanical properties of the membranes. This can be compensated through the introduction of hydrophilic and hydrophobic clay particles into the dope solution. Their method led to a significant improvement in the permeate flux of the MD process.

Qtaishat et al. verified the importance of the hydrophobic skin layer in composite membranes [138]. Characteristics such as the LEP, pore size, and porosity had a huge influence on the resulting flux. Besides that, hydrophilic layers with sponged-like structures exhibited enhanced flux as compared to those with finger-like structures. Poly

(urethane propylene glycol)-based SMMs displayed better performance than the poly (urea dimethylsiloxane urethane)-based SMMs. In another work, Qtaishat et al. blended polysulfone (PS) with SMMs of different fluorine contents and molecular weights [139]. Higher flux was observed for the following conditions: (i) increased fluorine content; (ii) 1-Methyl-2-pyrrolidinone (NMP) as a solvent; (iii) lower hydrophilic polymer concentration; (iv) decreased amount of non-solvent; and (v) lower LEP. The novel composite membranes had a permeate flux that was 43% higher than commercial PTFE membranes and therefore could potentially be used for desalination.

Peng et al. blended polyvinyl alcohol (PVA) with polyethylene glycol (PEG) and cross-linked by aldehydes [140]. The hydrophilic PVA/PEG layer was created on top of a hydrophobic PVDF substrate. The composite membrane was observed to be more durable and retained the flux of the hydrophobic substrate. Furthermore, it experienced lesser effects of the concentration polarization phenomenon. Notably, the composite membrane was able to achieve high removal efficiency as well as high purity distillate. It was suggested that the introduction of a hydrophilic layer could improve on the pore wetting issue faced by hydrophobic MD membranes.

Zuo and Wang carried out novel membrane surface modification on a PVDF substrate [37]. Plasma grafting of PEG and deposition of TiO_2 nanoparticles were performed to create a highly hydrophilic surface layer. The hydrophilic surface was observed to show lesser affinity for the oil droplets in the feed than the hydrophobic surface of the virgin membranes. Furthermore, no fouling or wetting was observed after a day of operation and this could be attributed to the benefits of the reduced hydrophobicity of the membrane and smaller pore size. At certain pH levels where the surface charges of the membrane and oil droplets were opposite, severe fouling could be observed. This

validates the point that there exists an important relationship between membrane surface chemistry and the feed. In recent studies, PVDF membranes with underwater superoleophobic property were prepared by spray coating of various nanocomposite layers with sophisticated micro-/nano-hierarchical structures to repel the adsorption of physically emulsified crude oil [55, 141].

The composite dual-layer membrane is an interesting strategy. However, to enhance on the anti-fouling and anti-wetting properties of the membrane, the hydrophilic-hydrophobic configuration should be adopted for the treatment of low surface tension feeds. It is paramount to optimize the thickness of the hydrophilic layer and the size of the membrane pores in order to achieve excellent rejection properties and high permeate fluxes.

2.3.2.5.4 Triple-layer membrane

Prince et al. invented a novel triple-layer nanofiber based membrane via wet casting and electrospinning [142]. The selective top hydrophobic layer prevents water molecules from entering the membrane. The micro-porous middle layer increases the LEP of the membrane by 1.6 times, allowing for long-term protection against pore wetting. The bottom hydrophilic layer serves the function of drawing vapor molecules from the middle layer by absorption [143]. These layers were bounded together by heat pressing and solvent binding. This novel membrane achieved stable high flux. Moreover, the permeate quality was consistent even after more than three days of continuous operation. While the results look promising, it is worth noting that this novel membrane had only been tested using synthetic seawater. Should it be tested in low surface tension wastewaters, it is highly likely that the top hydrophobic layer in this novel membrane will attract hydrophobic and/or amphiphilic foulants onto the membrane surface. The

adsorption of low surface tension contaminants onto the membrane surface can potentially reduced the LEP of the membrane. This is highly undesirable as membrane fouling and pore wetting may become prevalent.

2.3.2.5.5 Omniphobic membrane

In 2008, scientists from the Massachusetts Institute of Technology invented omniphobic surfaces, which can possibly repel everything. Recently, Lin et al. used this concept to fabricate omniphobic membranes for MD [144]. They coated silica nanoparticles (re-entrant structure) onto hydrophilic glass fiber membranes followed by surface fluorination (low surface tension) and polymer coating (metastable Cassie-Baxter state). No wetting was observed for 9 h in the presence of sodium dodecyl sulfate (SDS). These omniphobic membranes have the potential to be used for the treatment of produced water, which typically contains high concentrations of surfactants or low surface tension pollutants. This was made possible through the creation of re-entrant structures. This coupled with the low surface tension surfaces allowed for the existence of a metastable Cassie-Baxter state for liquid-solid-vapor interfaces. Based on this principle, the development of omniphobic membrane for MD applications has picked up the pace in recent years [51, 53, 54]. While the results look promising, it is worth noting that many of these studies focused on only one type of surfactant. Since real produced water samples often contain a wide range of constituents, the observations would have been of more value had they tested these membranes in more complex feed solutions such as surfactant-stabilized O/W emulsions. Fig. 2-2 shows the fouling- and wetting-resistant properties of novel membranes in surfactant-containing feed water as proposed by Wang and Lin [145].

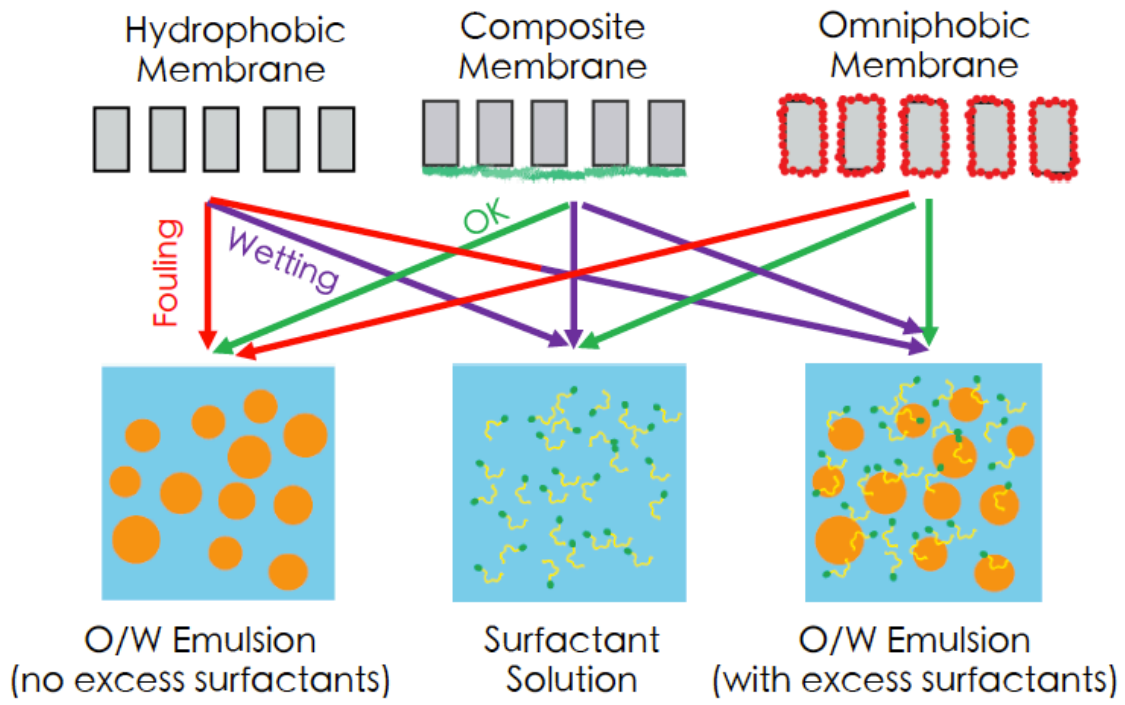


Fig. 2-2. Fouling- and wetting-resistant properties of different novel membranes in low surface tension feed solutions [145].

Overall, fouling and wetting in MD remain its main challenge towards practical implementation. While many researchers have made a great effort to address and try to overcome these issues, their studies mainly focused on the mechanisms of different types of fouling in MD. Common mitigation methods have been established or borrowed from other related membrane processes, especially membrane filtration and heat exchange processes. Hence, more specific fouling and wetting control techniques need to be developed for MD, based on its unique properties and characteristics, to narrow down on the remaining research gaps.

Chapter 3 Materials and Methods

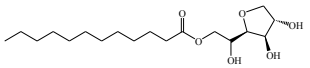
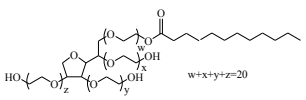
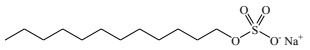
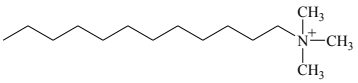
3.1. Materials and chemicals

Sodium chloride (NaCl, 99.5%), sorbitan monolaurate (Span® 20), polyoxyethylenesorbitan monolaurate (Tween® 20), anhydrous sodium acetate, and 2-propanol (IPA) were purchased from Merck Millipore (Singapore). Dopamine hydrochloride (DA), Polyethylenimine (PEI, Mw=800), tris(hydroxymethyl)aminomethane (Tris), sodium dodecyl sulfate (SDS), dodecyltrimethylammonium bromide (DTAB), petroleum (~18% aromatics), vacuum pump oil (VPO), sodium hydroxide (NaOH), hydrochloric acid (HCl), and sodium periodate (SP) were purchased from Sigma-Aldrich (Singapore). The properties of oils and surfactants used in this study are presented in Table 3-1 and Table 3-2, respectively. Milli-Q® water with a resistivity value of 18.2 MΩ cm was used in all experiments (produced by the Milli-Q® integral water purification system, Merck Millipore). Hydrophobic PVDF hollow fiber membranes with a nominal pore size of 0.027 μm were obtained from a commercial supplier. The received hollow fiber membranes were immersed in Milli-Q® water at 313 K for at least 3 h to get rid of chemical residues from the fabrication process. Subsequently, the membranes were dried overnight in a vacuum oven at 323 K (Heraeus Vacutherm® Oven, Thermo Fisher Scientific, Singapore). The dried membranes were then used as substrates for surface modification, and as references for the fouling and wetting experiments. The relevant membrane properties were characterized and summarized in Table 3-3. Lab-scale modules were prepared by sealing 4 pieces of 18 cm long hollow fiber in Teflon tubing. A new membrane module was used for each experiment. The effective membrane area for each module was 35 cm^2.

Table 3-1. Properties of oils used in this study.

Oil type	Relative density ($g\ ml^{-1}$)	Boiling point (K)	Flash point (K)	Components
Petroleum	0.79	453–493	334	~18% aromatics
VPO	0.88	662	523	Solvent-refined heavy paraffinic

Table 3-2. Properties of surfactants used in this study.

Surfactant	Molecular weight ($g\ mol^{-1}$)	HLB[a]	CMC[b] ($mg\ L^{-1}$)	Surface tension[c] ($mN\ m^{-1}$)	Chemical structure
Span® 20	346.5	8.6 [146]	1.6	~25 ± 0.12	
Tween® 20	1227.5	16.7 [146]	3.5	~36 ± 0.25	
SDS	288.4	40.0 [147]	129	~30 ± 0.17	
DTAB	308.3	24.3 [148]	N.A.[d]	~40 ± 0.22	

[a] Hydrophilic-lipophilic balance.
[b] Critical micelle concentration (in 3.5 wt% NaCl at 333 K).
[c] Surface tension was measured at 0.15 mM in 3.5 wt% NaCl using tensiometer (DCAT11, DataPhysics, Germany).
[d] Not applicable.

Table 3-3. PVDF membrane properties.

Dimension (mm)	Pore size (μm)	Contact angle, θ (°)	Porosity, ε (%)	LEP_w[a] (bar)	Tensile modulus, E_t (MPa)	Strain, δ_b (%)	Zeta potential[b] (mV)
d_0: 1.531 d_i: 0.872	r_{max}: 0.183 r_{mean}: 0.022	116	83	3.14	26.4	126.6	-52.5

[a] Water liquid entry pressure.
[b] Surface zeta potential was measured in NaCl solution at pH 7.

3.2. Membrane characterization tests

An in-house-made LEP experimental setup was used for the measurement of LEP_w of the pristine PVDF membrane as described in our previous research [22]. The mechanical properties of the membrane were measured by a Zwick Roell BT1-FR0.5TN.D14 Material Testing Machine at a constant elongation velocity of 50 mm min^{-1} under room temperature. The mean pore size and pore size distribution of the pristine PVDF and modified membranes were determined by a capillary flow porometer (CFP 1500A, Porous Material, Inc., USA). The hollow fiber membranes were glued to the sample holders using epoxy and wetted thoroughly overnight by Galwick^{TM}, a low surface tension wetting fluid. The detailed underlying working principles and experimental procedures had been described in our previous research works [20, 121]. The membrane porosity was calculated by dividing the volume of pores by the total volume of the membrane as described in our previous research [22].

The surface functional groups of the pristine PVDF and modified membranes were qualitatively analyzed at room temperature by a Fourier transform infrared spectroscope via attenuated total reflectance mode (ATR-FTIR) (IR-Prestige-21, Shimadzu, Japan) over a scan range of 400–4000 cm^{-1} with a resolution of 4 cm^{-1}. The Happ-Genzel function was selected as the apodization function. The presence of surfactants on the inner surface of the pristine PVDF membrane was also detected using the ATR-FTIR. The differences in the surface and cross-section morphologies of the pristine PVDF, fouled PVDF, and modified membranes were observed using a field emission scanning electron microscope (FESEM) (JSM-7200F, JEOL, Japan). The dried hollow fibers were fractured in liquid nitrogen and then sputter-coated with a layer of

platinum by a sputter coater (JEC-3000FC, JEOL, Japan) prior to the respective tests. The outer surface topographies and roughness of the pristine PVDF and modified membranes were observed through an atomic force microscope (AFM) (XE-100, Park Systems, Republic of Korea) with a scan area of 5 μm x 5 μm under the non-contact mode at ambient conditions.

The elemental compositions of the outer and inner surfaces of the pristine PVDF and modified membranes were measured using an X-ray photoelectron spectroscope (XPS) (AXIS Supra^{TM}, Kratos Analytical, UK) with a 500 mm Rowland circle monochromic Al Kα excitation source at 1486.7 eV. An emission current of 5 mA and operating voltage of 15 kV were employed. High-resolution spectra were collected using pass energies of 20 eV and 160 eV for narrow and broad scans, respectively. The sampling depth was approximately 10 nm with a takeoff angle of 0° with respect to the membrane surface. All binding energies for the elements of interest were corrected against an adventitious C 1s core level at 285.0 eV. All XPS peaks were fitted using the Shirley background together with the Gaussian-Lorentzian function by the CASA XPS software.

The dynamic contact angles of the virgin PVDF, fouled PVDF, and modified membranes were determined by a tensiometer (DCAT11, Data Physics, Germany). A hollow fiber sample glued to a holder was hung from the arm of an electro-balance and underwent through three cycles of immersion (surface detection threshold at 0.5 mg) into Milli-Q$^{®}$ water at an immersion depth of 5 mm. The dynamic contact angles were calculated from the wetting force according to the Wilhelmy method. Each membrane sample was measured ten times and an average value was calculated. To obtain accurate measurements for the modified membranes, their lumen sides were filled with epoxy

resin and allowed to dry overnight. This was to ensure that only the outer surfaces of the modified membranes were in contact with the Milli-Q® water during the test procedure. The critical micelle concentration (CMC) values of the respective surfactants were also determined by the tensiometer. Predetermined concentrations of surfactant solutions were prepared and injected into a dish that contained 3.5 wt% NaCl solution, which was maintained at 333 K by a recirculating water bath. The changes in the surface tension of the NaCl solution were measured. CMC was reached when the surface tension remained relatively constant. Each CMC value was measured three times and an average value was obtained.

The surface zeta potentials of the pristine PVDF and modified membranes were determined using an electrokinetic analyzer (SurPASS™ 3, Anton Paar, Austria) based on streaming potential measurements. 1 mM NaCl was prepared as the background electrolyte solution. 0.05 M HCl and NaOH were used for pH titration. Hollow fiber membranes were flattened and taped onto two sample holders mounted in an adjustable gap cell (20 mm x 10 mm). The gap height was adjusted to ~100 μm. The pH of the electrolyte solution was first adjusted to pH 10 by dosing it with NaOH. Subsequently, the electrolyte solution was dosed with HCl in a stepwise fashion to pH 3. During each measurement, the NaCl electrolyte solution flowed across the cell through depressurization of the liquid reservoir from 600 mbar to 200 mbar, causing electric charge separation. The resulting potential difference was detected and calculated using the Helmholtz-Smoluchowski equation [149].

The underwater oleophilicity and oleophobicity of the pristine PVDF and modified membranes were evaluated using the captive bubble method via a goniometer (OCA 25, DataPhysics, Germany). In this method, a drop of petroleum was injected

beneath the membrane taped onto a cell underwater. The interactions between the oil droplet and the respective membrane surfaces were observed. To evaluate the structural stability of the grafted layer on the modified membranes, each membrane sample was ultrasonic treated for 10 min at ambient temperature in an ultrasonic bath (FB 15068, Fisher Scientific, USA) with a frequency of 37 kHz.

3.3. Preparation and characterization of surfactant solutions and surfactant-stabilized O/W emulsions

Different low surface tension saline feeds were prepared for the DCMD experiments, including four surfactant solutions that were prepared by mixing 50 mg L^{-1} of Span® 20, Tween® 20, SDS, and DTAB in 3.5 wt% NaCl solution, respectively. The properties of these surfactants are listed in Table 3-2. Separately, surfactant-stabilized O/W emulsion was prepared by mixing 450 mg L^{-1} of petroleum/VPO, 50 mg L^{-1} of surfactant, and 8 L of 3.5 wt% NaCl solution in a high speed heavy-duty blender (CB15, Waring® Commercial, USA) for at least 3 min. NaCl was used to represent the dissolved solids present in produced water. The conductivities of the emulsions were measured to be around 50 mS cm^{-1}. The composition of the emulsion was modeled as closely to real produced water samples as possible. The oil droplet size distribution of the emulsion was measured by a mastersizer (Hydro2000SM, Malvern Instruments, UK) while its zeta potential was measured by a zetasizer (NanoZS, Malvern Instruments, UK). Fresh emulsions were prepared after every 24 h of operation to ensure that the feed remained kinetically stable because unstable emulsions might not accurately demonstrate the fouling and wetting behaviors of both the pristine PVDF and modified membranes.

3.4. DCMD performance tests

The DCMD experimental rig used for the experiments has been illustrated in our previous work [20]. The feed solutions were heated and maintained at 333 K and circulated on the shell side of the hollow fiber membranes. The permeate water was cooled and maintained at 293 K and circulated in the lumen side of the hollow fiber membranes in a countercurrent flow to the feed. The feed and permeate volumetric flow rates were maintained at 0.7 L min^{-1} and 0.25 L min^{-1} respectively, corresponding to Reynolds numbers of 1631 and 609 respectively. A higher flow rate was employed on the feed side to mitigate concentration and temperature polarizations [20]. The overflow from the permeate reservoir was collected into a tank placed on a weighing balance to determine the temporal changes in mass with an accuracy of ± 0.1 g. The temporal changes in permeate conductivity were recorded to an accuracy of ± 0.1 μS cm^{-1}. Most importantly, all tubes and membrane modules used in the experimental rig were insulated with insulation foam to minimize heat loss during the process.

This page is intentionally left blank

Chapter 4 Surfactant Effects on Water Recovery from Produced Water via Direct-contact Membrane Distillation[1]

4.1. Introduction

Over the years, there have been very few reports available in the literature on the application of MD for low surface tension feeds. While the influences of pretreatment, operating conditions, and novel membrane surface modifications have been intensively studied, there exists a gap in the knowledge base with regard to the three key constituents in real produced water streams (namely oils, surfactants, and salts) that have the greatest impact on MD performance. This in turn has discouraged the use of MD for extended applications.

This study aims at developing a fundamental understanding of the relationship between surfactant-stabilized O/W emulsions and PVDF membrane surface in the DCMD process. A PVDF membrane was selected because it is hydrophobic in nature, which is a fundamental requirement for MD operations. Specifically, a series of bench-scale experiments were conducted to investigate on the roles of different types and concentrations of oil and surfactant on the fouling and wetting behaviors of the PVDF membrane. Membrane autopsy was also conducted using Fourier transform infrared spectroscopy (FTIR) and field emission scanning electron microscopy (FESEM) to confirm the wetting and fouling phenomena in the DCMD process. It is expected that this study can provide guidance for developing new strategies to facilitate DCMD as an energy-efficient and effective technology for treating produced water.

[1] *This chapter is reproduced with permission from Chew, N.G.P., S. Zhao, C.H. Loh, N. Permogorov, R. Wang, Surfactant effects on water recovery from produced water via direct-contact membrane distillation, J. Membr. Sci. 528 (2017) 126–134. Copyright © 2017 Elsevier.*

4.2. Results and discussion

4.2.1. Oil droplet sizes and zeta potentials of surfactant-stabilized O/W emulsions

Three types of surfactant commonly used in the petroleum industry (Span® 20, Tween® 20, and SDS) and two types of oil (petroleum and VPO) were used to prepare the surfactant-stabilized O/W emulsions [150]. These O/W emulsions were modeled as similar to real oilfield-produced water samples as possible, which generally contain 2–565 mg L^{-1} of oil [3]. The mean droplet sizes and zeta potentials of these emulsions are listed in Table 4-1. The oil droplet size distributions of the emulsions are presented in Fig. 4-1. Oilfield-produced water typically has oil droplet sizes ranging from 2 to 30 μm [2]. However, the oil droplet sizes of all the emulsions were kept below 10 μm to form kinetically stable O/W emulsions [151]. It can be seen that the mean droplet size was dependent on the types of oil and surfactant. With the same oil/surfactant mass ratio and stirring time, the petroleum emulsion stabilized by Span® 20 had a larger mean oil droplet size as compared to other surfactants because oil droplets have a greater tendency to coalesce in this case. When comparing different types of oil stabilized by the same surfactant (Tween® 20 in this case), the oil droplet size of the VPO emulsion was larger than that of the petroleum emulsion due to the higher proportion of heavy hydrocarbons present in VPO [152]. According to the measured zeta potentials, the Span® 20 and Tween® 20-stabilized emulsions were nearly neutral while the SDS-stabilized emulsion was negatively charged.

Table 4-1. Number average mean droplet size, span of distribution, and zeta potential of the surfactant-stabilized O/W emulsions.

Composition	Mean droplet size[a] (μm)	Span of distribution[b]	Zeta potential (mV)
500 mg L^{-1} Span® 20/Petroleum Emulsion	7.74	2.05	-3.36 ± 0.44
500 mg L^{-1} Tween® 20/Petroleum Emulsion	2.16	2.82	-3.11 ± 0.32
500 mg L^{-1} SDS/Petroleum Emulsion	3.48	1.74	-37.2 ± 1.1
500 mg L^{-1} Tween® 20/VPO Emulsion	7.27	2.24	-3.38 ± 0.12
600 mg L^{-1} Tween® 20/Petroleum Emulsion	2.39	2.84	N.A[c]
1000 mg L^{-1} Tween® 20/Petroleum Emulsion	2.64	2.85	N.A[c]

[a] Mean droplet size was measured when the feed solution was heated up to 333 K.
[b] The larger the span of distribution is, the more polydisperse the emulsion.
[c] Not applicable. The zeta potentials of these emulsions were not measured.

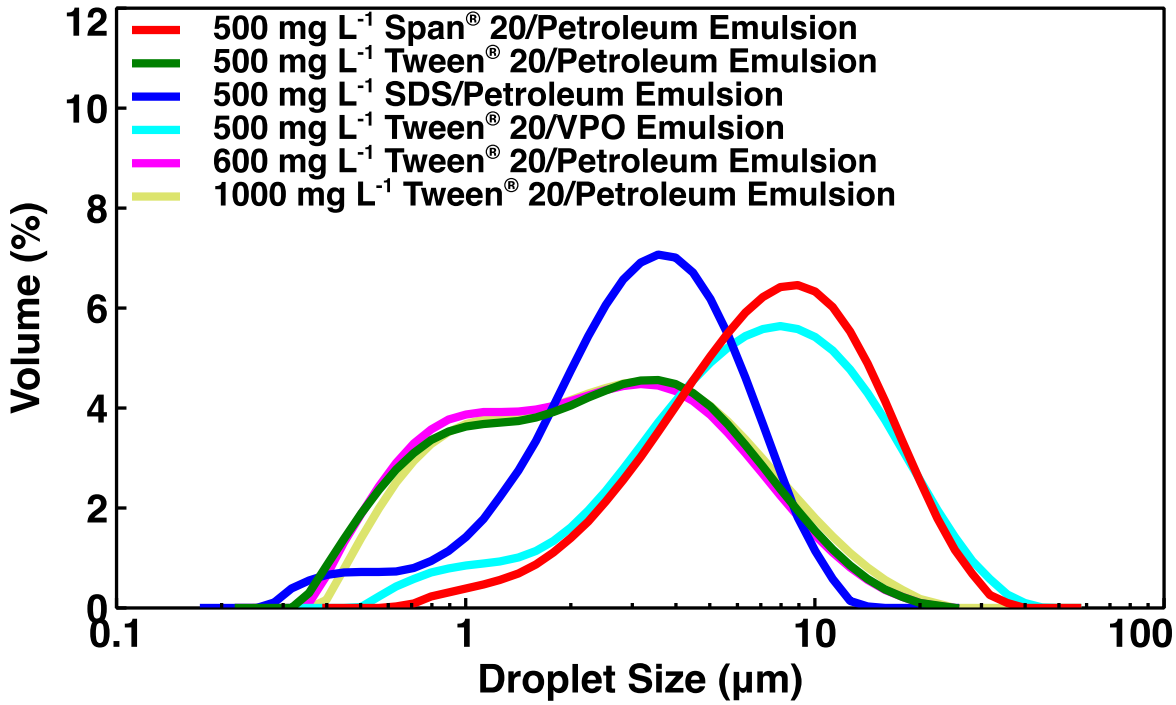


Fig. 4-1. Oil droplet size distributions of different O/W emulsions.

4.2.2. Effects of surfactant types

A baseline test was first conducted using 3.5 wt% NaCl as the feed solution, which represented the TDS present in produced water. The purpose of running a baseline test was to ascertain that the addition of NaCl did not contribute to changes in the permeate flux and conductivity, if any. As shown in Fig. 4-2, the permeate flux was steady and observed to be approximately 11 kg m^{-2} h^{-1} while the permeate conductivity was fairly constant throughout, ranging between 2–3 µS cm^{-1}. This suggests that scaling and wetting did not take place during the experiment.

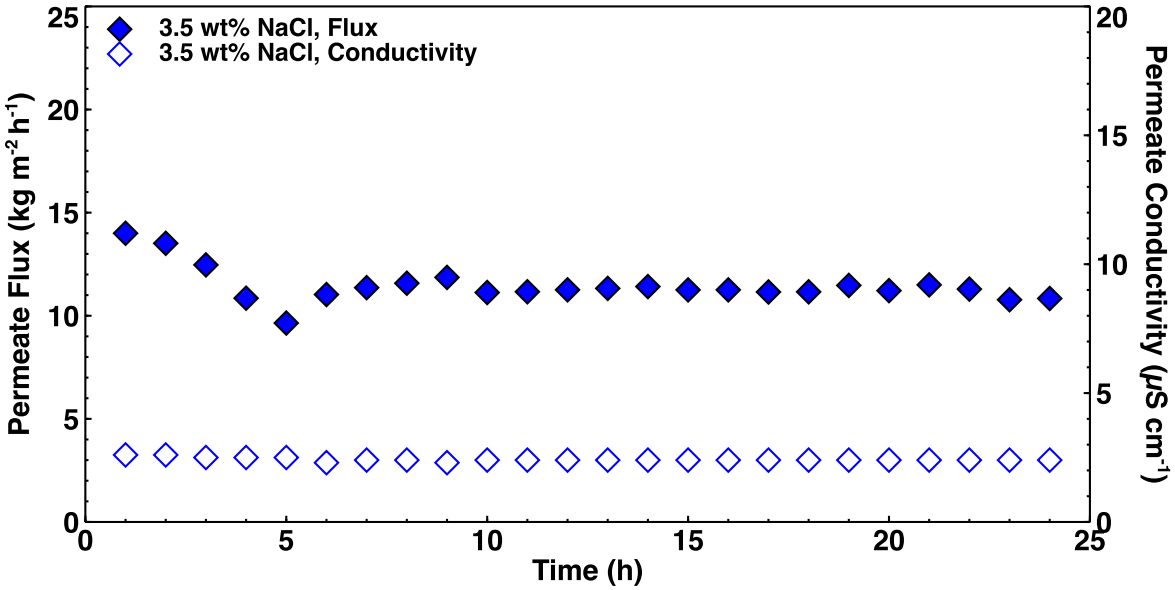


Fig. 4-2. Effects of 3.5 wt% NaCl solution on permeate flux (filled symbols) and conductivity (hollow symbols). Feed volumetric flow rate (Q_f) = 0.7 L min^{-1}; Permeate volumetric flow rate (Q_p) = 0.25 L min^{-1}; Feed temperature (T_f) = 333 K; Permeate temperature (T_p) = 293 K.

Fig. 4-3 shows the effects of different surfactants on the permeate flux and conductivity during the MD process. To ensure a fair comparison, the same molar concentration of surfactant was used. From Fig. 4-3, a significant rise in the permeate conductivities was observed, demonstrating the wetting of membrane during the MD process. The time for the onset of wetting was defined as the time when the permeate conductivity increased by 1 µS cm^{-1} due to the diffusion of NaCl into the permeate side.

The wetting times and the final permeate conductivities in different surfactant experiments are listed in Table 4-2. The results show that Tween® 20 exhibited the earliest wetting with an onset of wetting occurring at ~70 min, followed by Span® 20 (~105 min), and SDS (~520 min). The severity of membrane wetting was in the sequence of Tween® 20 > Span® 20 > SDS as well, and the final conductivities in the permeate tank were measured at 8.51, 3.56, and 0.153 mS cm^{-1}, respectively (as listed in Table 4-2).

The wetting behaviors could be controlled by surfactant adsorption on the membrane surface, which is related to the physical properties of the surfactants. As listed in Table 3-2, the surfactants used in this study exhibit different molecular weights, surface tensions, hydrophilic-lipophilic balance (HLB) values, and CMCs. The presence of surfactants lowers the surface tension of the medium rapidly [153-155]. Based on the Laplace-Young equation, LEP decreases with decreasing surface tension of liquid, resulting in higher tendency of membrane wetting [156]. However, Span® 20 caused a slower membrane wetting rate than Tween® 20 despite its lower surface tension. Hence, it seems that surface tension was not the determining factor for the time for onset of wetting and the extent of wetting. On the other hand, all these three surfactants have the same length of hydrophobic tails (12 alkyl units). Thus, the effect of different molecular weights of the surfactants is mainly attributed to the difference in their hydrophilic heads. Moreover, the dominant driving force for the surfactant adsorption is the hydrophobic effect (the tendency of the surfactant to escape from the aqueous environment), which is related to the hydrophobic/hydrophilic properties and CMC of the surfactants [151]. Therefore, the different wetting rates of these surfactants may be attributed to the difference in HLB and CMC among surfactants. As listed in Table 3-2, Span® 20, Tween® 20, and SDS have HLB values of 8.6, 16.7, and 40, respectively. The higher the surfactant's HLB value, the more hydrophilic it is [157]. In other words, a surfactant with

a lower HLB value will be more lipophilic and thus be easily adsorbed on a hydrophobic surface due to the hydrophobic effect [158]. Therefore, Span® 20 and Tween® 20 with relatively lower HLB values caused earlier wetting than the more hydrophilic SDS.

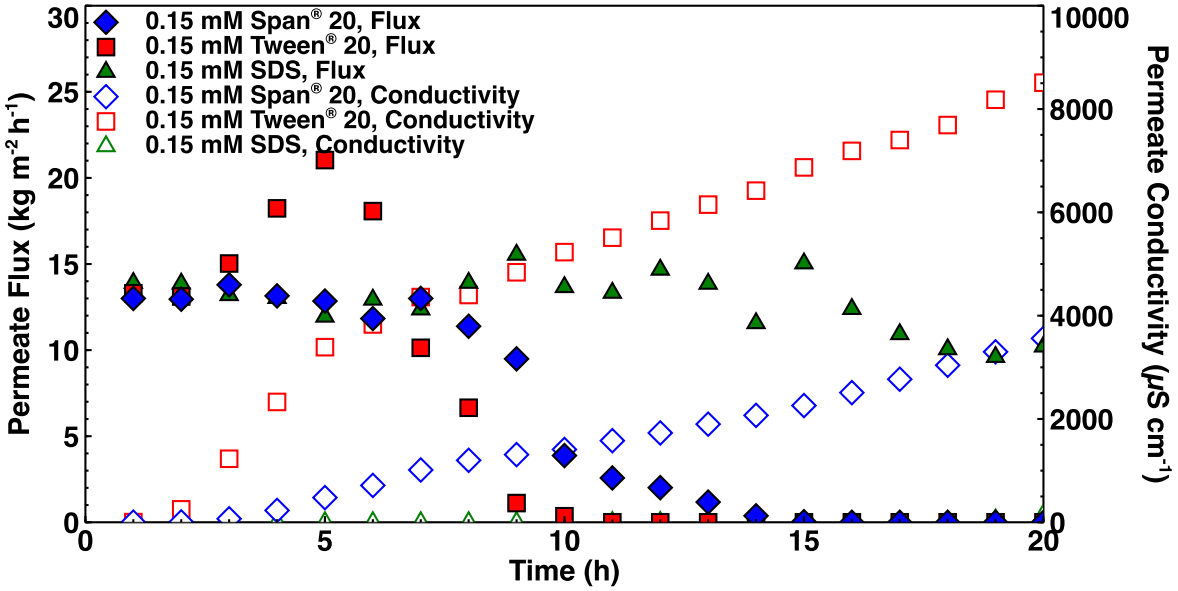


Fig. 4-3. Effects of surfactant types (same molar concentration) on permeate flux (filled symbols) and conductivity (hollow symbols). Q_f = 0.7 L min^{-1}; Q_p = 0.25 L min^{-1}; T_f = 333 K; T_p = 293 K.

Table 4-2. Wetting time, final permeate conductivity, and contact angle of surfactant-fouled membranes in DCMD using feed with different surfactants.

Membrane	Time for onset of wetting (min)	Final permeate conductivity (mS cm^{-1})	Contact angle (°)
No surfactant	-	-	116 ± 2
0.15 mM Span® 20	~105	3.56	72 ± 3
0.15 mM Tween® 20	~70	8.51	64 ± 2
0.15 mM SDS	~520	0.15	91 ± 1
50 mg L^{-1} Span® 20	~100	3.69	72 ± 1
50 mg L^{-1} Tween® 20	~130	12.55	63 ± 1
50 mg L^{-1} SDS	~140	0.95	85 ± 1

According to literature, surfactant adsorption on hydrophobic surfaces is non-cooperative, as they do not form micelles on the surfaces. Instead, the surfactant unimers

form a monolayer [151]. For non-ionic surfactants such as Span® 20 and Tween® 20, the adsorption on the hydrophobic PVDF membrane surface was dominated by hydrophobic interactions [151]. Considering the fact that 0.15 mM Span® 20 and Tween® 20 exceeded their respective CMC values, it was likely that the adsorbed unimers of Span® 20 and Tween® 20 tended to distribute more densely and thus stood erected on the PVDF membrane surface as illustrated in Fig. 4-4 [159]. Even though the alkyl chain length of a Span® 20 unimer is the same as that of a Tween® 20 unimer, the former has a much smaller hydrophilic head group as compared to the latter as stipulated by their respective HLB values [157]. The larger hydrophilic heads of Tween® 20 unimers were able to draw more water towards the membrane pores once these unimers got adsorbed onto the membrane surface. This may explain why earlier wetting and higher conductivity rising rate were observed for the Tween® 20 experiment.

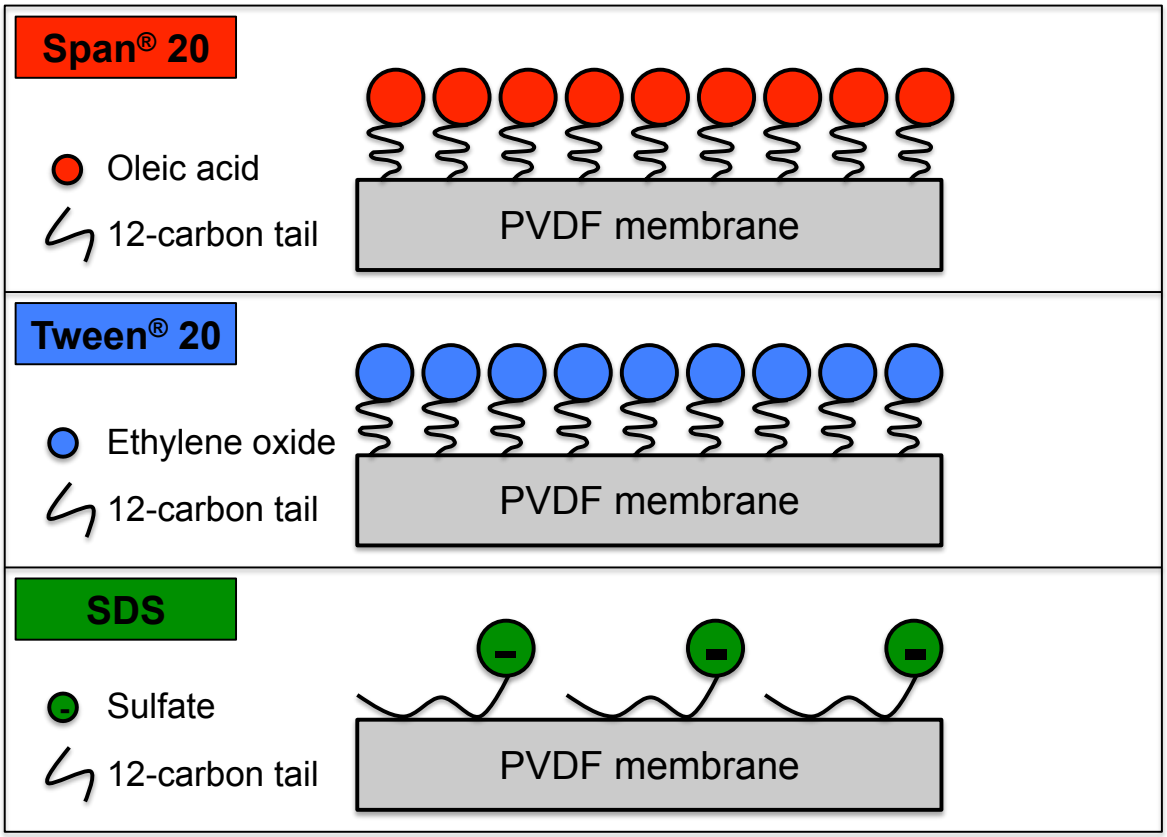


Fig. 4-4. Hypothetical illustration of the adsorption of surfactant unimers on the PVDF membrane surface.

In contrast to non-ionic surfactants, both hydrophobic interactions (nonpolar tails) and electrostatic interactions (polar heads) typically play crucial roles in the adsorption of ionic surfactants like SDS. The PVDF membrane surface was negatively charged, thus SDS would have experienced electrostatic repulsion resulting in fewer unimers getting adsorbed onto the membrane surface. On the other hand, being hydrophilic in nature, the SDS unimers would have the tendency to stay in water instead of attaching onto the PVDF membrane surface. As a result, very few SDS unimers would have adsorbed onto the membrane surface due to the hydrophobic nature of the PVDF membrane surface. In addition, the concentration of SDS in the feed solution was much lower than its CMC, suggesting that the unimers tended to be loosely packed even when a certain amount of SDS were adsorbed on the PVDF surface. Due to the low concentration of SDS on the PVDF membrane surface, it was very likely that the adsorbed unimers laid flat on the membrane surface as illustrated in Fig. 4-4.

As shown in Fig. 4-3, the permeate flux of the Span® 20 experiment remained fairly constant (13 kg m^{-2} h^{-1}) for 7 h even after the occurrence of wetting and then it gradually declined until no flux was observed after 15 h of operation. In the case of Tween® 20, a relatively constant flux was observed for 2 h. After which, there was a gradual increase in flux until 5 h of operation indicating membrane wetting and then there was a subsequent decline in flux. The flux reached zero at approximately 10 h. As discussed above, with the adsorption of Tween® 20 unimers on the membrane surface, their hydrophilic heads were able to draw more water towards the membrane pores. This resulted in the increase of permeate flux after the observed onset of wetting. Similar findings were presented in a recent publication [48]. The flux decline in the case of both Span® 20 and Tween® 20 suggests that membrane fouling indeed took place during the MD process. Since the concentrations of these two surfactants exceeded their respective

CMC values, micelles would have formed in the solutions. This might in turn lead to the blockage and closure of the membrane pores after membrane wetting. Moreover, micelles are able to grow from spherical aggregates to elongated ones with an increase of concentration [151]. In comparison to Span® 20, more severe fouling was observed in the case of Tween® 20 due to pore blockage by the larger micelles of Tween® 20. On the other hand, for SDS, a relatively constant flux (approx. 10 kg m^{-2} h^{-1}) was observed for 20 h of operation. This is because the concentration of SDS was well below its CMC value and almost no micelle would have formed in the solution. In addition, very few SDS unimers would have adsorbed onto the membrane surface due to the hydrophilic nature of SDS. Thus, the membrane experienced less fouling and the permeate flux remained fairly constant throughout the operation.

The water contact angles of the different surfactant-fouled membranes are listed in Table 4-2. It can be seen that the hydrophobicity of PVDF membrane decreased after the adsorption of surfactants and the contact angles of 0.15 mM Span® 20, Tween® 20, and SDS-fouled membranes were 72°, 64°, and 91° respectively. The decrease of PVDF membrane hydrophobicity can be explained by the hydrophobic interactions between the hydrophobic tails of surfactants and the membrane surface. The interactions orientated the hydrophilic head of surfactants facing outwards, causing the membrane surface to be covered by a hydrophilic layer. The contact angle values were in good agreement with the wetting behaviors of the respective surfactants. Since the membrane surface became the most hydrophilic after the adsorption of Tween® 20, more of the feed solution was able to flow through the wetted pores and this resulted in the highest permeate conductivity at the end of the operation. The results suggest that surfactants with higher HLB values could delay fouling and wetting of MD membranes.

In the industry, it is more common to use a fixed mass ratio of oil/surfactant in emulsions instead of a fixed molar ratio. As such, the effects of surfactant types with fixed mass concentration (50 mg L^{-1}) in the feed were also examined here, as shown in Fig. 4-5. The time for onset of wetting for the cases of 50 mg L^{-1} of Span® 20, Tween® 20, and SDS were ~100 min, ~130 min, and ~140 min, respectively (as listed in Table 4-2). By changing the experiment condition from fixed molar concentration to fixed mass concentration of surfactants, the amount of surfactant unimers changed. At a concentration of 50 mg L^{-1}, the molar concentration of Span® 20 remained similar (0.144 mM), while molar concentrations of Tween® 20 and SDS decreased (to 0.041 mM) and increased (to 0.173 mM), respectively, as compared with the case of 0.15 mM. Therefore, the amount of unimers also affected the wetting and fouling behaviors in addition to the HLB and CMC effects as discussed above. In both 50 mg L^{-1} and 0.15 mM cases, the concentrations of Span® 20 were similar. Hence, the fouling and wetting behaviors were similar. In the case of 50 mg L^{-1} Tween® 20, relatively fewer unimers in the feed solution resulted in less fouling and delayed onset of wetting in comparison to the 0.15 mM case. Since there was less fouling, the diffusion of NaCl was not as restricted as in the case of 0.15 mM Tween® 20. This resulted in a higher final conductivity in the permeate. In the case of 50 mg L^{-1} SDS, more SDS unimers were available to be adsorbed onto the membrane surface, making the membrane surface more hydrophilic. The contact angle values (as listed in Table 4-2) provided confirmation on this. Their hydrophilic heads were able to draw more water from the feed into the permeate. Therefore, the onset of wetting was brought forward and the final conductivity in the permeate was higher than that of the 0.15 mM SDS case.

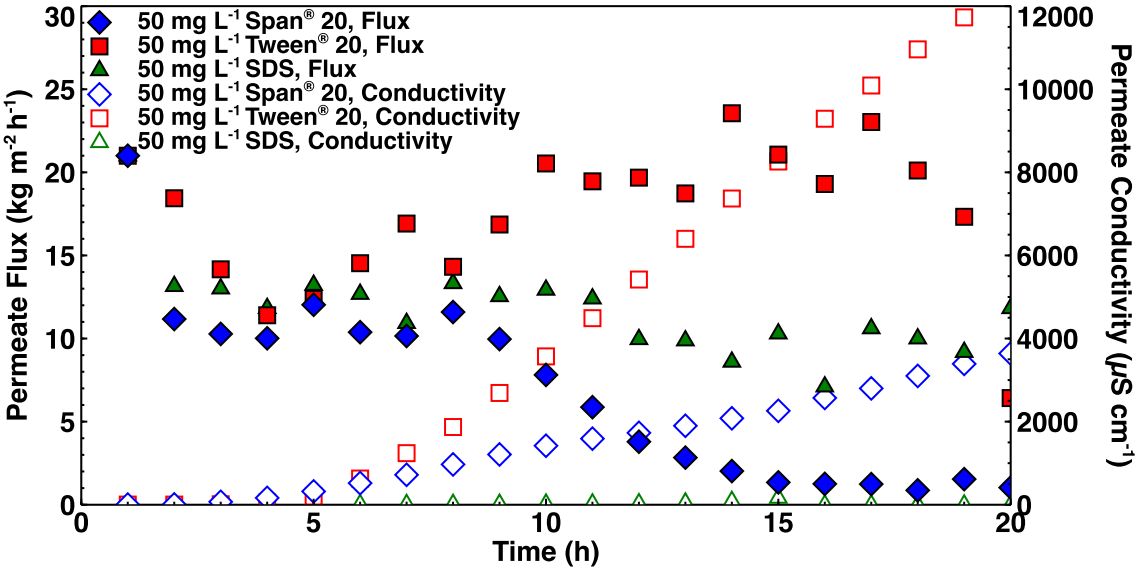


Fig. 4-5. Effects of surfactant types (same mass concentration) on permeate flux (filled symbols) and conductivity (hollow symbols). Q_f = 0.7 L min^{-1}; Q_p = 0.25 L min^{-1}; T_f = 333 K; T_p = 293 K.

4.2.3. Effects of the presence of oil

The effects of the presence of oil droplets on the permeate flux and conductivity are shown in Fig. 4-6. It was observed that the extents of membrane fouling and wetting were different when using Tween® 20 and Tween® 20-stabilized petroleum emulsion as feed. When only 50 mg L^{-1} Tween® 20 was present, wetting started to occur at ~130 min while the onset of wetting was delayed by 30 min in the case of the 1000 mg L^{-1} Tween® 20-stabilized petroleum emulsion. As proposed above, in the case of Tween® 20, the hydrophobic tails might be attached onto the PVDF membrane surface due to hydrophobic interaction while the hydrophilic ethylene oxide heads might be arranged towards the aqueous solution. These hydrophilic heads had good affinity to water, resulting in faster wetting of the membrane.

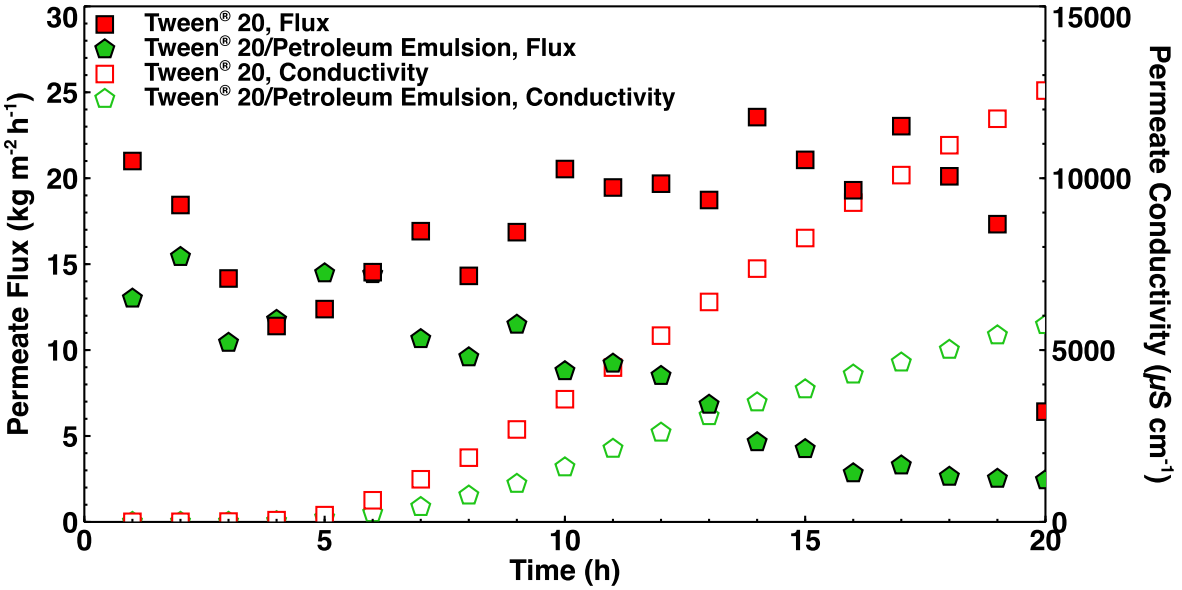


Fig. 4-6. Effects of the presence of oils on permeate flux (filled symbols) and conductivity (hollow symbols). Tween® 20 concentration was 50 mg L^{-1}. Tween® 20-stabilized petroleum emulsion was prepared using 50 mg L^{-1} of Tween® 20 and 950 mg L^{-1} of petroleum. Q_f = 0.7 L min^{-1}; Q_p = 0.25 L min^{-1}; T_f = 333 K; T_p = 293 K.

As for the Tween® 20-stabilized petroleum emulsion, more alkyl tails of the surfactant were bounded with the oil droplets, thus fewer free surfactant unimers were adsorbed on the membrane surface. Therefore, the onset of wetting was delayed in comparison to the Tween® 20 case. At the same time, with the prolonged operation time, more and more oil droplets were adsorbed onto the membrane surface due to its hydrophobicity. This caused some pores to be blocked and resulted in a gradual decline of the permeate flux. The accumulation of oil droplets formed a fouling layer that restrained the NaCl diffusion through the wetted pores of the membrane and a slower permeate conductivity rising rate was observed throughout the experiment. The results suggest that even though surfactants have a higher affinity for hydrophobic surfaces than hydrocarbons in general, oil does contribute to membrane fouling.

4.2.4. Effects of different surfactant-stabilized petroleum emulsions

Three 500 mg L^{-1} surfactant-stabilized petroleum emulsions were prepared at oil/surfactant mass ratio of 9/1 using Span® 20, Tween® 20 and SDS. The effects of these surfactant-stabilized petroleum emulsions on membrane fouling and wetting were investigated and the results are presented in Fig. 4-7. It can be observed that the extent of permeate flux decline was in the sequence of Tween® 20 < Span® 20 < SDS, suggesting that the SDS-stabilized petroleum emulsion caused the most severe membrane fouling followed by Span® 20 and Tween® 20. The membrane fouling in these cases might be ascribed to the adsorption of surfactants and oil droplets on the membrane surface and/or pores as well as pore blockage by the foulants. A hypothesis on the interactions between the surfactant-stabilized petroleum emulsions and the hydrophobic PVDF membrane surface is proposed and illustrated in Fig. 4-8.

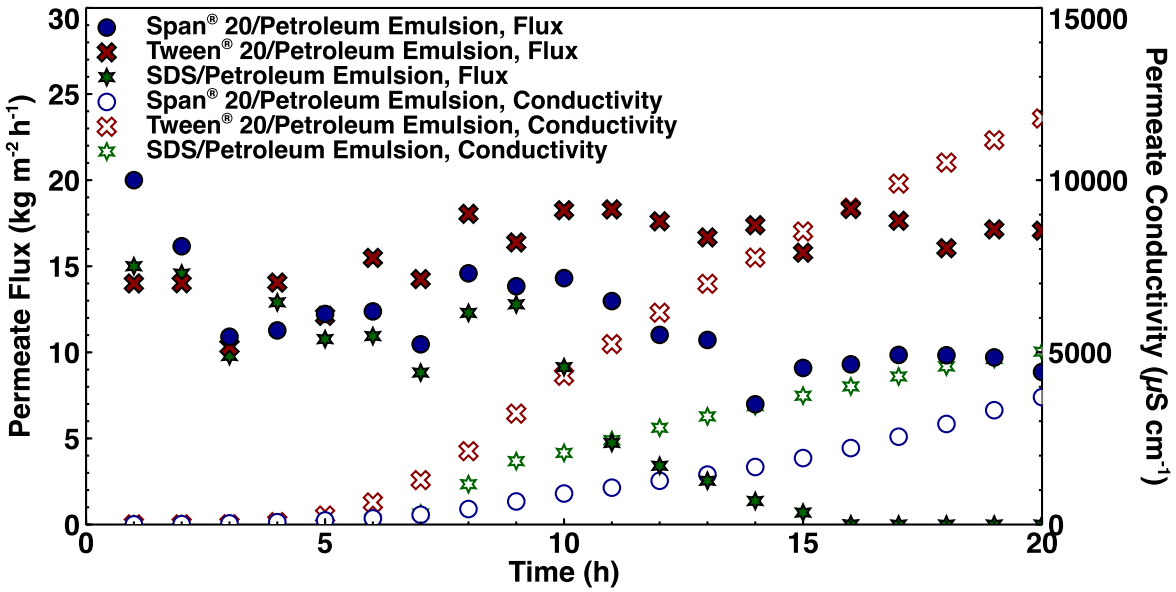


Fig. 4-7. Effects of different surfactant-stabilized petroleum emulsions on permeate flux (filled symbols) and conductivity (hollow symbols). Q_f = 0.7 L min^{-1}; Q_p = 0.25 L min^{-1}; T_f = 333 K; T_p = 293 K.

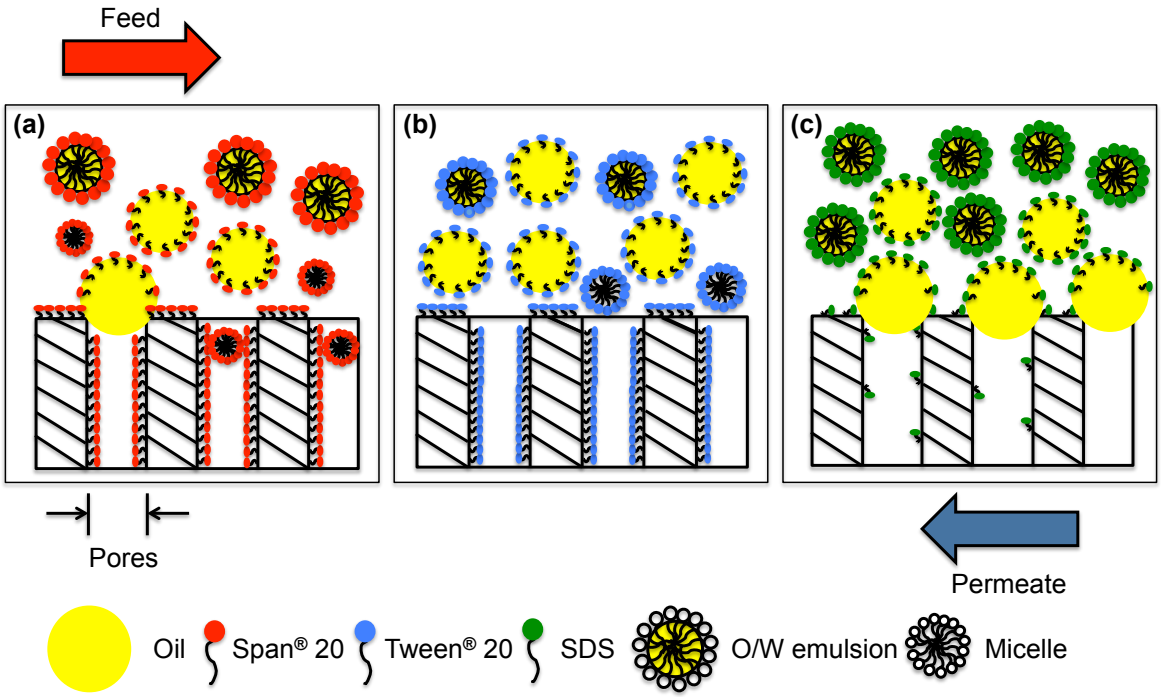


Fig. 4-8. Proposed interactions of (a) Span® 20-stabilized, (b) Tween® 20-stabilized, and (c) SDS-stabilized emulsions with the PVDF membrane surface.

The added concentration of Tween® 20, 50 mg L^{-1}, was above its CMC at 333 K (3.5 mg L^{-1}) and thus, micelles were formed in the feed solution. The Tween® 20 unimers would have stood erected on the PVDF membrane surface to form a monolayer due to hydrophobic interactions. After the adsorption of Tween® 20 unimers on the membrane surface, the hydrophilic heads orientated towards the feed solution. Hence, the PVDF membrane surface became more hydrophilic, which in turn promoted more severe pore wetting but restrained the adsorption of oil droplets on the membrane surface [152].

Similar to the Tween® 20 case, the Span® 20 unimers also formed a monolayer on the PVDF membrane surface due to hydrophobic interactions. As evidenced by the contact angles of the surfactant-fouled membranes presented in Table 4-2, the Span® 20-adsorbed surface is less hydrophilic than that of the Tween® 20, and thus relatively more oil droplets might be adsorbed on the membrane surface, aggravating the membrane fouling. In addition, micelles existed in the feed solution and resulted in partial pore

blockage since the Span® 20 concentration (50 mg L^{-1}) was higher than its CMC (1.6 mg L^{-1}). It was hypothesized that both the oil droplet adsorption and membrane pore blockage by Span® 20 micelles led to the more significant flux decline compared with the case of Tween® 20-stabilized emulsion. On the other hand, the membrane fouling restrained the diffusion of NaCl to the permeate side.

Due to the hydrophilic nature of SDS, relatively less SDS unimers were adsorbed onto the PVDF membrane as discussed previously in section 4.2.2. Therefore, the membrane surface was the least hydrophilic as evidenced by the contact angle of the SDS-fouled membrane shown in Table 4-2. Hence, the oil droplets had a higher tendency to be attached onto membrane surface, resulting in a more severe fouling. Due to the adsorption of more surfactant-stabilized oil droplets on membrane, the hydrophilic head of SDS might attract more feed to pass through the membrane, which resulted in a relatively more severe increase of the permeate conductivity. Despite the more severe fouling caused by the SDS-stabilized emulsion, the NaCl diffusion was surprisingly faster than the case of the Span® 20-stabilized emulsion. The reason for this phenomenon is unclear and further investigation is needed in the future study.

4.2.5. Effects of oil concentration

500, 600 and 1000 mg L^{-1} Tween® 20-stabilized petroleum emulsions were prepared to study the effects of oil concentration on the permeate flux and conductivity. The mass concentration of Tween® 20 was fixed at 50 mg L^{-1} and the mean oil droplet sizes of the different emulsions were kept similar as listed in Table 4-1. The results are shown in Fig. 4-9. It is evident that the increase in oil concentration led to more serious fouling, as represented by the more severe decline in permeate flux. With the increase of oil concentration, more oil droplets were adsorbed onto the membrane surface and caused

membrane pore blockage. Thus, a more significant decrease of the permeate flux was observed. Similarly, the trend observed in the permeate conductivity was as expected. Wetting became slower when more oil droplets blocked the membrane pores. The results suggest that MD could be an effective option for recovering water from produced water at low oil concentration.

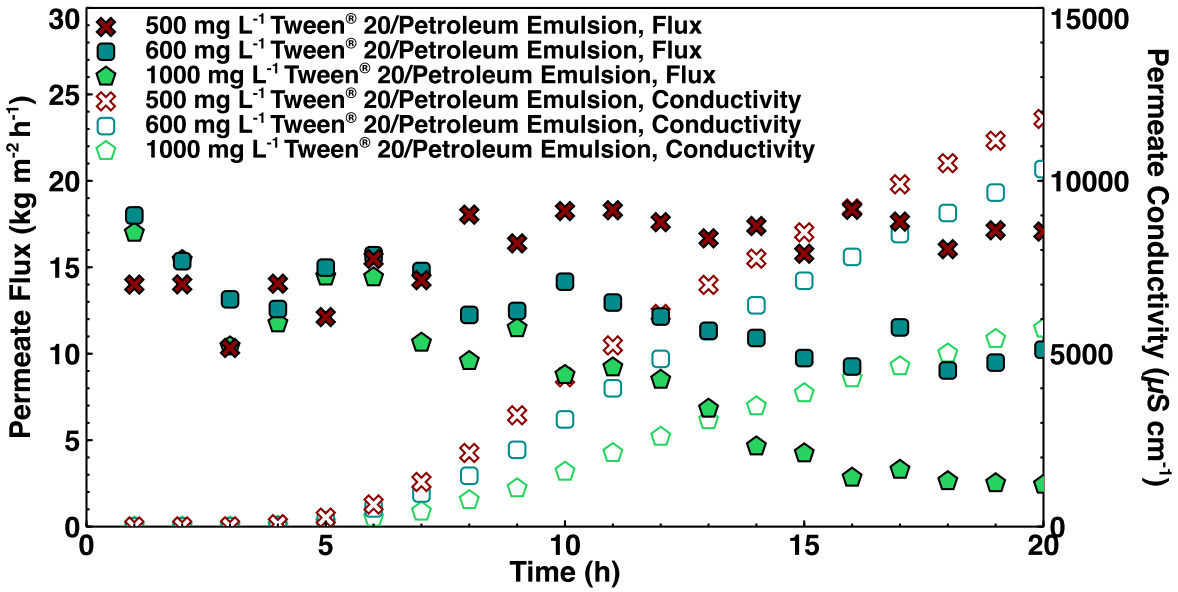


Fig. 4-9. Effects of oil concentration on permeate flux (filled symbols) and conductivity (hollow symbols). Q_f = 0.7 L min^{-1}; Q_p = 0.25 L min^{-1}; T_f = 333 K; T_p = 293 K.

4.2.6. Effects of oil types

The effects of Tween® 20-stabilized VPO emulsion on the permeate flux and conductivity are shown in Fig. 4-10. Generally, petroleum oil includes paraffins (15-60%), napthenes (30-60%), aromatics (3-30%), and asphaltics while VPO contains heavy distillates that are longer-chained hydrocarbon compounds with relatively higher boiling points and are hardly volatile. In comparison with the Tween® 20-stabilized petroleum emulsion, more severe fouling was observed for the VPO emulsion. This is believed to be ascribed to the higher proportions of heavy hydrocarbons present in VPO [152]. This

suggests that MD could be considered for water recovery from produced water containing higher proportions of lighter hydrocarbons.

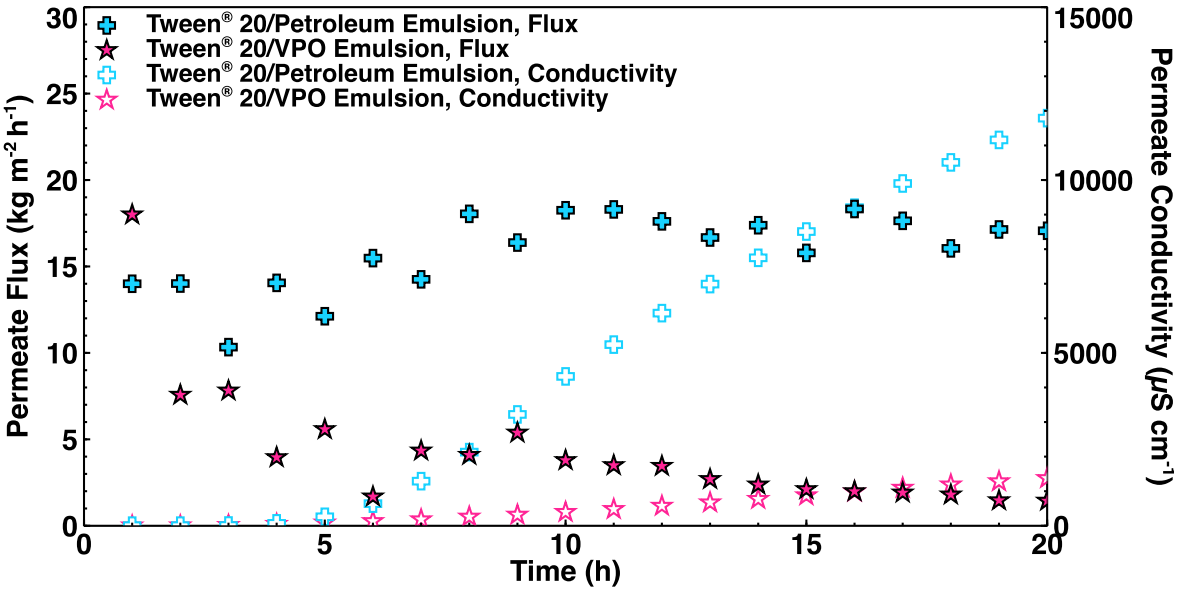


Fig. 4-10. Effects of oil types on permeate flux (filled symbols) and conductivity (hollow symbols). Q_f = 0.7 L min^{-1}; Q_p = 0.25 L min^{-1}; T_f = 333 K; T_p = 293 K.

4.2.7. Confirmation of surfactant penetration into membrane pores and membrane fouling

It was hypothesized that pore wetting leads to an increase in permeate conductivity as presented in Table 4-2. In order to validate this, penetration of surfactants into the membrane pores were verified using the ATR-FTIR characterization test on the inner surfaces of the wetted PVDF membranes. The FTIR spectra of the pristine and wetted PVDF membranes were plotted against that of pure Span® 20, Tween® 20, and SDS, as presented in Fig. 4-11.

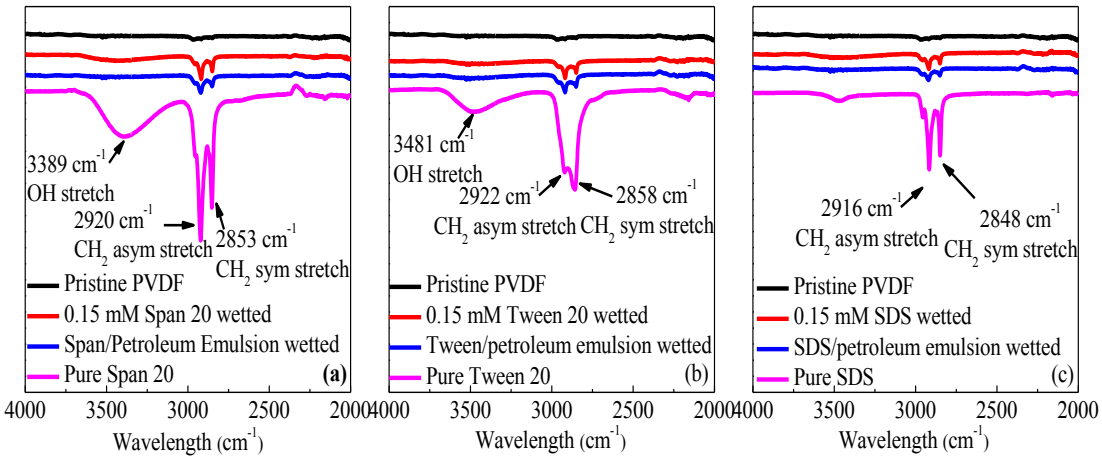


Fig. 4-11. FTIR spectra of the pristine and wetted PVDF membranes. Transmittance normalized against CF peak. (a) Span® 20 experiments, (b) Tween® 20 experiments, (c) SDS experiments.

As shown in Fig. 4-11(a), Span® 20 has three characteristic peaks: the 2853 cm^{-1} and 2920 cm^{-1} peaks were attributed to CH_2 symmetric and asymmetric stretching respectively, while the broad peak around 3389 cm^{-1} was assigned to O-H stretching. These peaks were only observable on the wetted PVDF membranes but were undetected on the pristine PVDF membrane, demonstrating the presence of Span® 20 on the inner surfaces of the wetted PVDF membranes. Similar results were also observed for membranes wetted in the case of both Tween® 20 and SDS. The FTIR spectra coupled with the rise in permeate conductivity in all experiments were indicative of the occurrence of membrane wetting.

The outer surface morphologies of the pristine and fouled PVDF membranes were characterized using FESEM and the images are shown in Fig. 4-12. Abundant pores could be clearly observed on the pristine PVDF membrane. However, the membrane surfaces were covered by foulants after the MD experiments no matter which type of feed solution was used. As shown in Fig. 4-12(e and h), the oil foulant layer formed by the Tween® 20-stabilized VPO emulsion seemed denser than the layer formed by the Tween® 20-

stabilized petroleum emulsion, demonstrating the more severe membrane fouling caused by VPO emulsion as discussed in section 4.2.6.

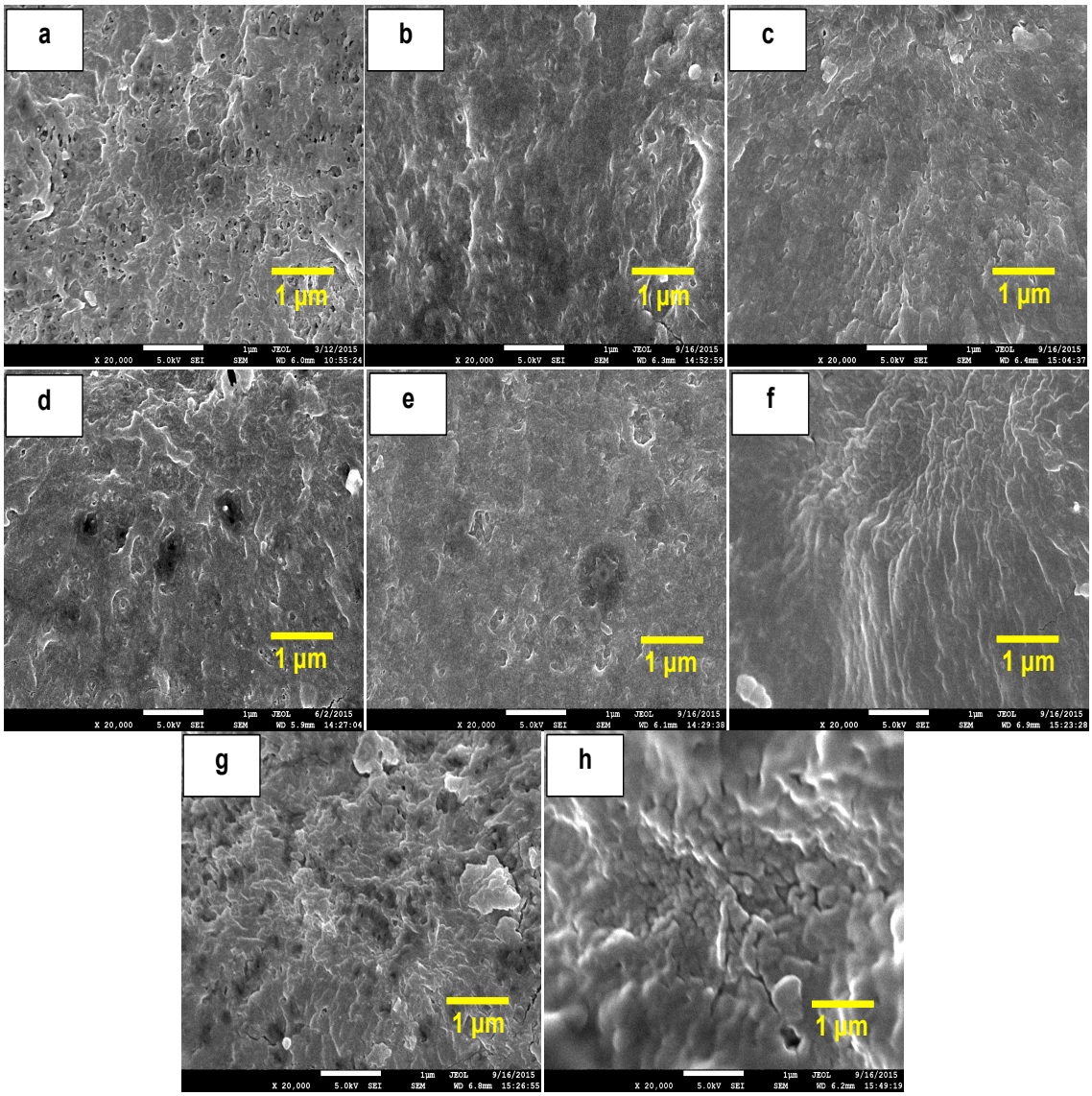


Fig. 4-12. FESEM images of (a) pristine PVDF membrane and membranes fouled by (b) 50 mg L^{-1} Span® 20, (c) 50 mg L^{-1} Tween® 20, (d) 50 mg L^{-1} SDS, (e) 500 mg L^{-1} Tween® 20/Petroleum Emulsion, (f) 500 mg L^{-1} Span® 20/Petroleum Emulsion, (g) 500 mg L^{-1} SDS/Petroleum Emulsion, and (h) 500 mg L^{-1} Tween® 20/VPO Emulsion.

4.3. Conclusions

This study attempts to provide an in-depth understanding of the relationship between different surfactant-stabilized O/W emulsions and the hydrophobic PVDF membrane surface in DCMD. The results reveal that the time for onset of wetting for

different surfactants was dependent on their HLB values. A surfactant with lower HLB value tended to be adsorbed more on the membrane surface and caused an earlier onset of wetting.

The presence of oils in the emulsion delayed the onset of wetting of the membrane. Fouling was observed to be less severe for emulsions stabilized by surfactants with a lower HLB value. The severity of membrane fouling increased with increasing oil concentration. Moreover, membrane fouling caused by the VPO emulsion was also more severe due to the higher proportions of heavy hydrocarbons in VPO. These results suggest that MD should be considered as an option for recovering water from produced water with lower oil concentration and higher proportions of lighter hydrocarbons.

This study revealed that robust membranes with better anti-fouling and anti-wetting properties are required to eliminate or minimize the issues of fouling and wetting. These findings suggest that novel membrane surface modification, which will be discussed in Chapters 5 and 6, is required to achieve anti-fouling and anti-wetting properties. This, coupled with process optimization, is expected to advance DCMD as an economically viable technology for treating produced water.

Chapter 5 Superoleophobic Surface Modification for Robust Membrane Distillation Performance[2]

5.1. Introduction

In Chapter 4, we developed a fundamental understanding of the relationship between surfactant-containing feed water and a commercial hydrophobic PVDF hollow fiber membrane. While conventional MD membranes fabricated from hydrophobic polymeric materials, such as PVDF, have shown stable performances in relatively clean wastewaters, they are vulnerable to membrane fouling and pore wetting when used to treat challenging feeds that contain hydrophobic and amphiphilic pollutants such as oils and surfactants. This compromises on the recovery rate and distillate quality. Based on the foundation built in Chapter 4, we will apply targeted surface modification techniques in Chapters 5 and 6 to engineer robust membrane surfaces with fouling- and wetting-resistant properties for surfactant-containing feed water. As discussed in Chapter 2, a superoleophobic layer can be deposited onto hydrophobic polymeric substrates to fabricate composite membranes with fouling- and wetting-resistant properties. Yet, existing surface modification techniques are often too complex for real applications. Therefore, it is paramount to develop facile surface modification techniques to engineer robust MD membranes.

Over the last decade, the mussel-inspired chemistry of dopamine has been widely used for a variety of surface modifications due to its unique advantages of material-independent attachment and surface post-functionalization [160]. Compared with physical

[2] *This chapter is reproduced with permission from Chew, N.G.P., S. Zhao, C. Malde, R. Wang, Superoleophobic surface modification for robust membrane distillation performance, J. Membr. Sci. 541 (2017) 162–173. Copyright © 2017 Elsevier.*

coating, the resulting polydopamine (PDA) coating has stronger binding affinity to the membrane surface [161]. Moreover, co-deposition of dopamine with other molecules such as polyethylenimine (PEI) can greatly increase the stability of the grafted layer under harsh conditions [162]. As a result, this versatile and robust technique has been adopted in a broad range of membrane processes such as MF [163-166], UF [167, 168], NF [169], and FO [170, 171] for various purposes such as improving anti-fouling performance and enhancing structural stability.

This study aims at developing robust membrane surfaces with anti-fouling and anti-wetting properties to be used in DCMD operations for water recovery from produced water. Specifically, a composite membrane with Janus wetting properties was fabricated by single-step co-deposition of the hydrophilic PDA/PEI layer on the outer surface of a hydrophobic PVDF hollow fiber substrate. Janus membranes have asymmetric properties on either side of the membrane [172]. The surface chemistry, wetting properties, and structure of the modified PVDF membrane were studied comprehensively. Subsequently, bench-scale DCMD experiments were carried out using a series of low surface tension feeds including various types of surfactant solutions and surfactant-stabilized (O/W) emulsions. The performances of the modified PVDF membrane were analyzed and compared against those of the pristine PVDF membrane to ascertain its suitability and robustness for long-term produced water treatment. To the best of our knowledge, this is the first report about the co-deposition of PDA/PEI on a hydrophobic PVDF hollow fiber substrate that can be used for DCMD applications against low surface tension feeds.

5.2. Experimental

5.2.1. Fabrication of composite PVDF hollow fiber membrane

The in-air hydrophilic/underwater superoleophobic composite membrane was fabricated by co-deposition of PDA/PEI on a hydrophobic PVDF substrate, which is illustrated in Fig. 5-1. Firstly, 2 g L^{-1} of DA and 50 mM of Tris were weighed and dissolved into 2 g L^{-1} of PEI solution. Similar procedures have been reported elsewhere [163, 173, 174]. After that, the pristine PVDF membranes were immersed in the PDA/PEI solution with shaking at 40 rpm for a certain time (Orbital Maxi MD Humidity, OVAN, Spain). Precautions were taken to ensure that only the outer surfaces of the hydrophobic PVDF hollow fibers were modified, so that the membrane pores beneath the surface remained hydrophobic for vapor transport. Finally, the composite membranes were rinsed thoroughly with Milli-Q® water and freeze-dried overnight (Alpha 2-4, Martin Christ, Germany). Hereon, the PDA/PEI coated PVDF membrane will be referred to as PVDF-P membrane.

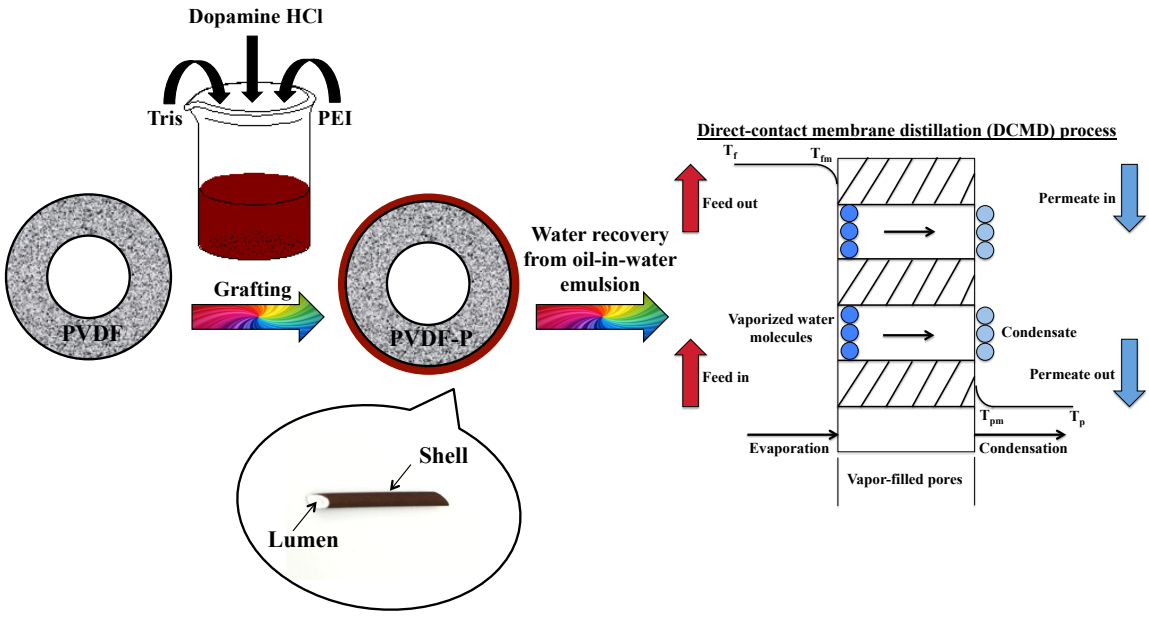


Fig. 5-1. Schematic of co-deposition of PDA/PEI on the outer surface of a PVDF membrane and its application in water recovery from oil-in-water emulsions via DCMD.

5.3. Results and discussion

5.3.1. Membrane surface characterizations

Fig. 5-2 shows the outer surface and cross-section morphologies of the pristine PVDF and PVDF-P membranes. It was evident from these images that the changes in surface morphology of the pristine PVDF membrane after modification were rather radical. As shown in Fig. 5-2(a1) and (a2), the pristine PVDF membrane surface had abundant pores. The co-deposition of PDA/PEI formed agglomerates on the membrane surface that thoroughly covered the surface and blocked membrane pores (shown in Fig. 5-2(b1) and (b2)). These deposited agglomerates created a hierarchical structure with a higher roughness, which was attested by the surface roughness parameters presented in Table 5-1. According to the Wenzel model, roughness plays a critical role in enhancing surface intrinsic wetting ability [175], which will be further discussed in section 5.3.3. Fig. 5-2(b3) suggests that the thickness of the grafted layer was around 1 μm and did not penetrate into the bulk of the pristine PVDF substrate. The stability of the grafted layer on the membrane surface was assessed by subjecting the PVDF-P membrane to bath sonication. The FESEM images of the outer surface and cross-section morphologies of the PVDF-P membrane after ultrasonication are shown in Fig. 5-2(c1) to (c3). The result shows that the grafted layer remained intact and minimal changes to the surface morphology were observed. The FESEM images were indicative of the robust structural stability of the PVDF-P membrane under harsh conditions.

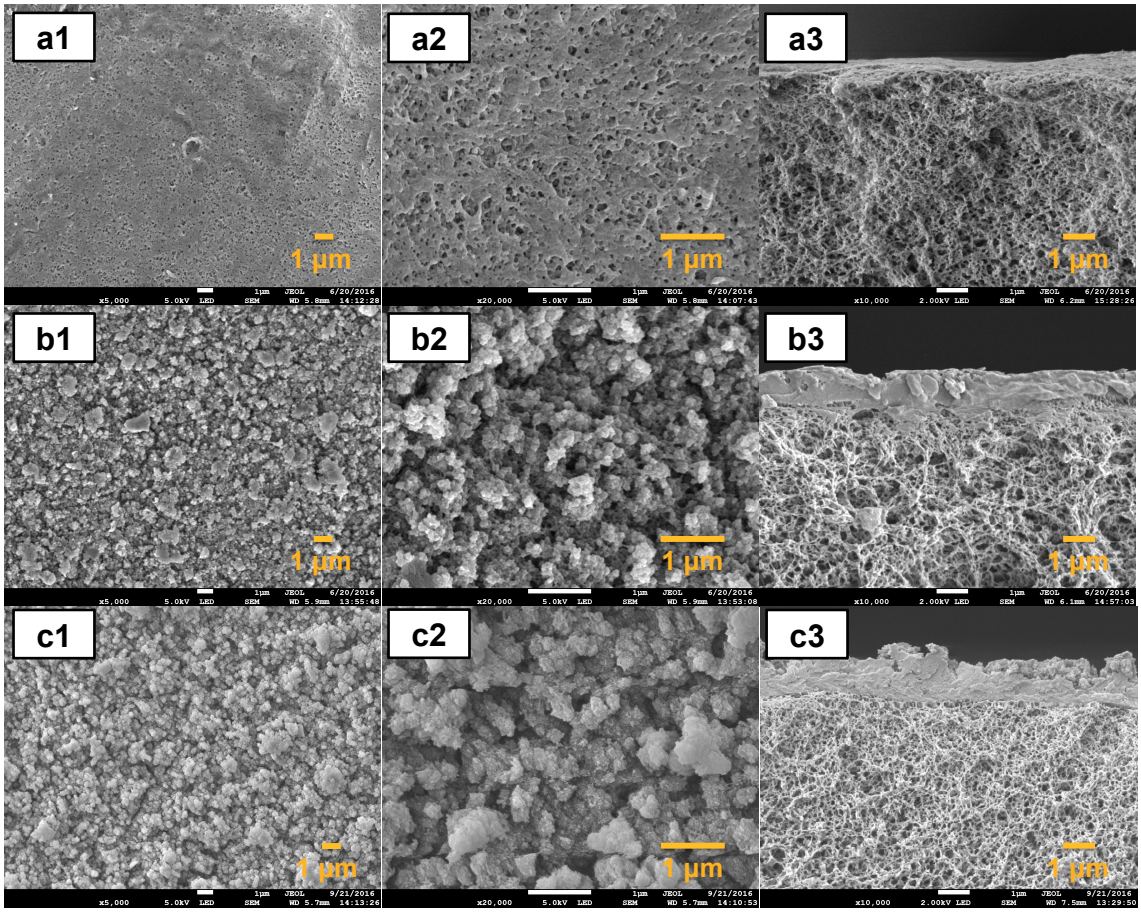


Fig. 5-2. FESEM images of the outer surface morphologies of the pristine PVDF (a1 and a2), PVDF-P (b1 and b2), and ultrasonicated PVDF-P (c1 and c2) membranes; FESEM images of the cross-section morphologies of the pristine PVDF (a3), PVDF-P (b3), and ultrasonicated PVDF-P (c3) membranes.

Table 5-1. Surface roughness parameters and water contact angles of the pristine PVDF and PVDF-P membranes.

Membranes	Roughness			Water contact angle (°)
	R_a[a] (nm)	R_q[b] (nm)	R_z[c] (nm)	
PVDF	25.6 ± 1.2	31.9 ± 0.8	258.3 ± 2.2	109.5 ± 1.2
PVDF-P	197.0 ± 1.8	243.1 ± 3.1	1689.2 ± 1.4	25.7 ± 4.0

[a] Average roughness.
[b] Root-mean-squared roughness.
[c] Ten point average roughness.

The distinct difference in pore size distribution between the pristine PVDF and PVDF-P membranes suggests that the co-deposition of PDA/PEI altered the structural property of the pristine PVDF membrane. As shown in Fig. 5-3, it can be observed that the pristine PVDF membrane had a well-defined bimodal distribution with a mean pore

size of 0.027 μm. On the other hand, the PVDF-P membrane had a much narrower pore size distribution with a smaller mean pore size of 0.017 μm, which is in agreement with the FESEM images. The co-deposition of PDA/PEI would have effectively covered most of the pores on the outer surface of the PVDF-P membrane and caused a reduction in its pore size. As such, it is expected that the PVDF-P membrane would be less vulnerable to pore wetting due to the additional protection provided by the grafted layer [20].

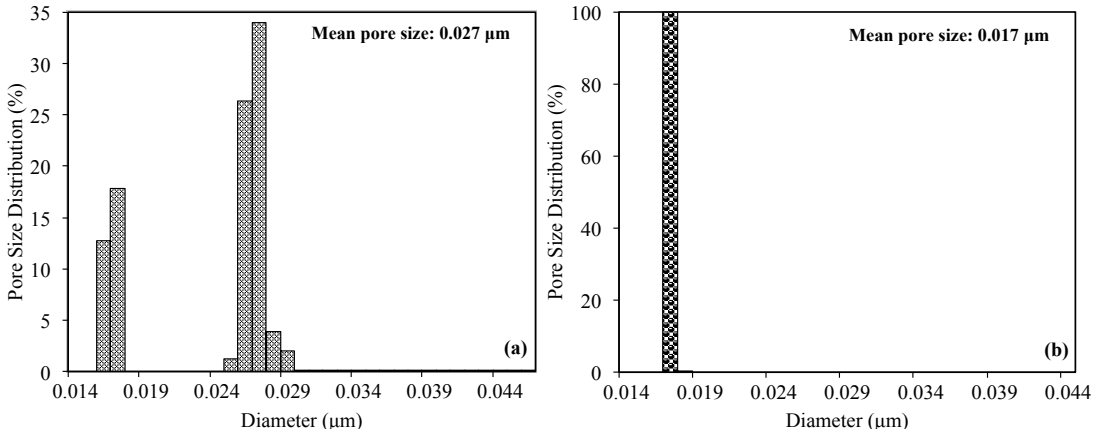


Fig. 5-3. Pore size distributions of the (a) pristine PVDF and (b) PVDF-P membranes.

5.3.2. Deposition of PDA/PEI on the PVDF-P membrane surface

In Fig. 5-4, the ATR-FTIR spectra provided an evidence on the co-deposition of PDA/PEI on the PVDF-P membrane surface as shown by the presence of two noticeable absorption peaks at 1541 cm^{-1} and 1660 cm^{-1}, which were attributed to the N-H bending in PDA and C = N stretching within the PDA/PEI cross-links, respectively [162]. Besides that, the broad peak observed between 3000 and 3600 cm^{-1} on the PVDF-P membrane surface could be attributed to the N-H stretching and O-H stretching in the amine- and hydroxyl-functional groups found on its surface [174, 176].

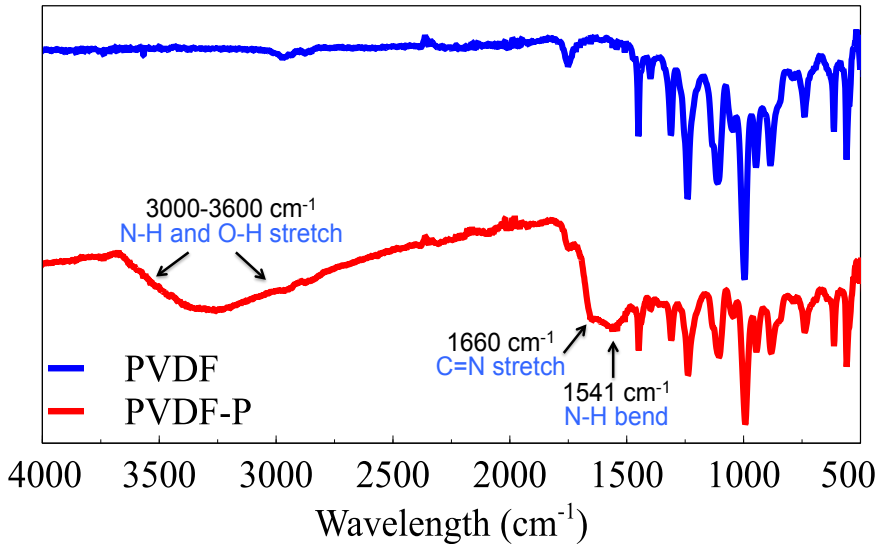


Fig. 5-4. ATR-FTIR spectra of the outer surfaces of the pristine PVDF and PVDF-P membranes. Transmittance was normalized against the CF peak.

In order to further understand the elemental composition and chemical state of the PDA/PEI grafting layer, XPS analyses were carried out. The survey scan spectra of the pristine PVDF and PVDF-P membranes along with the deconvolution spectra of the PVDF-P membrane outer surface are presented in Fig. 5-5 while the surface elemental compositions of both the pristine PVDF and PVDF-P membranes are summarized in Table 5-2. The inner surface elemental compositions of both the pristine PVDF and PVDF-P membranes were similar, which proves that there was no penetration of the hydrophilic grafting solution through the hydrophobic pores of the PVDF substrate. As shown in Fig. 5-5(a), the disappearance of the F 1s and Cl 2p peaks along with the appearance of N 1s peak on the outer surface of the PVDF-P membrane suggested the successful co-deposition of PDA/PEI and its complete coverage on the membrane surface. As listed in Table 5-2, the C 1s and O 1s concentrations of the PVDF-P membrane outer surface were increased after modification and the N/O ratio reached 0.9, which was close to the value reported by Yang et al. [162]. As shown in the deconvoluted spectra of the PVDF-P membrane in Fig. 5-5(b)–(d), the C 1s core-level spectrum could be curve-fitted with three peak components at binding energies (BE) of 284.8 eV, 285.9

eV, and 287.5 eV, which corresponded to the C-C/C-H, C-O/C-N, and C = O bonds, respectively. The N 1s core-level spectrum was curve-fitted with two peak components, one at a BE of 399.8 eV for the C-N bond and the other at a BE of 402.0 eV for the protonated amine-functional group. The O 1s core-level spectrum was also curve-fitted with two peak components at BE of 531.2 eV and 532.6 eV, which were assigned to the C = O and C-O bonds groups, respectively. The XPS analysis results were supportive of the following proposed PDA reaction mechanisms with PEI.

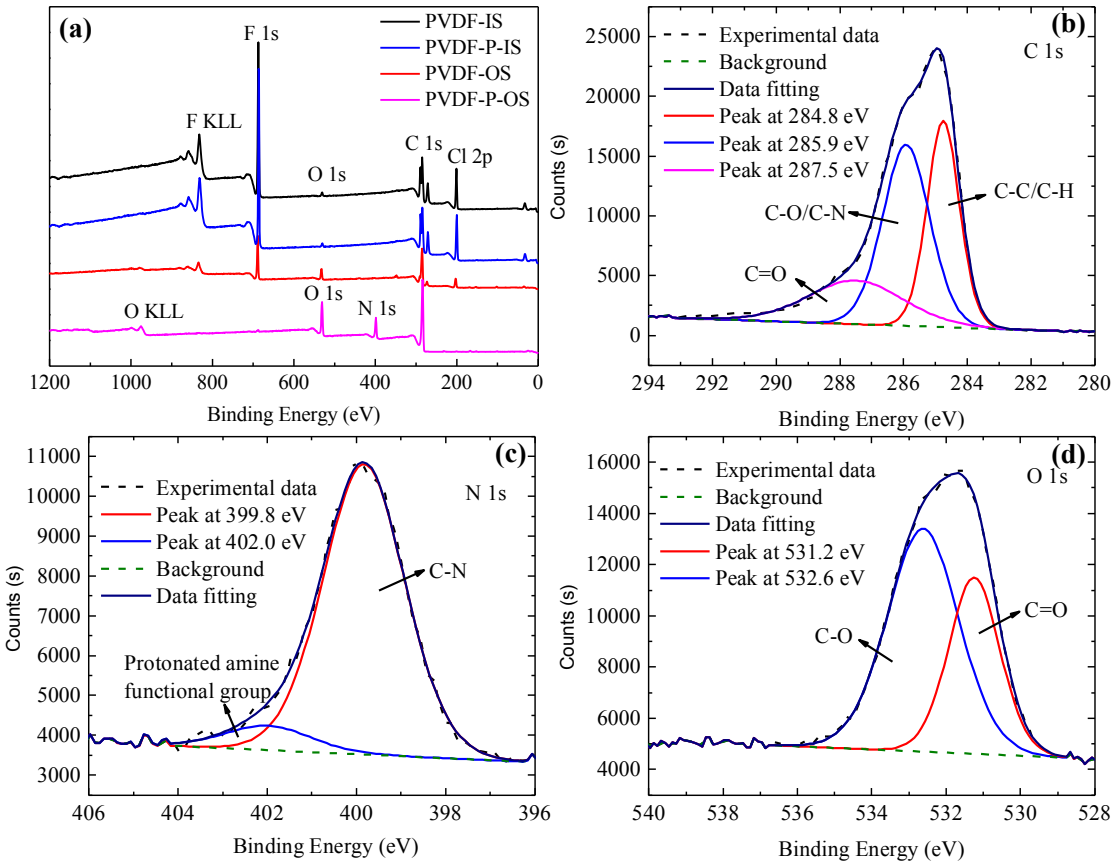


Fig. 5-5. (a) XPS survey scan spectra of the inner (IS) and outer (OS) surfaces of the pristine PVDF and PVDF-P membranes. Deconvolution of (b) C 1s, (c) N 1s, and (d) O 1s spectra of the outer surface of the PVDF-P membrane.

Table 5-2. The elemental compositions (in atomic percentage) of the inner (IS) and outer (OS) surfaces of the pristine PVDF and PVDF-P membranes.

Membrane	O 1s (At%)	C 1s (At%)	F 1s (At%)	Cl 2p (At%)	N 1s (At%)
PVDF-IS	1.21	56.85	28.81	13.31	-
PVDF-P-IS	0.96	54.43	31.23	13.37	-
PVDF-OS	6.55	71.63	15.60	6.22	-
PVDF-P-OS	12.63	75.80	0.35	0.20	11.02

The oxidative self-polymerization of dopamine involves its catechol group autooxidizing to form dopamine quinone [177], which in turn follows several reaction pathways to form PDA [178-183]. The primary amine-functional groups on PEI may react with dopamine quinones to form Michael-type adducts or Schiff bases through Michael addition or Schiff base reaction, respectively, as illustrated in Fig. 5-6. Thus, the incorporation of PEI can form covalent cross-linking with PDA due to the reaction among catechol and amino groups [162].

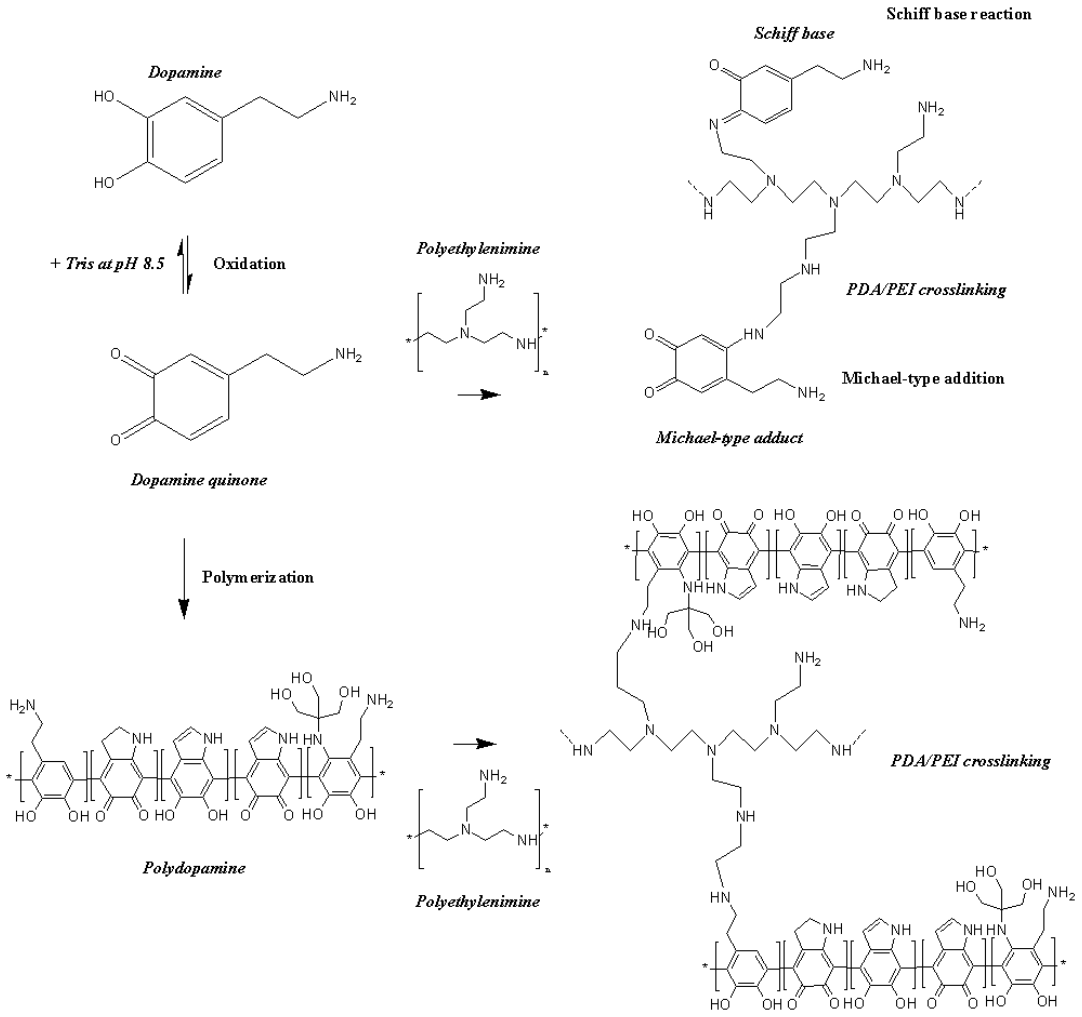


Fig. 5-6. Proposed polydopamine reaction mechanisms with polyethylenimine.

The surface charge properties of the pristine PVDF and PVDF-P membranes were studied using the streaming potential measurement at a pH range of 3–10 and the results are shown in Fig. 5-7. Throughout the entire tested pH range, the pristine PVDF membrane was mostly negatively charged. The co-deposition of PDA/PEI slightly neutralized the negative charge on the PVDF membrane surface, resulting in a right shift of the zeta potential curve. The isoelectric point of the PVDF-P membrane was 3.8.

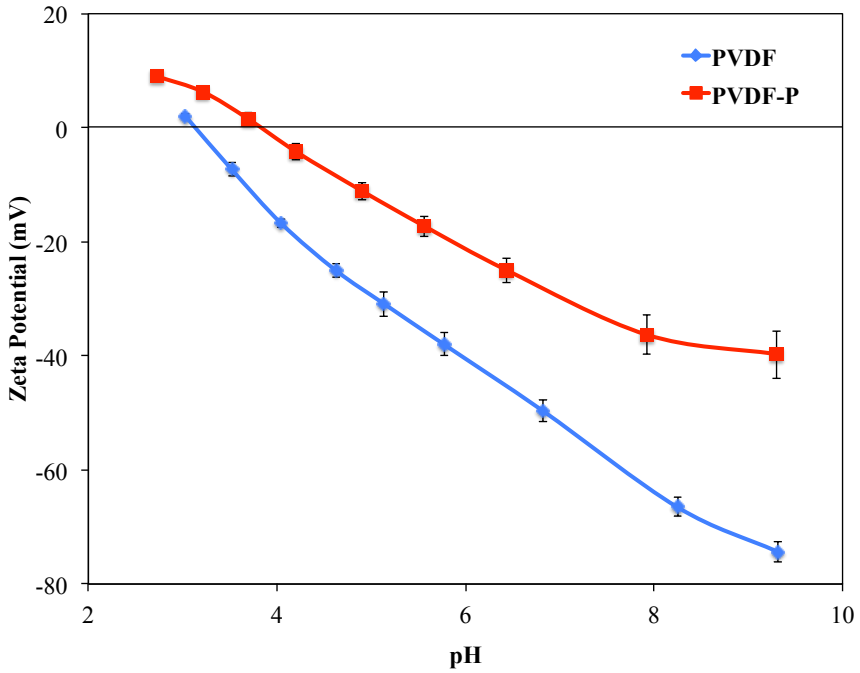


Fig. 5-7. Surface zeta potentials of the pristine PVDF and PVDF-P membranes as a function of pH. 1 mM NaCl was used as the electrolyte solution.

5.3.3. Wetting properties of the pristine and modified membranes

As listed in Table 5-1, the pristine PVDF and PVDF-P membranes had water contact angles of 109.5 ± 1.2° and 25.7 ± 4.0°, respectively. This suggests that the pristine PVDF membrane underwent transition from being hydrophobic to hydrophilic after surface modification. The presence of polar amine- and hydroxyl-functional groups of PDA/PEI imparted hydrophilicity to the PVDF-P membrane surface. In addition, the hierarchical surface structure further enhanced the hydrophilic effects [175]. In order to investigate on the intrinsic wetting properties of the membranes in the presence of oil droplets, the underwater captive bubble method was employed. The relevant captured images of the interactions are depicted in Fig. 5-8. It was evident that the pristine PVDF membrane surface was underwater oleophilic, which was instantaneously wetted by the oil droplet upon contact. The oil contact angle approached 0° within 15 s. On the other hand, the PVDF-P membrane surface exhibited underwater superoleophobicity. The oil droplet would not leave the needle and stick onto the membrane surface even after several

attempts. The oil droplet remained spherical in shape and no apparent deformation was observed. The underwater superoleophobicity of the PVDF-P membrane could be explained from the thermodynamically favorable interaction between its surface hydrophilic groups and surrounding water molecules. The hydrophilic moieties on the grafted layer could interact strongly with surrounding water molecules and other polar molecules to form hydrogen bonds, which resulted in an interfacial hydration layer. This hydrogen-bonded hydration layer provided a significant energetic barrier for the oil droplets to overcome in order to be attached onto the PVDF-P membrane surface. This suggests that the PVDF-P membrane had an oil adhesion-resistant surface and could possibly be anti-fouling when used for treating O/W emulsions.

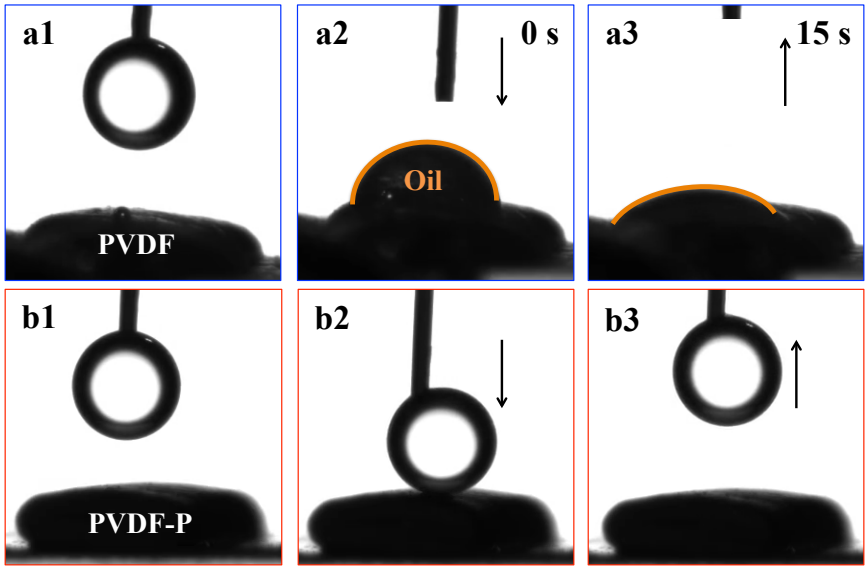


Fig. 5-8. Captured images of the underwater interactions between oil droplets tethered via a needle and the pristine PVDF (a1-a3) and PVDF-P (b1-b3) membrane surfaces.

5.3.4. Membrane performance in DCMD tests

5.3.4.1. Saline feeds with four types of surfactant

To ascertain that the PDA/PEI grafted layer did not affect the intrinsic MD performance of the PVDF-P membrane, a baseline test was first conducted by using 3.5

wt% NaCl feed solution and the results are shown in Fig. 5-9. It can be observed that the permeate flux of the PVDF-P membrane was comparable to that of the pristine PVDF membrane throughout the operation, which suggests that the grafted layer did not provide additional resistance to vapor transport through the hydrophobic pores. As observed in the outer surface morphology of the PVDF-P membrane (Fig. 5-2(b1) and (b2)), there were micro-channels within the hierarchical structure formed by the PDA/PEI asperities. These micro-channels allowed water molecules to flow through the hydrophilic grafted layer. Even though the pore size of the PVDF-P membrane outer surface became smaller after functional group modification, the compromise between smaller membrane pores and a hydrophilic surface ensured a comparable flux for the PVDF-P membrane. Similar to the pristine PDVF membrane, no wetting was observed for the PVDF-P membrane after 24 h of operation. This vindicates that only the shell side of the PVDF-P membrane was coated with a hydrophilic layer and as such, the substrate pores remained hydrophobic for the vapor transport while rejecting the non-volatile NaCl solute.

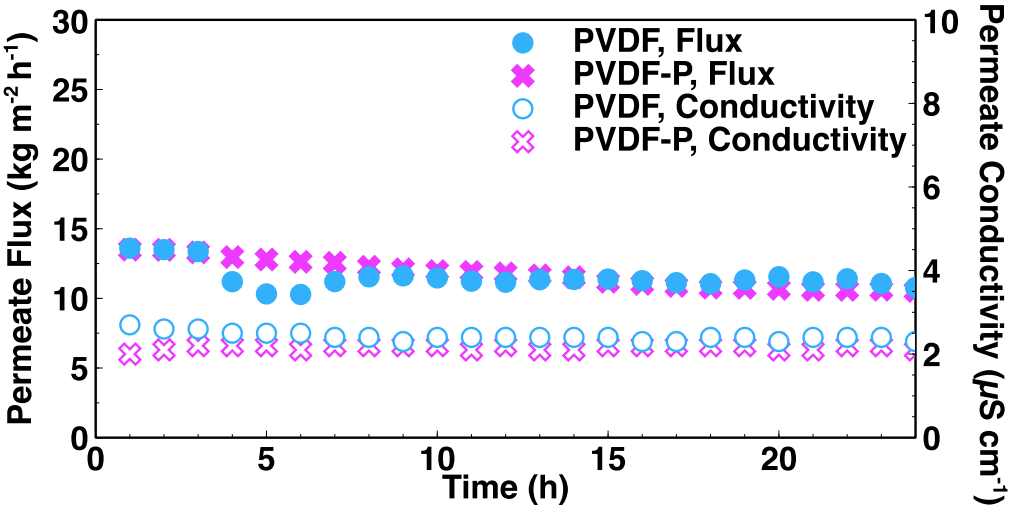


Fig. 5-9. DCMD performances of the pristine PVDF and PVDF-P membranes by feeding 3.5 wt% NaCl. Feed volumetric flow rate (Q_f) = 0.7 L min^{-1}; Permeate volumetric flow rate (Q_p) = 0.25 L min^{-1}; Feed temperature (T_f) = 333 K; Permeate temperature (T_p) = 293 K.

After the baseline test, DCMD experiments were performed on both the pristine PVDF and PVDF-P membranes by feeding 50 mg L^{-1} of non-ionic (Span® 20 and Tween® 20), anionic (SDS), and cationic (DTAB) surfactants. High salinity wastewater, such as oilfield or shale gas produced water, often contains surfactants that reduce its surface tension significantly and in turn poses a challenge to MD membranes. To ensure a fair comparison, surfactants with a 12-carbon hydrophobic tail were selected. The HLB values of these surfactants and surface tensions of the respective solutions are provided in Table 3-2. HLB is an empirical value that defines the relationship of the polar and non-polar groups of a surfactant. The lower the HLB value, the more hydrophobic (oil-soluble) the surfactant is. The significantly different wetting and fouling behaviors of these two membranes are illustrated in Fig. 5-10. In the case of Span® 20 (Fig. 5-10(a)), the pristine PVDF membrane experienced severe wetting and fouling, as indicated by the rapidly increased permeate conductivity and declined water flux. In comparison, the PVDF-P membrane showed more stable MD performance, where neither fouling nor wetting was observed after 80 h of operation. The permeate of the PVDF-P membrane was of excellent quality, with its conductivity remaining stable at 3.5 μS cm^{-1} throughout the operation. The stark contrast in the performances of the pristine PVDF and PVDF-P membranes was believed to be due to their different surface hierarchical structures and opposing wetting properties. As discussed in Chapter 4 [33], Span® 20 is a relatively hydrophobic surfactant with a low HLB value of 8.6. As such, the Span® 20 unimers have the tendency to adsorb onto hydrophobic surfaces to form a monolayer via hydrophobic interactions [151]. For the pristine PVDF membrane, the drastic water flux decline and permeate conductivity increase were due to the adsorption of Span® 20 unimers onto its hydrophobic membrane surface and pores, which resulted in complete pore blockage and severe pore wetting [33]. In comparison, the hydrophilic coating on the PVDF-P membrane surface avoided such hydrophobic interactions. The hydrophilic moieties on

the PVDF-P membrane surface strongly interacted with water to form a hydration layer on its surface, which in turn prevented the hydrophobic tails of surfactants from attaching. Such an anti-fouling mechanism is supported by its underwater superoleophobicity as suggested by the captive bubble measurement. Similar phenomenon was also observed in the case of Tween® 20 as feed, in which a very stable permeate flux was achieved for the PVDF-P membrane after 115 h of operation while the permeate conductivity remained relatively low at 20 μS cm^{-1} (Fig. 5-10(b)). The greatly improved anti-fouling and anti-wetting properties of the PVDF-P membrane make it robust for water recovery from low surface tension feeds containing non-ionic surfactant unimers such as Span® 20 and Tween® 20 by MD.

As shown in Fig. 5-10(c), the PVDF-P membrane experienced no wetting after 90 h of operation when 50 mg L^{-1} of SDS was used as feed. Its final permeate conductivity was only 3.5 μS cm^{-1} as compared to 5,660 μS cm^{-1} in the case of the pristine PVDF membrane. However, membrane fouling was observed on both the pristine PVDF and PVDF-P membranes as indicated by the flux decline. The fouling mechanisms for these two membranes were different, which will be discussed below. Different from non-ionic surfactants, both the hydrophobic and electrostatic interactions play crucial roles in the adsorption of ionic surfactants. In the case of the pristine PVDF membrane, its negatively charged surface could repel the similarly charged SDS unimers. However, this was offset by the dominant hydrophobic interactions between the hydrophobic tails of the SDS unimers and the hydrophobic PVDF membrane surface. Such hydrophobic interactions resulted in the adsorption of some SDS unimers, as represented by the flux decline after approximately 12 h of operation. The fouling extent caused by SDS was not as severe as that from Span® 20 and this was due to its relatively hydrophilic nature, which commensurate with its higher HLB value [48]. Like the other surfactants, the adsorption

of surface active agent SDS also resulted in pore wetting as represented by the increase in permeate flux and permeate conductivity towards the end of the operation. On the other hand, the hydrophilic PDA/PEI grafting layer on the PVDF-P membrane surface could alleviate the hydrophobic interactions while the electrostatic interactions were the dominant factor for membrane fouling. In theory, the negatively charged PVDF-P membrane surface should have repelled the negatively charged SDS unimers in the solution at around pH 7. However, the electrostatic attraction between the protonated amine-functional groups on the PVDF-P membrane surface and the sulfate groups present in the hydrophilic heads of the SDS unimers resulted in membrane fouling [184, 185]. Fortunately, this fouling was reversible. The permeate flux of the PVDF-P membrane was able to return to its initial level by cleaning it repeatedly with Milli-Q® water, as shown in Fig. 5-10(c). The PVDF-P membrane remained anti-wetting despite the electrostatic adsorption of the SDS unimers because the grafted PDA/PEI layer protected the mouth of the membrane pores, which in turn could maintain the LEP of these pores.

In contrast to anionic surfactant SDS, the PVDF-P membrane did not experience any fouling or wetting after 137 h of operation when feeding 50 mg L^{-1} of cationic surfactant DTAB (Fig. 5-10(d)). Its permeate flux was stable while the permeate quality was excellent throughout the operation, achieving a final electrical conductivity of 4.3 μS cm^{-1}. Its anti-fouling performance could be explained by the presence of the hydration layer and electrostatic repulsive forces between the positively charged quaternary ammonium heads of the DTAB unimers and the protonated amine-functional groups present in the grafted layer. In contrast, the lack of positive functional groups on the negatively charged surface of the pristine PVDF membrane would attract some DTAB unimers due to both hydrophobic and electrostatic interactions, leading to wetting of the membrane pores. It recorded a final permeate conductivity of 1,026 μS cm^{-1} after 24 h of

operation. From the above discussions, it could be inferred that the presence of protonated amine-functional groups on the outer surface of the PVDF-P membrane was effective in preventing the adsorption of cationic surfactants.

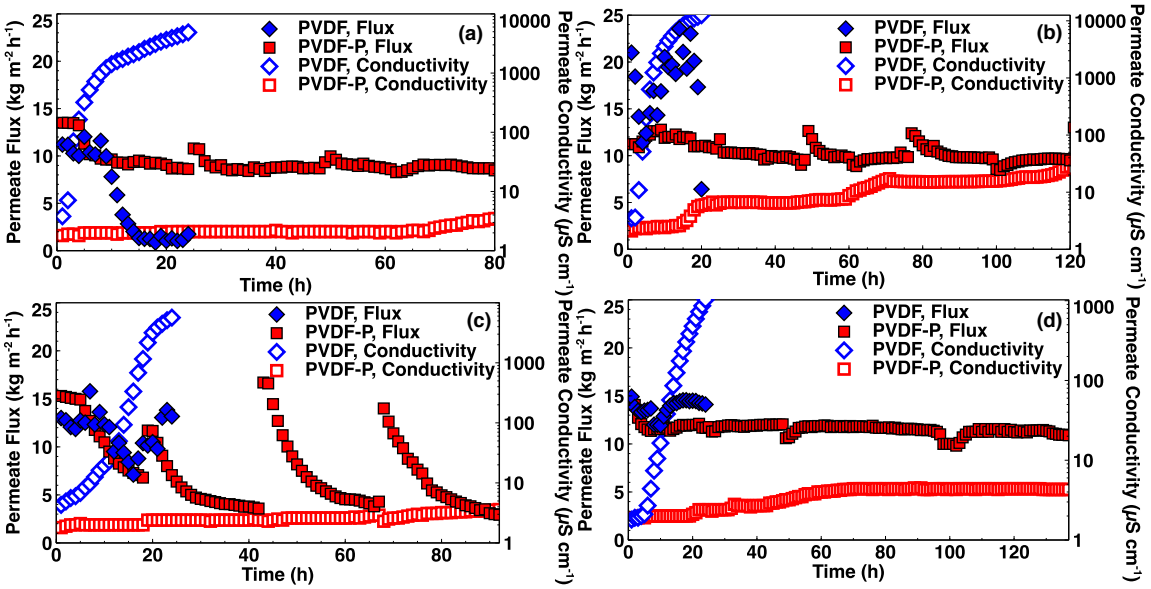


Fig. 5-10. DCMD performances of the pristine PVDF and PVDF-P membranes by feeding 50 mg L^{-1} of (a) Span® 20, (b) Tween® 20, (c) SDS, and (d) DTAB in 3.5 wt% NaCl. For the SDS experiment, PVDF-P membrane was flushed with Milli-Q® water when flux reached the lowest point. For each experiment, the feed tank was periodically refilled with overflow from the permeate reservoir to maintain the feed concentration. Q_f = 0.7 L min^{-1}; Q_p = 0.25 L min^{-1}; T_f = 333 K; T_p = 293 K.

5.3.4.2. Surfactant-stabilized petroleum-in-water emulsions

After the DCMD experiments with various surfactants, the fouling and wetting behaviors of the pristine PVDF and PVDF-P membranes were further evaluated by feeding 500 mg L^{-1} of surfactant-stabilized petroleum-in-water emulsion. The O/W emulsion was made kinetically stable by adding the surfactant DTAB in order to keep its oil droplet size below 10 μm [151]. The mean oil droplet size was 2.43 μm, which was much bigger than the nominal pore sizes of the pristine PVDF and PVDF-P membranes and was likely to cause pore blockage on the respective membrane surfaces. The pH and

corresponding zeta potential of the DTAB-stabilized petroleum-in-water emulsion were measured to be 5.7 and 22.9 ± 1.4 mV, respectively.

As presented in Fig. 5-11, the PVDF-P membrane showed robust long-term MD performance, maintaining a stable flux for up to a week of operation with a final permeate conductivity of 5.5 μS cm^{-1}. It was hypothesized that its anti-fouling and anti-wetting properties were ascribed to the tightly bounded hydration layer on its hydrophilic outer surface as illustrated in Fig. 5-12 [186]. When the O/W emulsion came into contact with the PVDF-P membrane surface, the hydrophilic moieties could interact strongly with water molecules to form a hydrogen-bonded network within the hierarchical structure of the grafted layer. This strong surface hydration layer provided a significant energetic barrier for the oil droplets to overcome in order to be adsorbed onto the PVDF-P membrane interface. Oil-adhesion on the membrane surface is only possible when the water molecules are expelled from the hierarchical structure, which is usually caused by dehydration. Dehydration leads to the unfavorable decrease in entropy, which in turn reduces the energetic barrier and facilitates membrane fouling [187]. Also, the electrostatic repulsive forces that existed between the positively charged O/W emulsion and protonated amine-functional groups on the PVDF-P membrane surface made it difficult for the attachment of oil droplets. In other words, the strongly hydrogen-bonded hydration layer coupled with the electrostatic repulsion interactions rendered the PVDF-P membrane surface to be oil adhesion-resistant. In contrast, the lack of such a protection layer on the pristine PVDF membrane surface made it susceptible to oil-adhesion and pore wetting. Both the hydrophobic interactions (between the hydrophobic membrane surface and oil droplets) and electrostatic attractive forces (between the negatively charged membrane surface and positively charged O/W emulsion) made it easier for the attachment and accumulation of oil droplets on the pristine PVDF membrane surface. To

put it succinctly, the anti-fouling and anti-wetting abilities of MD membranes could be achieved through the efficacious combinative effects of surface hydration and electrostatic repulsion.

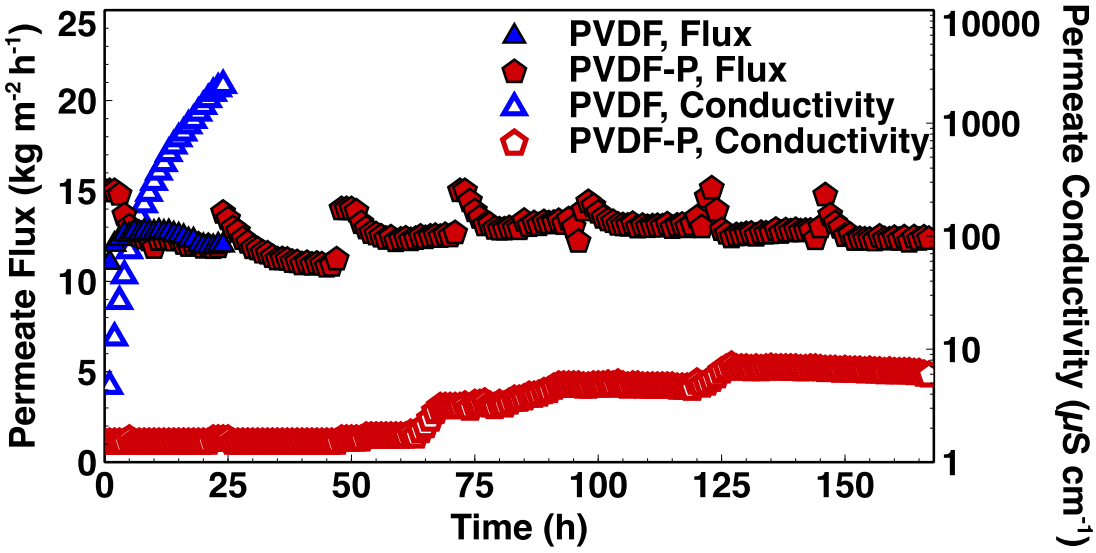


Fig. 5-11. DCMD performances of the pristine PVDF and PVDF-P membranes by feeding 500 mg L^{-1} of DTAB-stabilized petroleum-in-water emulsion. Fresh emulsions were prepared every 24h for the PVDF-P experiment. Q_f = 0.7 L min^{-1}; Q_p = 0.25 L min^{-1}; T_f = 333 K; T_p = 293 K.

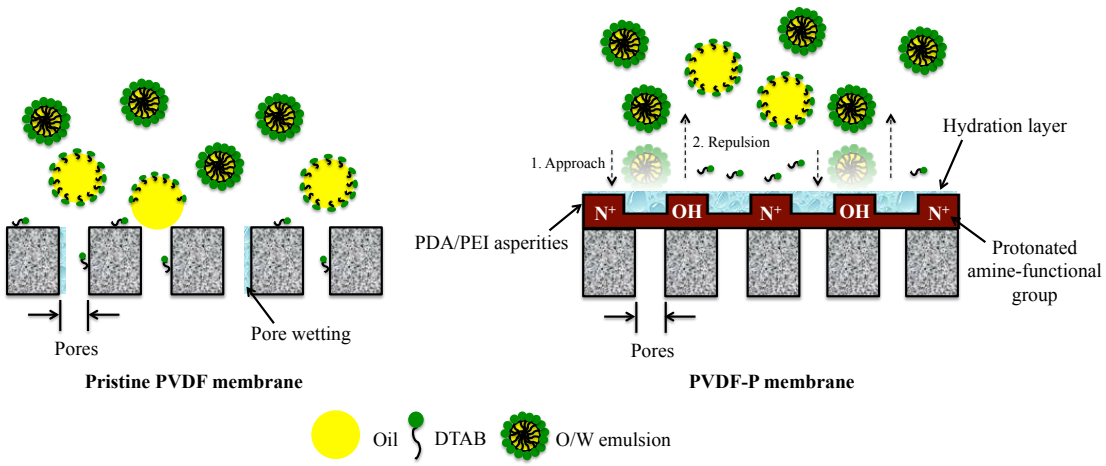


Fig. 5-12. Schematic of interaction of DTAB-stabilized O/W emulsion with the pristine PVDF and PVDF-P membranes.

5.3.5. Comparisons to other MD membranes

Table 5-3 summarizes the DCMD performance of the PVDF-P membrane for various feed solutions along with other MD membranes from literature. It can be seen that the PVDF-P membrane exhibits robust long-term performance with stable flux and excellent permeate quality (permeate conductivities were less than 5.5 μS cm^{-1} and salt rejection rates were above 99.9%) by feeding high concentration surfactant solutions and O/W emulsions for up to one week of operation. This is superior to all other previously reported MD membranes. For example, compared with the SiO_2-incorporated PVDF membrane [188], the PVDF-P membrane reported in this work delivered better anti-fouling and anti-wetting performances by feeding surfactants of 5 times the concentration. The study conducted by Wang et al. reported salt rejections instead of final permeate conductivity values [55, 141]. However, the final permeate conductivity values are better representations of the permeate quality in MD operations. The robustness of the PVDF-P membrane suggests its potential for water recovery from low surface tension feeds such as produced water via the DCMD process.

Table 5-3. Comparison of performances among various MD membranes.

Membrane	Feed	Test duration (h)	$C_{p,final}$ ($\mu S\ cm^{-1}$)	Salt rejection (%)	Reference
PVDF-P	50 mg L^{-1} Span® 20	80	3.5	99.99	Current work
PVDF-P	50 mg L^{-1} Tween® 20	115	20	99.96	Current work
PVDF-P	50 mg L^{-1} SDS	90	3.5	99.99	Current work
PVDF-P	50 mg L^{-1} DTAB	137	4.3	99.99	Current work
PVDF-P	500 mg L^{-1} DTAB/Oil	168	5.5	99.99	Current work
SiO_2/PVDF	10 mg L^{-1} SDBS[a]	104	~80	99.9	[188]
SiO_2/PVDF	10 mg L^{-1} kerosene	200	~100	99.8	[188]
SiNPs/PVDF	1000 mg L^{-1} crude oil	36	N.A[b]	~100	[55]
PDA/SiNPs/ PVDF	1000 mg L^{-1} crude oil	12	N.A[b]	99.9	[141]

[a] Sodium dodecyl benzene sulfonate.
[b] Not applicable. The final permeate conductivity values of these experiments were not provided.

5.4. Conclusions

A composite PVDF membrane with in-air hydrophilic/underwater superoleophobic properties was fabricated via a facile method through single-step co-deposition of PDA/PEI onto a hydrophobic PVDF substrate. The fouling and wetting behaviors of the pristine PVDF and modified PVDF membranes were systematically studied via DCMD experiments by feeding amphiphilic surfactants and O/W emulsion. The results reveal that the modified PVDF membrane exhibited excellent anti-wetting properties regardless of the type of surfactant. In addition, it exhibited excellent anti-fouling properties against both non-ionic and cationic surfactants. More importantly, the modified membrane showed very promising stability (one week of operation) in the recovery of water from DTAB-stabilized petroleum-in-water emulsion without experiencing fouling and wetting. The robust MD performance was possible because of the following two reasons. Firstly, an interfacial hydration layer was formed within the hierarchical structure of the hydrophilic grafting layer, which prevented the attachment of oil droplets. Secondly, the protonated amine-functional groups on the membrane outer surface were able to repel the positively charged O/W emulsion. Interestingly, the thin grafting layer did not impede on the permeate flux of the modified membrane and instead protected the membrane pores from oil adsorption. This study suggests that the underwater superoleophobic mussel-inspired modified PVDF membrane could potentially be used for highly effective and environmentally friendly water recovery from low surface tension solutions such as produced water via DCMD.

Chapter 6 Polyvinylidene Fluoride Membrane Modification via Oxidant-induced Dopamine Polymerization for Sustainable Direct-contact Membrane Distillation[3]

6.1. Introduction

Most of the surface modification techniques involving dopamine investigated thus far have proven to be laborious and time-consuming. Often, the deposition of polydopamine (PDA) through these conventional techniques is non-homogenous, of low thickness, and of limited hydrophilicity. In the previous study as discussed in Chapter 5, the coating process took more than a day to achieve the desired thickness [56]. Even so, the deposited layer presented limited hydrophilicity. Furthermore, the modified membrane was especially vulnerable to wetting in some non-ionic surfactant solutions and fouling in anionic surfactant solutions. It has been suggested that the use of oxidants, in replacement of dissolved oxygen, can overcome these limitations [189-191].

This study focuses on developing a robust MD membrane with enhanced flux for water recovery from wastewaters containing low surface tension solutes via direct-contact membrane distillation (DCMD). Specifically, a superoleophobic composite membrane with sandwich structure was fabricated through facile single-step deposition of hydrophilic PDA layer in the presence of an oxidant, namely sodium periodate (SP), on both the outer and inner surfaces of a commercial hydrophobic PVDF hollow fiber substrate. The surface chemistry and hierarchical structure of the modified PVDF membrane were studied comprehensively through a range of characterization techniques.

[3] *This chapter is reproduced with permission from Chew, N.G.P., S. Zhao, C. Malde, R. Wang, Polyvinylidene fluoride membrane modification via oxidant-induced dopamine polymerization for sustainable direct-contact membrane distillation. Copyright © 2018 Elsevier.*

The fouling and wetting propensities of the modified PVDF membrane were investigated via a bench-scale DCMD experimental rig by feeding a series of low surface tension saline wastewater. Its performances were analyzed and then compared against those of the pristine PVDF and previously reported composite membranes (Chapter 5) to ascertain its applicability and robustness for long-term treatment of low surface tension feeds. To the best of our knowledge, this is the first report on oxidant-induced dopamine modification on a hydrophobic PVDF hollow fiber substrate for extended applications of DCMD.

6.2. Experimental

6.2.1. Fabrication of composite PVDF membrane

The composite membrane was fabricated by facile deposition of PDA on both the outer and inner surfaces of a hydrophobic PVDF substrate to create a sandwich structure as illustrated in Fig. 6-1. The coating solution was first prepared by dissolving 2 g L^{-1} DA into 50 mM sodium acetate buffer with 20 mM SP as the oxidant [191]. The solution was adjusted with 2 M HCl to pH 5. Hereon, the coating solution will be referred to as the PDASP solution. For outer surface modification, both ends of each hollow fiber membrane were sealed to ensure that only its outer surface was modified while the membrane pores beneath the surface remained hydrophobic for vapor transport. The pristine PVDF hollow fiber membranes were partially pre-wetted with predetermined concentrations of IPA for a designated time prior to being immersed in the PDASP solution with shaking at 30 rpm (Orbital Maxi MD Humidity, OVAN, Spain) for designated times (2 h or 6 h) under ambient conditions. Hereon, the modified membranes with different deposition times will be referred to as the 2h-mPVDF and 6h-mPVDF membranes, respectively. Finally, the modified membranes were washed thoroughly with Milli-Q® water and dried overnight in the vacuum oven at 323 K.

To perform inner surface modification on the 2h-mPVDF and 6h-mPVDF membranes, freshly prepared PDASP solution was circulated in the membrane lumen by a peristaltic pump at 0.01 L min^{-1} for 1 h on a bench-scale cross-flow setup as illustrated in Fig. 6-1. Throughout the reaction, the PDASP solution was covered with aluminum foil and stirred at 300 rpm under ambient conditions. The membrane lumen was washed thoroughly with Milli-Q® water after modification.

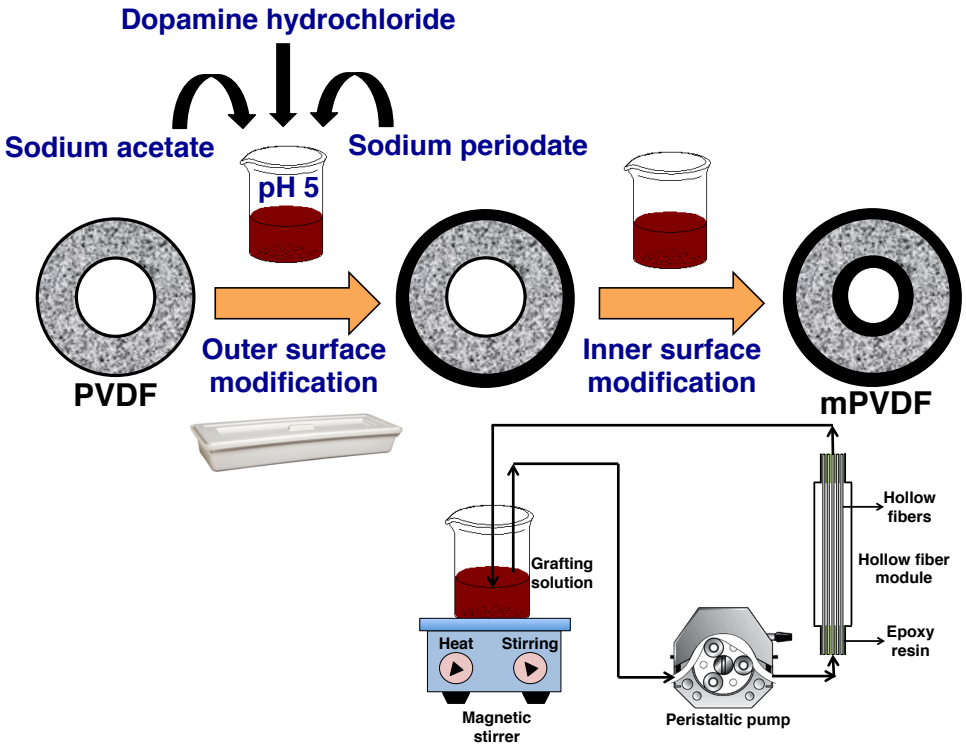


Fig. 6-1. Schematic of oxidant-induced deposition of PDA on the outer and inner surfaces of a PVDF hollow fiber membrane.

6.2.2. Raw seawater

In order to compare the DCMD performances of the pristine and modified PVDF (2h-mPVDF and 6h-mPVDF) membranes in real applications, a systematic study was carried out against seawater samples collected from a local desalination plant. The seawater samples were stored at ambient conditions and used as received. No pre-

treatment was carried out prior to the respective experiments. The water quality of the seawater is listed in Table 6-1. The detailed analytical measurement methods were described in our previous study [192].

Table 6-1. Main compositions of the seawater used in this study.

Parameter	Value
pH	7.8 ± 0.2
Conductivity (mS cm^{-1})	48.4 ± 1.1
Dissolved oxygen (mg L^{-1})	5.5 ± 1.2
Ca (mg L^{-1})	362
Mg (mg L^{-1})	1252
Na (mg L^{-1})	10600
Cl (mg L^{-1})	18890

6.3. Results and discussion

6.3.1. Observations of membrane surface morphology

The outer surface and cross-section morphologies of the pristine PVDF, 2h-mPVDF, and 6h-mPVDF membranes were observed using FESEM and the images are shown in Fig. 6-2. The changes in surface morphology were apparent after PDA deposition. As shown in Fig. 6-2(a1) and (a2), the pristine PVDF membrane surface was smooth with abundant pores. The oxidant-induced polymerization of dopamine deposited a thin layer of agglomerates, as large as 1 μm, on the pristine PVDF membrane surface after 2 h (as observed in Fig. 6-2(b1–b3)), which thoroughly covered the highly porous surface. When the coating duration was extended to six hours, minute PDA particles were deposited on the PVDF membrane surface to create a hierarchical structure with high surface roughness as corroborated by the roughness parameters listed in Table 6-2. High surface roughness contributes greatly to membrane superhydrophilicity as evidenced by the low water contact angle, 13.2 ± 2.4°, of the 6h-mPVDF membrane [193-195]. The surface hierarchical structure, coupled with superhydrophilicity, can potentially impart

underwater superoleophobic properties to the modified membrane, which will be discussed in section 6.3.3. Fig. 6-2(b3) and (c3) reveal that the deposited layer did not permeate into the bulk of the PVDF substrate, hence ensuring that the membrane pores beneath the surface remained hydrophobic for vapor transport. Moreover, the deposited layer was structurally stable. It remained intact and minimal changes to its surface morphology were observed even after ultrasonication as evidenced by Fig. 6-2(d1)-(d3).

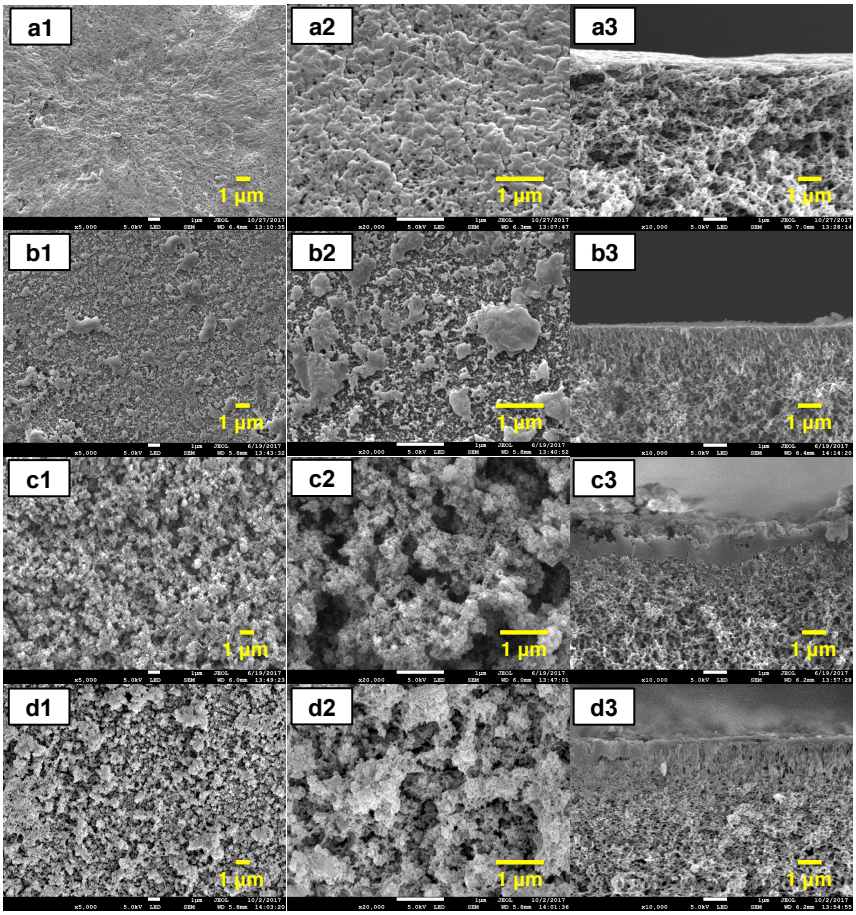


Fig. 6-2. FESEM images of the outer surface morphologies of the pristine PVDF (a1 and a2), 2h-mPVDF (b1 and b2), 6h-mPVDF (c1 and c2), and ultrasonicated 6h-mPVDF (d1 and d2) membranes. FESEM images of the cross-section morphologies of the pristine PVDF (a3), 2h-mPVDF (b3), 6h-mPVDF (c3), and ultrasonicated 6h-mPVDF (d3) membranes.

Table 6-2. Surface roughness parameters and water contact angles of the pristine PVDF and 6h-mPVDF membranes.

Membranes	Roughness			Water contact angle (°)
	R_a[a] (nm)	R_q[b] (nm)	R_z[c] (nm)	
PVDF	25.6 ± 1.2	31.9 ± 0.8	258.3 ± 2.2	109.5 ± 1.2
6h-mPVDF	113.0 ± 2.1	145.0 ± 2.8	895.9 ± 1.9	13.2 ± 2.4

[a] Average roughness.
[b] Root-mean-squared roughness.
[c] Ten point average roughness.

The pore size distributions of the pristine PVDF and 6h-mPVDF membranes are illustrated in Fig. 6-3. While both membranes have distinct bimodal distributions, they have contrasting mean pore sizes. The pristine PVDF membrane has a larger mean pore size (0.027 μm) as compared to the 6h-mPVDF membrane (0.018 μm), which is consistent with the FESEM images. This is indicative of the alteration in intrinsic pore structure of the pristine PVDF membrane after oxidation-induced polymerization of dopamine on its surface. Introduction of PDA onto the membrane surface would have restricted some of the bigger pores and covered the smaller pores found in the pristine PVDF membrane. Consequently, the 6h-mPVDF membrane is expected to be less susceptible to fouling and pore wetting owing to the additional protection offered by the deposited layer.

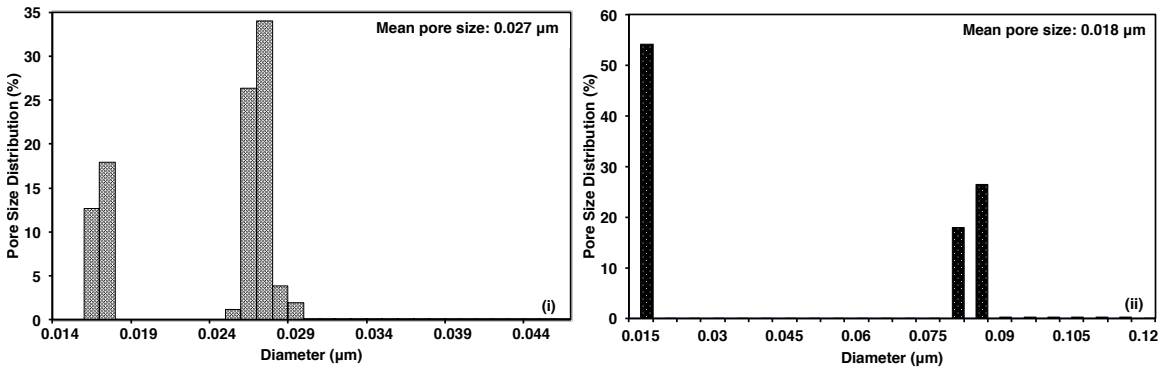


Fig. 6-3. Pore size distributions of the (i) pristine PVDF and (ii) 6h-mPVDF membranes.

6.3.2. Characterizations of membrane surface chemistry

The changes in surface functional groups of the membrane after PDA deposition was characterized by ATR-FTIR and the spectra are presented in Fig. 6-4. Two distinct absorption peaks at 1508 cm^{-1} and 1606 cm^{-1} were detected on the mPVDF membranes, which are assigned to the primary amine N-H bending and C = C aromatic stretch within the PDA structure, respectively [196]. The absorption peak observed at 1701 cm^{-1} on the mPVDF membranes is indicative of carbonyl/carboxyl groups, suggesting the successful deposition of carboxyl-functional groups during the accelerated oxidative process induced by SP under slightly acidic conditions [191, 196]. This in turn rendered the mPVDF membrane surface more hydrophilic than the previously reported PDA/PEI coated membrane [56].

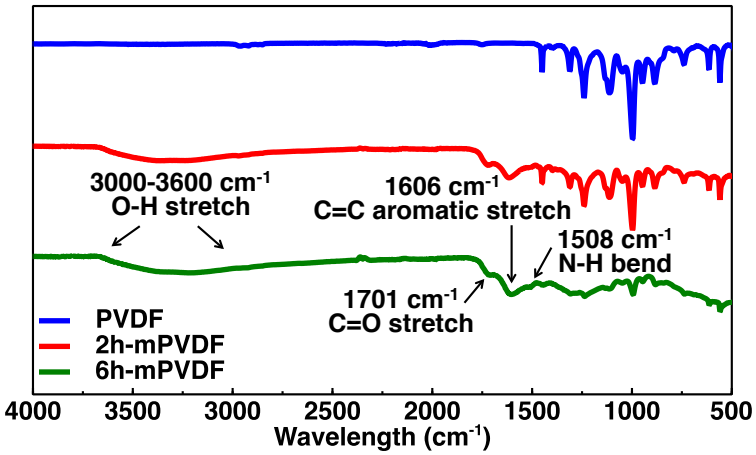


Fig. 6-4. ATR-FTIR spectra of the outer surfaces of the pristine PVDF, 2h-mPVDF, and 6h-mPVDF membranes. Transmittance was normalized against the CF peak.

The surface chemical compositions of the pristine PVDF and oxidant-induced PDA coated membranes were compared via XPS analysis as shown in Table 6-3 and Fig. 6-5. It can be seen that the outer and inner surface elemental compositions of both membranes were dissimilar. The F 1s and Cl 2p peaks that were initially present on both the outer and inner surfaces of the pristine PVDF membrane could not be observed on

either surface of the 6h-mPVDF membrane after modification. The synchronous appearance of the O 1s, N 1s, and I 3d peaks on both the outer and inner surfaces of the 6h-mPVDF membrane mirrored the successful deposition of PDA. The significant increase in atomic concentration of O 1s after surface modification was consistent with the ATR-FTIR results, suggesting the formation of carboxyl-functional groups and oxidative o-quinone cleavage during oxidant-induced polymerization of dopamine [191, 196, 197]. The O/C ratios of the outer and inner surfaces of the 6h-mPVDF membrane were 0.39 and 0.35, respectively. These ratios were noticeably higher than dopamine's stoichiometric ratio of 0.25 as reported by Lee et al. [198], which was a further proof of the oxidative effect initiated through the addition of SP. Previous studies reported that prolonged oxidation time could lead to the loss of amine groups and decarboxylation of pyrrole moieties, resulting in a smaller N/C ratio [191, 196]. However, the N/C ratios of both the outer and inner surfaces of the 6h-mPVDF membrane were similar despite their contrasting deposition times. This was possible through the suppression of the oxidative breakdown process by preparing fresh coating solution every 2 h for outer surface modification. As shown in the deconvolution spectra of the 6h-mPVDF membrane in Fig. 6-5(b)-(d), the C 1s core-level spectrum revealed three peak components at BE of 284.8 eV, 285.8 eV, and 288.5 eV, which were assigned to the chemical states of C-C/C-H, C-O/C-N, and C = O, respectively. The N 1s core-level spectrum was curve-fitted with two components, one at a BE of 400.1 eV for the chemical state of C-N and the other at a BE of 402.3 eV for the chemical state of protonated amine-functional group. The O 1s spectrum presented two peak components at BE of 531.6 eV and 533.9 eV, which were assigned to the C-O and C = O of the carboxylic acid moieties, respectively. The XPS analysis results were consistent with the structural components of the SP-oxidized PDA as proposed by previous studies [191, 196].

Table 6-3. Elemental compositions (in atomic percentage) of the outer (OS) and inner (IS) surfaces of the pristine PVDF and 6h-mPVDF membranes.

Membrane	C 1s	F 1s	O 1s	Cl 2p	N 1s	I 3d	N/C	O/C
PVDF-OS	54.9	37.2	1.9	6.0	-	-	-	0.03
6h-mPVDF-OS	65.5	-	25.5	-	7.8	1.2	0.12	0.39
PVDF-IS	49.1	42.5	0.4	8.0	-	-	-	0.01
6h-mPVDF-IS	68.6	-	23.9	-	7.2	0.4	0.10	0.35

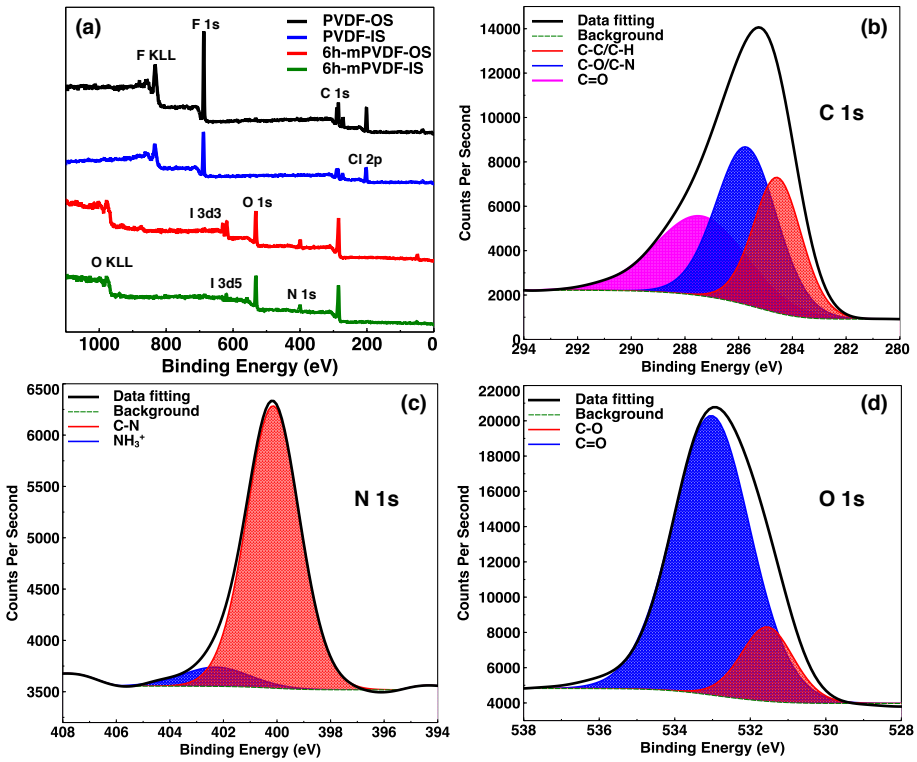


Fig. 6-5. (a) XPS survey scan spectra of the outer (OS) and inner (IS) surfaces of the pristine PVDF and 6h-mPVDF membranes. Deconvolution spectra of (b) C 1s, (c) N 1s, and (d) O 1s on the outer surface of the 6h-mPVDF membrane (the inner surface coating time is 1 h).

The surface charge property of a membrane is very important for MD applications because the electrostatic interaction between foulants and the membrane surface influences membrane fouling and wetting behaviors [141]. Therefore, the pH dependence of surface zeta potential of the 6h-mPVDF membrane was studied and compared with the pristine PVDF membrane via streaming potential measurements. As shown in Fig. 6-6, the pristine PVDF was mostly negatively charged throughout the tested pH range, which was consistent with data found in literature [199]. In comparison with the pristine PDVF

membrane, the 6h-mPVDF membrane was less negatively charged. Amine- and phenolic hydroxyl-functional groups endowed PDA with amphoteric properties. The former protonated from –NH to $–NH_2^+$ at low pH while the latter dissociated from –OH to $–O^-$ at high pH [200, 201]. Apart from that, its negative charge at high pH could also be ascribed to dissociation of the carboxyl-functional groups.

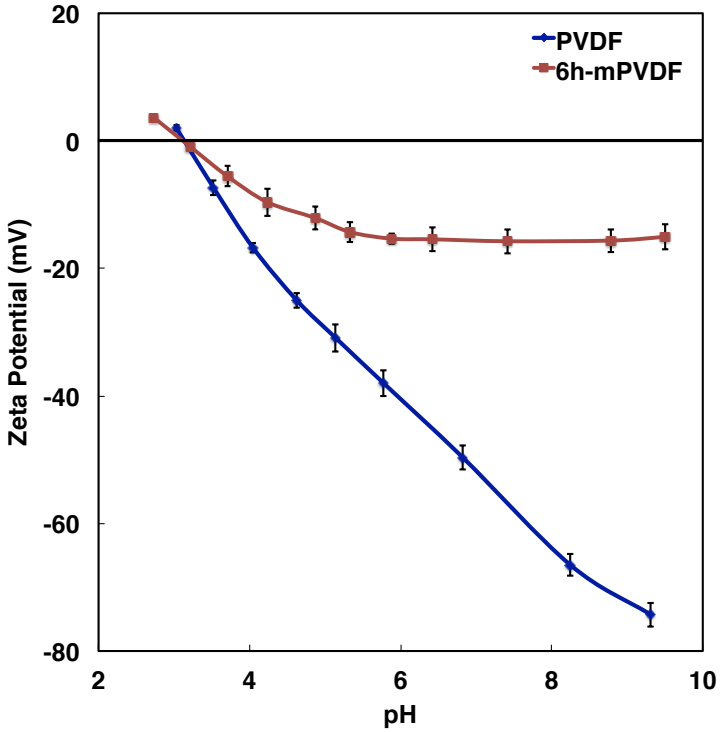


Fig. 6-6. Surface zeta potentials of the pristine PVDF and 6h-mPVDF membranes as a function of pH. 1 mM NaCl was used as the background electrolyte solution.

6.3.3. Underwater oil-membrane interactions

With reference to Table 6-2, the pristine PVDF membrane was in-air hydrophobic and the 6h-mPVDF membrane was in-air superhydrophilic with water contact angle values of 109.5 ± 1.2° and 13.2 ± 2.4°, respectively. The 6h-mPVDF membrane's superhydrophilicity could be attributed to the deposition of polar amine-, hydroxyl-, and carboxyl-functional groups during surface modification. In addition, the hierarchical structures with high surface roughness of the 6h-mPVDF membrane were instrumental in

augmenting its intrinsic wetting properties [175]. The addition of a liquid droplet (i.e. petroleum droplet) to textured surfaces can lead to a Cassie-Baxter state that supports a composite interface, which facilitates non-wetting and easy droplet roll-off [50, 202]. The underwater captive bubble method was applied to probe further into the mechanics of the Cassie-Baxter state at the oil-water-solid interface in the hierarchical structure on the 6h-mPVDF membrane surface. A petroleum droplet, Milli-Q® water, and a piece of 6h-mPVDF membrane represented the oil, water, and solid phase, respectively. The relevant captured images of the underwater interactions are illustrated in Fig. 6-7. Upon contact, the petroleum droplet immediately adhered onto the pristine PVDF membrane surface and spread across the entire surface within 15 s. In contrast, there was neither deformation of the petroleum droplet nor petroleum residue on the 6h-mPVDF membrane surface upon contact. Similar observations were recorded even when there was forced contact between the petroleum droplet and the 6h-mPVDF membrane surface, attesting its underwater superoleophobic property. The hierarchical structure, coupled with surface superhydrophilicity, imparted the underwater superoleophobic property of the modified membrane. In such a scenario, an interfacial hydration layer was formed on the membrane surface and trapped water within the hierarchical structure, prohibiting oil attachment on the surface. The oil adhesion-resistant property of the 6h-mPVDF membrane renders it a suitable candidate for effective oil-water separation via DCMD.

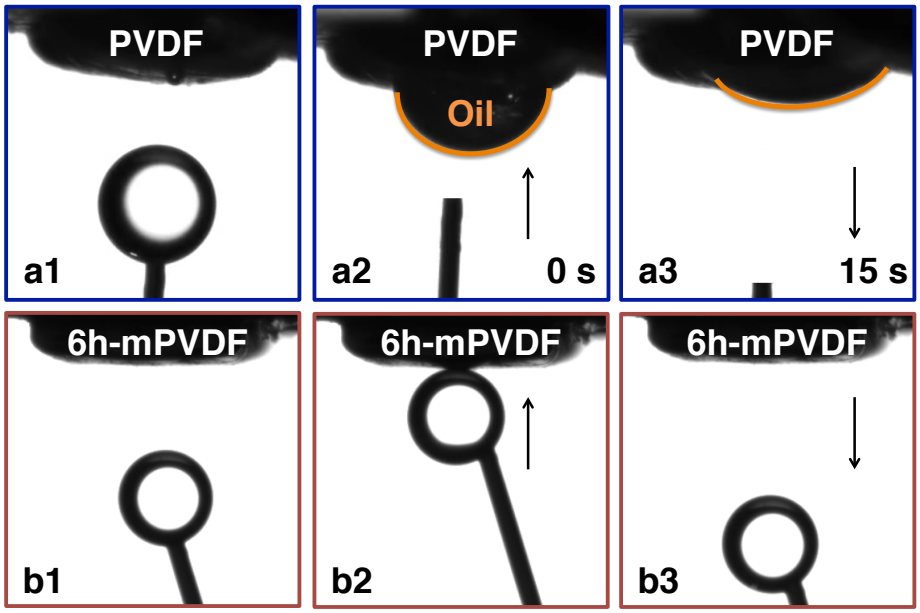


Fig. 6-7. Captured images of the underwater interactions between petroleum droplets tethered via a needle and the pristine PVDF (a1-a3) and 6h-mPVDF (b1-b3) membrane surfaces.

6.3.4. Membrane performance in DCMD tests

6.3.4.1. Saline feeds with anionic, cationic, and non-ionic surfactants

To investigate the intrinsic MD performances of the modified PVDF membranes, baseline tests were first conducted using 3.5 wt% NaCl solution as feed. The permeate flux and conductivity over a period of 24 h of the 2h-mPVDF-O (only outer surface modification was performed) and 2h-mPVDF (outer and inner surface modifications were performed) membranes were recorded and compared with the pristine PVDF and previously reported PDA/PEI coated membranes, which are presented in Fig. 6-8. It was evident that all of four membranes exhibited stable fluxes and conductivities throughout the operation. The deposited PDA layer did not provide additional mass transfer resistance to vapor transport across the membrane pores and there was no salt breakthrough. The permeate flux of the 2h-mPVDF membrane was the highest, presenting approximately 70% flux enhancement over the pristine PVDF membrane. The average permeate fluxes of the pristine PVDF, PDA/PEI, 2h-mPVDF-O, and 2h-mPVDF membranes were 11.16 kg m^{-2} h^{-1}, 11.76 kg m^{-2} h^{-1}, 16.77 kg m^{-2} h^{-1}, and 18.96 kg m^{-2} h^{-1},

respectively. Similarly, the 6h-mPVDF membrane demonstrated stable flux and permeate conductivity during the test.

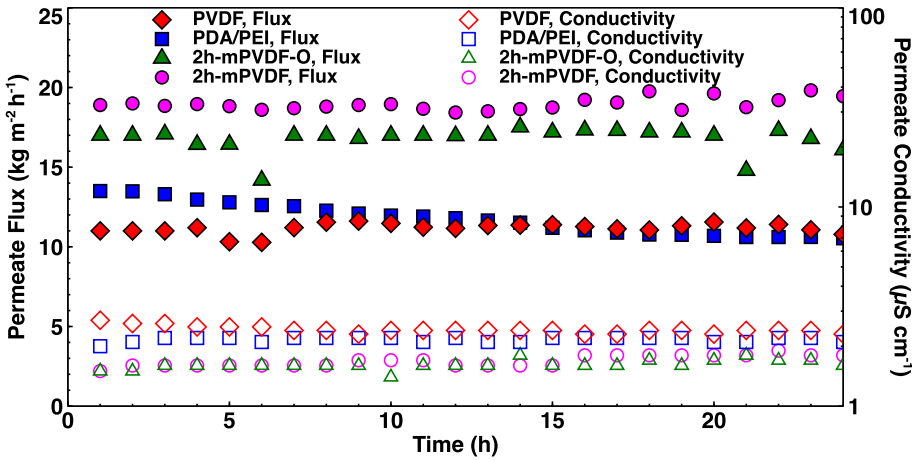


Fig. 6-8. DCMD performances of the pristine PVDF, PDA/PEI, 2h-mPVDF-O and 2h-mPVDF membranes by feeding 3.5 wt% NaCl. Feed volumetric flow rate (Q_f) = 0.7 L min^{-1}; Permeate volumetric flow rate (Q_p) = 0.25 L min^{-1}; Feed temperature (T_f) = 333 K; Permeate temperature (T_p) = 293 K.

It was hypothesized that the membrane's improved flux could be ascribed to the deposition of carboxyl groups on its outer surface, which led to favorable polar-polar interactions with the vapor molecules as illustrated in Fig. 6-9. This in turn enhanced their absorption. Subsequently, the hydrophobic PVDF substrate was able to repel both water and non-volatile NaCl solute while insuring that distillate of excellent quality was collected. Finally, the carboxyl groups present on the inner surface of the 2h-mPVDF membrane served as sites for vapor-liquid interactions, thus leading to faster vapor removal from the substrate pores into the distillate stream [59, 60, 63-67].

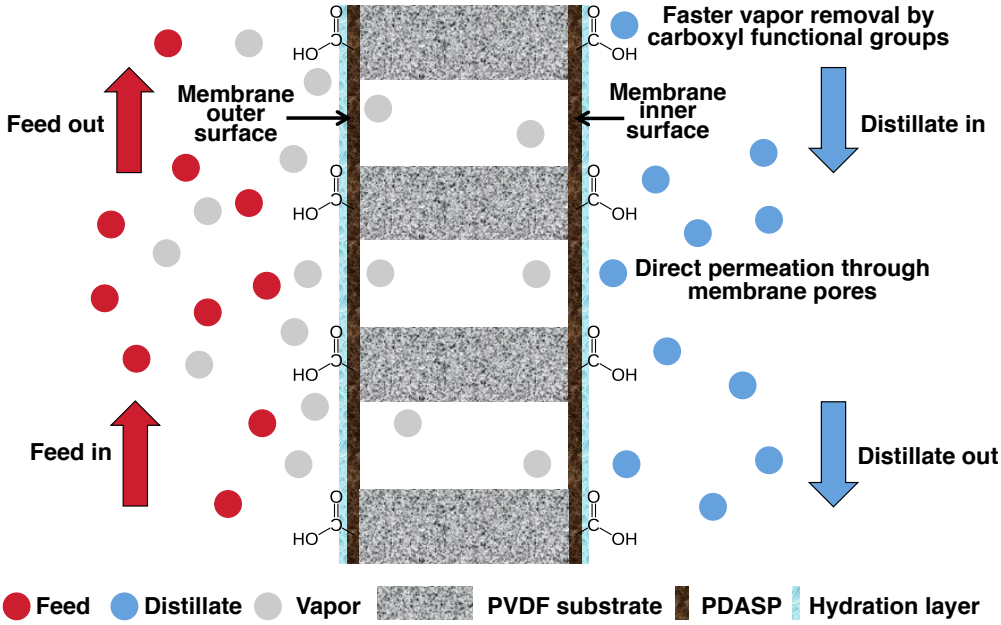


Fig. 6-9. Schematic diagram of proposed mechanisms for flux enhancement through oxidant-induced surface modification.

Following the baseline experiments, the fouling and wetting behaviors of the modified PVDF membrane in the presence of 50 mg L^{-1} of anionic (SDS), cationic (DTAB), and non-ionic (Tween® 20) surfactant solutions were analyzed and compared with those of the pristine PVDF and previously reported PDA/PEI coated membranes. As depicted in Fig. 6-10, these three types of membrane exhibited significantly different fouling and wetting behaviors in the presence of 50 mg L^{-1} of SDS solution. The pristine PVDF membrane experienced severe wetting, as demonstrated by the rapid increase in the permeate conductivity. The PDA/PEI membrane presented reversible fouling but no wetting during the operation. On the other hand, the 6h-mPVDF membrane demonstrated excellent anti-fouling and anti-wetting properties, maintaining a stable flux and excellent distillate quality throughout the experiment. The stark difference in the performances of these membranes was believed to be ascribed to their different surface chemistries and wetting properties as well as hierarchical structures, which will be further discussed below. The pristine PVDF membrane is inherently hydrophobic with a smoother surface. The hydrophobic interaction between the hydrophobic tails of SDS unimers and the PVDF membrane surface brought about the adsorption of SDS unimers on the membrane

surface, which resulted in pore blockage and severe pore wetting [33]. On the other hand, the PDA/PEI coated membrane had an underwater superoleophobic surface with hierarchical structure. It showed excellent anti-wetting property but poor anti-fouling property in the SDS solution. This could be explained by its surface charge property. The PDA/PEI membrane was tailored in such a way that protonated amine-functional groups were deposited on its surface. The negatively charged SDS unimers would have a natural tendency to adhere on certain regions of the PDA/PEI membrane with the positively charged amine-functional groups, resulting in blockage of the micro-channels within the hierarchical structure. This fouling was reversible and the permeate flux could be recovered by simply washing with Milli-Q® water. Besides that, the deposited PDA/PEI layer offered additional protection to the membrane pores and maintained the liquid entry pressure, rendering them less vulnerable to wetting [56]. Last but not least, the excellent fouling- and wetting-resistant properties of the 6h-mPVDF membrane were ascribed to its underwater superoleophobic surface with hierarchical structures and negative charges, which was able to eliminate both the hydrophobic and electrostatic interactions. Even though protonated amine-functional groups were also detected on the 6h-mPVDF membrane surface, there were fewer of these groups as compared with the PDA/PEI membrane surface. This was corroborated with the chemical structures of the respective deposited layers [56, 191, 196]. As such, the electrostatic repulsion between the negatively charged SDS unimers and the negatively charged 6h-mPVDF membrane surface was more dominant than the electrostatic attraction between these unimers and the protonated amine-functional groups. With fewer SDS unimers adsorbed on its surface, the 6h-mPVDF membrane remained robust throughout the operation.

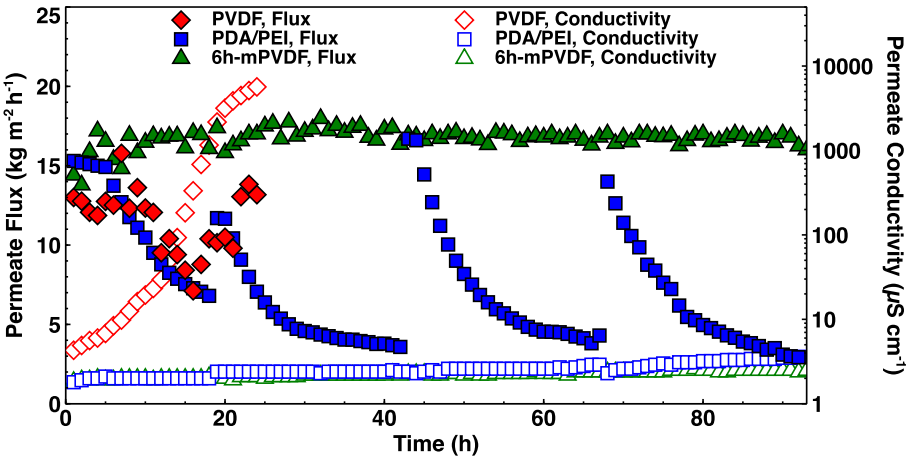


Fig. 6-10. DCMD performances of the pristine PVDF, PDA/PEI, and 6h-mPVDF membranes by feeding 50 mg L^{-1} of SDS in 3.5 wt% NaCl. For each experiment, the feed tank was periodically refilled with overflow from the permeate reservoir to maintain the feed concentration. Q_f = 0.7 L min^{-1}; Q_p = 0.25 L min^{-1}; T_f = 333 K; T_p = 293 K.

In the case of cationic surfactant DTAB (Fig. 6-11), both of the composite membranes (PDA/PEI and 6h-mPVDF membranes) experience neither fouling nor wetting throughout the entire test duration, which was attested by their respective stable fluxes and high salt rejection rates (> 99.99%). The 6h-mPVDF membrane presented a relatively higher flux and better distillate quality (final permeate conductivity of 2.2 μS cm^{-1}) as compared to the PDA/PEI membrane (4.3 μS cm^{-1}). Both of these membranes were intrinsically negatively charged but the presence of protonated amine-functional groups could prevent the adsorption of positively charged DTAB unimers. This, coupled with the interfacial hydration layer, could circumvent the issues of fouling and wetting. When the deposited layer comes into contact with the bulk water, water molecules penetrate into its hydrophilic structure to form a hydrogen-bonded network within the deposited layer. Surface hydration leads to an increased resistance against surfactant adsorption, leading to fouling-resistant property. This in turn ensured that the composite membranes remained anti-wetting throughout the test duration. In contrast, the lack of protonated amine-functional groups on the negatively charged and hydrophobic pristine PVDF membrane surface could promote electrostatic attraction as well as hydrophobic

interaction between the membrane surface and the DTAB unimers. This in turn led to pore wetting as substantiated by the increase in permeate conductivity.

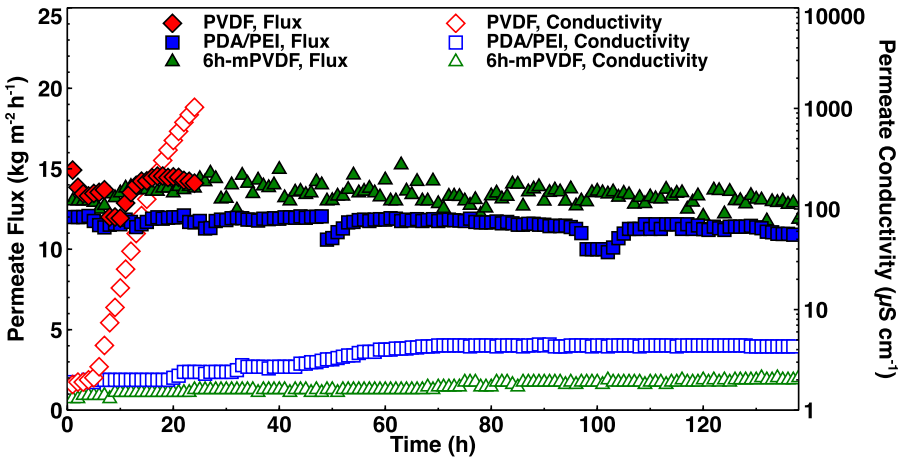


Fig. 6-11. DCMD performances of the pristine PVDF, PDA/PEI, and 6h-mPVDF membranes by feeding 50 mg L^{-1} of DTAB in 3.5 wt% NaCl. For each experiment, the feed tank was periodically refilled with overflow from the permeate reservoir to maintain the feed concentration. Q_f = 0.7 L min^{-1}; Q_p = 0.25 L min^{-1}; T_f = 333 K; T_p = 293 K.

Tween® 20 is one of the most challenging surfactants, with reference to the onset and severity of wetting, as attested by our previous studies shown in Chapters 4 and 5 [33, 56]. In the case of 50 mg L^{-1} Tween® 20, the pristine PVDF membrane was severely wetted, as indicated by the rapid increase in permeate flux and conductivity during 20 h of operation as shown in Fig. 6-12. By contrast, both of the composite membranes (PDA/PEI and 6h-mPVDF membranes) showed robust stable performances. Moreover, the 6h-mPVDF membrane outperformed the PDA/PEI membrane, presenting higher permeate flux and better distillate quality. As discussed in previous chapters [33, 56], Tween® 20, with a lower HLB value, shows a greater affinity for hydrophobic surfaces as compared to surfactants with higher HLB values (SDS and DTAB). Thus, a monolayer of Tween® 20 unimers formed on the hydrophobic PVDF membrane surface via hydrophobic interaction. However, the negative charge on the pristine PVDF membrane would not have contributed to the attachment of this non-ionic surfactant. The adsorbed Tween® 20 unimers on the membrane surface would draw more water molecules towards

the membrane pores via their hydrophilic heads, resulting in severe wetting. On the other hand, the formation of hydration layer on the composite membrane surfaces significantly prevented the adhesion of surfactant unimers, maintaining the stable performances of these membranes. The 6h-mPVDF membrane, with a lower water contact angle of 13.2 ± 2.4°, is more hydrophilic than the PDA/PEI membrane (water contact angle of 25.7 ± 4.0°). The more hydrophilic polar functional groups on the 6h-mPVDF membrane surface endowed it with a more robust performance as compared to the PDA/PEI membrane.

These three cases involving different types of surfactant solution have demonstrated that composite membranes, such as the 6h-mPVDF membrane, when endowed with superoleophobic property could effectively overcome fouling and wetting issues in DCMD applications for low surface tension feeds.

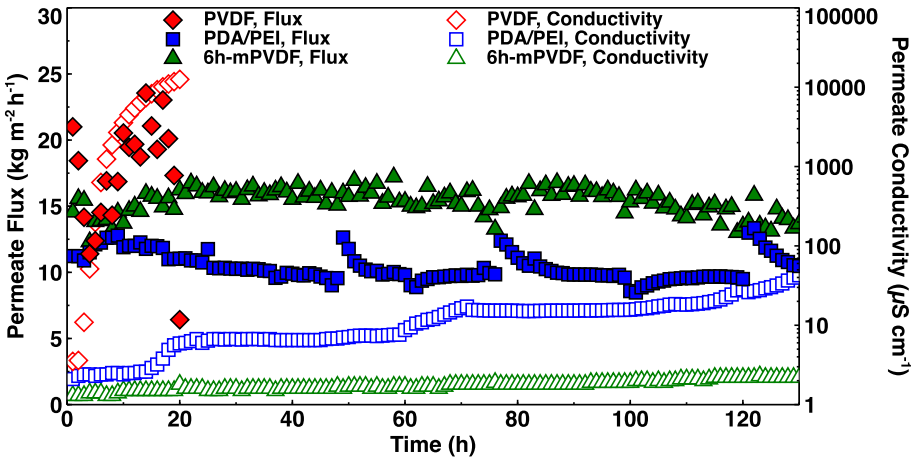


Fig. 6-12. DCMD performances of the pristine PVDF, PDA/PEI, and 6h-mPVDF membranes by feeding 50 mg L^{-1} of Tween® 20 in 3.5 wt% NaCl. For each experiment, the feed tank was periodically refilled with overflow from the permeate reservoir to maintain the feed concentration. Q_f = 0.7 L min^{-1}; Q_p = 0.25 L min^{-1}; T_f = 333 K; T_p = 293 K.

6.3.4.2. Surfactant-stabilized petroleum-in-water emulsion

After investigating the challenges of different types of surfactant on the MD performance of the modified PVDF membrane, its feasibility for water recovery from O/W emulsions was studied and the results are shown in Fig. 6-13. The 500 mg L^{-1} of petroleum-in-water emulsion was prepared by adding Tween® 20 to form a kinetically stable emulsion with mean oil droplet size of less than 10 μm. This serves as an indicator of the applicability of the modified membranes for produced water treatment since removal of fine oil droplets (< 10 μm) is often challenging. As shown in Fig. 6-13, severe pore wetting was observed for the pristine PVDF membrane, as revealed by the substantial increase in both the permeate flux and conductivity. In contrast, the 6h-mPVDF showed robust performance throughout the entire operation, presenting a stable flux and excellent distillate quality. The Tween® 20-stabilized petroleum-in-water emulsion had a mean droplet size of 2.16 μm and a near neutral zeta potential of -3.11 ± 0.32 mV. Thus, the electrostatic interaction between the petroleum droplets and membrane surface would only have a minor effect on the membrane performance, while the surface wetting property and hierarchical structures play a critical role in governing the fouling and wetting behaviors. The severe wetting behavior of the pristine PVDF membrane was ascribed to its hydrophobic nature, which led to the adsorption of Tween® 20 unimers and petroleum droplets on its surface and/or pores via hydrophobic interaction [33]. The anti-fouling and anti-wetting properties of composite membranes, such as the 6h-mPVDF membrane, are attributed to the combined effects of the surface superhydrophilicity and hierarchical structures. The hydrophilic moieties (amine-, hydroxyl-, and carboxyl-functional groups) on the deposited PDA layer had the tendency to interact strongly with surrounding water molecules through polar interaction. This strong affinity to water in turn kept the outer surface of the 6h-mPVDF membrane hydrated and a hydrogen bonded network was formed within the hierarchical structure.

Subsequently, the hydration layer provided a significant energetic barrier for the petroleum droplets and Tween® 20 unimers to overcome to be attached onto the surface [203, 204]. This was evidenced by the captive bubble experiments as shown in Fig. 6-7. Water molecules within the interfacial hydration layer possessed low rotational and translational dynamics [205], which could only be displaced from the membrane interface during an unfavorable enthalpy gain episode. Therefore, Tiraferri et al. suggested that maximizing the interfacial energy between the membrane surface and its surrounding water molecules could be an effective anti-fouling strategy [206]. By improving surface hydrophilicity, foulant adhesion tendency is likely to be reduced. As proven in Fig. 6-13, the more hydrophilic 6h-mPVDF membrane showed better fouling- and wetting-resistant properties than the PDA/PEI membrane.

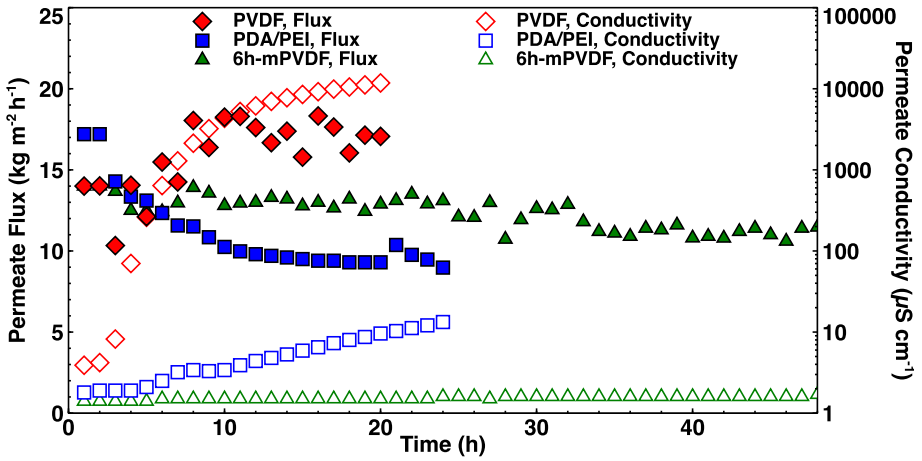


Fig. 6-13. DCMD performances of the pristine PVDF, PDA/PEI, and 6h-mPVDF membranes by feeding 500 mg L^{-1} of Tween® 20-stabilized petroleum-in-water emulsion. Fresh emulsions were prepared daily for the respective experiments. Q_f = 0.7 L min^{-1}; Q_p = 0.25 L min^{-1}; T_f = 333 K; T_p = 293 K.

6.3.4.3. Raw seawater

To ascertain that the newly engineered membranes (2h-mPVDF and 6h-mPVDF) could be used for real applications, their performances in seawater desalination were analyzed and compared with that of the pristine PVDF membrane as shown in Fig. 6-14.

In the case of the pristine PVDF membrane, no significant fouling was observed and the permeate flux remained fairly constant throughout the test duration. However, pore wetting was first observed after 30 h of operation. The permeate conductivity rose from 1.5 μS cm^{-1} to 196.4 μS cm^{-1} after 48 h of operation, which translated to a salt rejection rate of 99.6%. In contrast, both the 2h-mPVDF and 6h-mPVDF membranes produced high quality distillates with final permeate conductivity values at 2.7 and 3.3 μS cm^{-1} after 140 h of operation, respectively (the salt rejection rates were higher than 99.99%). The 2h-mPVDF membrane presented a higher initial flux than the 6h-mPVDF membrane. The difference in initial flux could be attributed to the thickness of the deposited layer as observed in Fig. 6-2(b3) and (c3). The 2h-mPVDF membrane had a more 'open' structure across its thinner deposited layer. On the other hand, the 6h-mPVDF membrane had a denser structure across the whole thickness that inevitably provided some mass transfer resistance to vapor flow, albeit small. However, when the deposited layer was thinner and less dense, the membrane became more susceptible to fouling in the long run as exhibited by the 2h-mPVDF membrane's gradual decline in flux towards the end of the experiment. Hence, there exists a tradeoff between a membrane's robustness and the water recovery rate. A thinner deposited layer may lead to higher initial flux but may not be as robust as a thicker layer in terms of anti-fouling and anti-wetting properties.

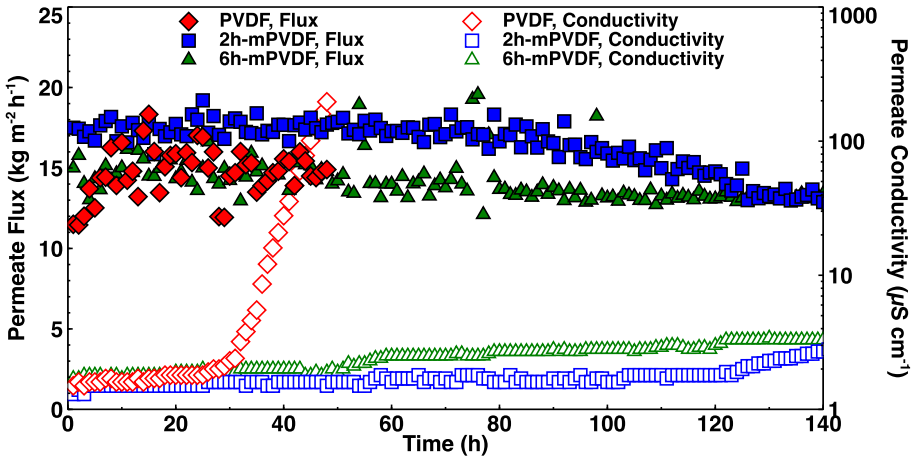


Fig. 6-14. DCMD performances of the pristine PVDF and mPVDF membranes by feeding seawater. For each experiment, the feed tank was periodically refilled with overflow from the permeate reservoir to maintain the feed concentration. Q_f = 0.7 L min^{-1}; Q_p = 0.25 L min^{-1}; T_f = 333 K; T_p = 293 K.

6.4. Conclusions

In this work, we fabricated a composite PVDF hollow fiber membrane with sandwich structure via single-step oxidant-induced dopamine polymerization. In comparison with conventional PDA deposition techniques using dissolved oxygen, this facile and expeditious approach achieved a deposited layer with improved hydrophilicity. The fouling and wetting behaviors of this newly developed membrane in low surface tension saline feeds via bench-scale DCMD experiments were investigated thoroughly. Its performances were compared to those of commercial hydrophobic PVDF and previously reported composite membranes. The novel membrane presented excellent fouling- and wetting-resistant properties against different types of surfactant solution. It also remained robust in O/W emulsion and seawater, during which a stable flux and highly purified distillate were achieved. This could be ascribed to the sustenance of the metastable Cassie-Baxter state within the hierarchical structures formed on the superhydrophilic membrane surface. The deposited layer did not provide additional resistance to vapor transport and instead brought about a flux increment of up to 70% at a feed temperature

of 333 K. These results suggest that the newly engineered membrane endowed with underwater superoleophobicity could be used for extended applications of DCMD.

This page is intentionally left blank

Chapter 7 Conclusions and Recommendations

7.1. Overall conclusions

This thesis presents the performance enhancement of the MD process for extended applications by first understanding the relationship between low surface tension pollutants and a commercial hydrophobic PVDF hollow fiber membrane surface followed by applying novel surface modification techniques on the outer and inner surfaces of the PVDF membrane. Currently, there is a lack of understanding in the roles of oils, surfactants, and salts on membrane fouling and pore wetting in DCMD operations. As such, there is no pinpointing to the exact cause of deteriorated membrane performance in terms of permeate flux and distillate quality, which in turn has limited the use of MD membranes to treating relatively 'clean' waters. In view of that, a detailed study was conducted via a bench-scale DCMD experimental rig on the effects of surfactant types, oil concentration, and oil types to elucidate the fouling and wetting mechanisms involved.

With this foundation, robust dual-layer and sandwich-structured composite PVDF hollow fiber membranes were engineered via novel surface modification techniques. These modified membranes exhibited fouling- and wetting-resistant properties in the presence of low surface tension contaminants. This suggests that the composite membranes could potentially be used for water recovery from low surface tension feeds. Both novel membranes were characterized via standard protocols in terms of structure and morphology, surface functional groups, surface zeta potential, pore size, pore size distribution, water contact angle, mechanical properties, DCMD performance, and etc. The major findings are summarized as follows:

- The time for the onset of wetting for different surfactants is highly dependent on their respective HLB values. Surfactants with a lower HLB value (more hydrophobic) have a higher tendency of attaching onto the hydrophobic PVDF membrane surface as compared to surfactants with a higher HLB value (less hydrophobic). Wetting occurs more readily when more surfactant unimers get adsorbed onto the membrane surface **(Chapter 4)**;

- In O/W emulsions, the presence of oil delays the onset of wetting of a membrane due to increased interaction between oil droplets and surfactant unimers resulting in fewer surfactant unimers adhering onto the membrane surface **(Chapter 4)**;

- Higher oil concentration and higher proportion of heavy hydrocarbons increase the severity of membrane fouling. This suggests that conventional MD membranes are only suitable to be used for water recovery from relatively clean waters that only contain non-volatile solutes **(Chapter 4)**;

- Inspired by mussels' byssus, a strategy to engineer composite PVDF hollow fiber membrane with a thin superhydrophilic layer on top of a hydrophobic substrate has been developed. While effective, this remains a time-consuming technique **(Chapter 5)**.

- The use of oxidant can accelerate dopamine polymerization and reduce the time required for surface modification significantly. This novel technique has been applied to develop composite PVDF hollow fiber with sandwich

structure **(Chapter 6)**.

- By tailoring rough hierarchical structures on the porous PVDF substrate, it creates a protective layer on existing membrane pores and prevents the adhesion of organics. The formation of an interfacial hydration layer on the superhydrophilic surface, coupled with the presence of protonated amine-functional groups, endows the composite PVDF membrane with underwater superoleophobic properties **(Chapters 5 and 6)**.

- Bench-scale DCMD experiments demonstrate that the newly developed membranes are able to present stable long-term performance for up to one week of operation. More importantly, the modified layers exhibit excellent durability under ultrasonic treatment **(Chapters 5 and 6)**.

- The newly fabricated membranes prepared via surface modification are robust against different low surface tension contaminants. The underwater superoleophobic nature of these membranes renders them suitable for not only seawater desalination but also water recovery from low surface tension feeds acquired from different industries **(Chapters 5 and 6)**.

7.2. Recommendations for future research

In order to extent application of the MD process beyond small-scale and off-grid installations, more research is required with respect to foulant-membrane interactions as well as the development of robust membranes.

While this thesis has attempted to better understand the influence of key components (surfactants, oils, and NaCl) and mixtures of these components on membrane performance in the DCMD process, more studies are required since the results achieved may be unique to the types of surfactant and oil investigated here. Moreover, it is paramount to establish the interaction between different components via molecular dynamics simulations. This would be useful in providing an insight on the interaction strength as well as means to avert undesirable interactions between the components. Besides that, real-time non-invasive fouling monitoring methods such as electrical impedance spectroscopy and ultrasonic time domain reflectometry could be applied to provide more reliable information on fouling events.

In terms of engineering robust MD membrane surfaces through novel surface modification techniques, composite omniphobic membranes could be another solution to membrane fouling and pore wetting. Tailoring an in-air superhydrophilic/underwater superoleophobic skin layer on top of an omniphobic substrate could impart fouling- and wetting-resistant properties to the composite membrane. An interfacial hydration layer would form on the skin layer and prevent fouling caused by oil droplets. On the other hand, the omniphobic substrate would prevent low surface tension feeds from wicking through its network of re-entrant structures. It has been proven that omniphobic membranes are resistant to wetting by oils and surfactants ascribing to re-entrant structures [145]. This could potentially circumvent on the issues of membrane fouling and pore wetting faced in long-term MD operations.

The past several years have witnessed significant progress in research activities regarding novel surface modification techniques targeting low surface tensions and crucial challenges. The continuous effort on exploration of composite membranes with

highly controlled hierarchical structures will address most, if not all, of the challenges and extend application of MD process to challenging industrial wastewaters containing low surface tension contaminants.

This page is intentionally left blank

References

[1] IEA, World Energy Outlook 2013, (2013) 700.

[2] D. Rangarajan T., B. Ali Heydari, H. Amr, State of the art treatment of produced water, Water Treatment Walid Elshorbagy and Rezaul Kabir Chowdhury, IntechOpen, 2013.

[3] A. Fakhru'l-Razi, A. Pendashteh, L.C. Abdullah, D.R.A. Biak, S.S. Madaeni, Z.Z. Abidin, Review of technologies for oil and gas produced water treatment, J. Hazard. Mater., 170 (2009) 530-551.

[4] D.L. Shaffer, L.H. Arias Chavez, M. Ben-Sasson, S. Romero-Vargas Castrillon, N.Y. Yip, M. Elimelech, Desalination and reuse of high-salinity shale gas produced water: Drivers, technologies, and future directions, Environ. Sci. Technol., 47 (2013) 9569-9583.

[5] A. Alkhudhiri, N. Darwish, N. Hilal, Produced water treatment: Application of air gap membrane distillation, Desalination, 309 (2013) 46-51.

[6] L. Toop, Produced water treatment trends move towards reuse, in: Oil and gas product news, Dow, 2016.

[7] A. Hong, A.G. Fane, R. Burford, Factors affecting membrane coalescence of stable oil-in-water emulsions, J. Membr. Sci., 222 (2003) 19-39.

[8] A.S.C. Chen, J.T. Flynn, R.G. Cook, A.L. Casaday, Removal of oil, grease, and suspended solids from produced water with ceramic crossflow microfiltration, SPE Prod. Eng., 6 (1991) 131-136.

[9] S.H.D. Silalahi, T. Leiknes, Cleaning strategies in ceramic microfiltration membranes fouled by oil and particulate matter in produced water, Desalination, 236 (2009) 160-169.

[10] A. Motta, C. Borges, K. Esquerre, A. Kiperstok, Oil produced water treatment for oil removal by an integration of coalescer bed and microfiltration membrane processes, J. Membr. Sci., 469 (2014) 371-378.

[11] D. Ali, M.M. Husein, T.G. Harding, Produced water treatment by micellar-enhanced ultrafiltration, Environ. Sci. Technol., 44 (2010) 1767-1772.

[12] D. Wandera, S.R. Wickramasinghe, S.M. Husson, Modification and characterization of ultrafiltration membranes for treatment of produced water, J. Membr. Sci., 373 (2011) 178-188.

[13] D. Wandera, H.H. Himstedt, M. Marroquin, S.R. Wickramasinghe, S.M. Husson, Modification of ultrafiltration membranes with block copolymer nanolayers for produced water treatment: The roles of polymer chain density and polymerization time on performance, J. Membr. Sci., 403-404 (2012) 250-260.

[14] P. Xu, J.E. Drewes, Viability of nanofiltration and ultra-low pressure reverse osmosis membranes for multi-beneficial use of methane produced water, Sep. Purif. Technol., 52 (2006) 67-76.

[15] S. Mondal, S.R. Wickramasinghe, Produced water treatment by nanofiltration and reverse osmosis membranes, J. Membr. Sci., 322 (2008) 162-170.

[16] N. Tomer, S. Mondal, D. Wandera, S.R. Wickramasinghe, S.M. Husson, Modification of nanofiltration membranes by surface-initiated atom transfer radical polymerization for produced water filtration, Sep. Sci. Technol., 44 (2009) 3346-3368.

[17] N. Liu, L. Li, B. McPherson, R. Lee, Removal of organics from produced water by reverse osmosis using MFI-type zeolite membranes, J. Membr. Sci., 325 (2008) 357-361.

[18] M. Melo, H. Schluter, J. Ferreira, R. Magda, A. Junior, O. de Aquino, Advanced performance evaluation of a reverse osmosis treatment for oilfield produced water aiming reuse, Desalination, 250 (2010) 1016-1018.

[19] B.D. Coday, P. Xu, E.G. Beaudry, J. Herron, K. Lampi, N.T. Hancock, T.Y. Cath, The sweet spot of forward osmosis: Treatment of produced water, drilling wastewater, and other complex and difficult liquid streams, Desalination, 333 (2014) 23-35.

[20] X. Yang, R. Wang, L. Shi, A.G. Fane, M. Debowski, Performance improvement of PVDF hollow fiber-based membrane distillation process, J. Membr. Sci., 369 (2011) 437-447.

[21] G. Chen, X. Yang, Y. Lu, R. Wang, A.G. Fane, Heat transfer intensification and scaling mitigation in bubbling-enhanced membrane distillation for brine concentration, J. Membr. Sci., 470 (2014) 60-69.

[22] Y. Liao, R. Wang, M. Tian, C. Qiu, A.G. Fane, Fabrication of polyvinylidene fluoride (PVDF) nanofiber membranes by electro-spinning for direct contact membrane distillation, J. Membr. Sci., 425-426 (2013) 30-39.

[23] M. Safavi, T. Mohammadi, High-salinity water desalination using VMD, Chem. Eng. J., 149 (2009) 191-195.

[24] A. Alkhudhiri, N. Darwish, N. Hilal, Treatment of high salinity solutions: Application of air gap membrane distillation, Desalination, 287 (2012) 55-60.

[25] A.F. Janson, S. Adham, F. Benyahia, R. Dores, A. Husain, J. Minier-Matar, Membrane distillation of high salinity brines using low grade waste heat, in: AMTA/AWWA Membrane Technology Conference and Exposition 2013, February 25, 2013 - February 28, 2013, American Water Works Association, San Antonio, TX, United states, 2013, pp. 1175-1189.

[26] Y.M. Manawi, M.A.M.M. Khraisheh, A.K. Fard, F. Benyahia, S. Adham, A predictive model for the assessment of the temperature polarization effect in direct

contact membrane distillation desalination of high salinity feed, Desalination, 341 (2014) 38-49.

[27] J. Li, Y. Guan, F. Cheng, Y. Liu, Treatment of high salinity brines by direct contact membrane distillation: Effect of membrane characteristics and salinity, Chemosphere, 140 (2015) 143-149.

[28] N. Dow, S. Gray, J.-d. Li, J. Zhang, E. Ostarcevic, A. Liubinas, P. Atherton, G. Roeszler, A. Gibbs, M. Duke, Pilot trial of membrane distillation driven by low grade waste heat: Membrane fouling and energy assessment, Desalination, 391 (2016) 30-42.

[29] R. Schwantes, A. Cipollina, F. Gross, J. Koschikowski, D. Pfeifle, M. Rolletschek, V. Subiela, Membrane distillation: Solar and waste heat driven demonstration plants for desalination, Desalination, 323 (2013) 93-106.

[30] A.E. Jansen, J.W. Assink, J.H. Hanemaaijer, J. van Medevoort, E. van Sonsbeek, Development and pilot testing of full-scale membrane distillation modules for deployment of waste heat, Desalination, 323 (2013) 55-65.

[31] H.C. Duong, P. Cooper, B. Nelemans, T.Y. Cath, L.D. Nghiem, Evaluating energy consumption of air gap membrane distillation for seawater desalination at pilot scale level, Sep. Purif. Technol., 166 (2016) 55-62.

[32] A. Alkhudhiri, N. Darwish, N. Hilal, Membrane distillation: A comprehensive review, Desalination, 287 (2012) 2-18.

[33] N.G.P. Chew, S. Zhao, C.H. Loh, N. Permogorov, R. Wang, Surfactant effects on water recovery from oil-in-water emulsions via direct-contact membrane distillation, J. Membr. Sci., 528 (2017) 126-134.

[34] M. Gryta, K. Karakulski, Application of membrane distillation for the concentration of oil-water emulsions, Desalination, 121 (1999) 23-29.

[35] M. Gryta, K. Karakulski, A.W. Morawski, Purification of oily wastewater by hybrid UF/MD, Water Res., 35 (2001) 3665-3669.

[36] D. Singh, K.K. Sirkar, Desalination of brine and produced water by direct contact membrane distillation at high temperatures and pressures, J. Membr. Sci., 389 (2012) 380-388.

[37] G. Zuo, R. Wang, Novel membrane surface modification to enhance anti-oil fouling property for membrane distillation application, J. Membr. Sci., 447 (2013) 26-35.

[38] S. Zhang, P. Wang, X. Fu, T.-S. Chung, Sustainable water recovery from oily wastewater via forward osmosis-membrane distillation (FO-MD), Water Res., 52 (2014) 112-121.

[39] G. Schmidt, Silicone surfactants. Part III. Organomodified polydimethylsiloxanes as surface active ingredients in textile and fibre industries, Tenside, Surfactants, Detergents, 27 (1990) 324-328.

[40] A.C. Hari, R.A. Paruchuri, D.A. Sabatini, T.C.G. Kibbey, Effects of pH and cationic and nonionic surfactants on the adsorption of pharmaceutical to a natural aquifer material, Environ. Sci. Technol., 39 (2005) 2592-2598.

[41] M.A. Aboulhassan, S. Souabi, A. Yaacoubi, M. Baudu, Removal of surfactant from industrial wastewaters by coagulation flocculation process, Int. J. Environ. Sci. Technol., 3 (2006) 327-332.

[42] R. Fijan, S. ostar-Turk, R. Lapasin, Rheological study of interactions between non-ionic surfactants and polysaccharide thickeners used in textile printing, Carbohydr. Polym., 68 (2007) 708-717.

[43] D. Madunic-Cacic, M. Sak-Bosnar, O. Galovic, N. Sakac, R. Mateic-Puac, Determination of cationic surfactants in pharmaceutical disinfectants using a new sensitive potentiometric sensor, Talanta, 76 (2008) 259-264.

[44] M.A. Kandadai, P. Mohan, G. Lin, A. Butterfield, M. Skliar, J.J. Magda, Comparison of surfactants used to prepare aqueous perfluoropentane emulsions for pharmaceutical applications, Langmuir, 26 (2010) 4655-4660.

[45] C.D. Ampatzidis, E.M.A. Varka, T.D. Karapantsios, Interfacial activity of amino acid-based glycerol ether surfactants and their performance in stabilizing O/W cosmetic emulsions, Colloids Surf. A: Physicochemical Eng. Aspects, 460 (2014) 176-183.

[46] J.F. Ontiveros, C. Pierlot, M. Catte, V. Molinier, J.L. Salager, J.M. Aubry, A simple method to assess the hydrophilic lipophilic balance of food and cosmetic surfactants using the phase inversion temperature of C10E4/n-octane/water emulsions, Colloids Surf. A: Physicochemical Eng. Aspects, 458 (2014) 32-39.

[47] C. Baudequin, Z. Mai, M. Rakib, I. Deguerry, R. Severac, M. Pabon, E. Couallier, Removal of fluorinated surfactants by reverse osmosis - Role of surfactants in membrane fouling, J. Membr. Sci., 458 (2014) 111-119.

[48] P.-J. Lin, M.-C. Yang, Y.-L. Li, J.-H. Chen, Prevention of surfactant wetting with agarose hydrogel layer for direct contact membrane distillation used in dyeing wastewater treatment, J. Membr. Sci., 475 (2015) 511-520.

[49] A. Abbasian, S.R. Ghaffarian, N. Mohammadi, M.R. Khosroshahi, M. Fathollahi, Study on different planforms of paint's solvents and the effect of surfactants (on them), Prog. Org. Coat., 49 (2004) 229-235.

[50] A. Tuteja, C. Wonjae, J.M. Mabry, G.H. McKinley, R.E. Cohen, Robust omniphobic surfaces, Proc. Natl. Academy Sci. U.S.A, 105 (2008) 18200-18205.

[51] J. Lee, C. Boo, W.-H. Ryu, A.D. Taylor, M. Elimelech, Development of Omniphobic Desalination Membranes Using a Charged Electrospun Nanofiber Scaffold, ACS Appl. Mater. Interfaces, 8 (2016) 11154-11161.

[52] C. Boo, J. Lee, M. Elimelech, Engineering surface energy and nanostructure of microporous films for expanded membrane distillation applications, Environ. Sci. Technol., 50 (2016) 8112-8119.

[53] C. Boo, J. Lee, M. Elimelech, Omniphobic polyvinylidene fluoride (PVDF) membrane for desalination of shale gas produced water by membrane distillation, Environ. Sci. Technol., 50 (2016) 12275-12282.

[54] Y.C. Woo, Y. Chen, L.D. Tijing, S. Phuntsho, T. He, J.-S. Choi, S.-H. Kim, H.K. Shon, CF4plasma-modified omniphobic electrospun nanofiber membrane for produced water brine treatment by membrane distillation, J. Membr. Sci., 529 (2017) 234-242.

[55] Z. Wang, D. Hou, S. Lin, Composite membrane with underwater-oleophobic surface for anti-oil-fouling membrane distillation, Environ. Sci. Technol., 50 (2016) 3866-3874.

[56] N.G.P. Chew, S. Zhao, C. Malde, R. Wang, Superoleophobic surface modification for robust membrane distillation performance, J. Membr. Sci., 541 (2017) 162-173.

[57] Y.-X. Huang, Z. Wang, J. Jin, S. Lin, Novel Janus Membrane for Membrane Distillation with Simultaneous Fouling and Wetting Resistance, Environ. Sci. Technol., (2017).

[58] Z. Wang, S. Lin, The impact of low-surface-energy functional groups on oil fouling resistance in membrane distillation, J. Membr. Sci., 527 (2017) 68-77.

[59] M. Bhadra, S. Roy, S. Mitra, Enhanced desalination using carboxylated carbon nanotube immobilized membranes, Sep. Purif. Technol., 120 (2013) 373-377.

[60] K. Gethard, O. Sae-Khow, S. Mitra, Water desalination using carbon-nanotube-enhanced membrane distillation, ACS Appl. Mater. Interfaces, 3 (2011) 110-114.

[61] G.A. Polotskaya, A.V. Penkova, A.M. Toikka, Fullerene-containing polyphenylene oxide membranes for pervaporation, Desalination, 200 (2006) 400-402.

[62] H.-C. Yang, W. Zhong, J. Hou, V. Chen, Z.-K. Xu, Janus hollow fiber membrane with a mussel-inspired coating on the lumen surface for direct contact membrane distillation, J. Membr. Sci., 523 (2017) 1-7.

[63] K. Gethard, O. Sae-Khow, S. Mitra, Carbon nanotube enhanced membrane distillation for simultaneous generation of pure water and concentrating pharmaceutical waste, Sep. Purif. Technol., 90 (2012) 239-245.

[64] S. Roy, M. Bhadra, S. Mitra, Enhanced desalination via functionalized carbon nanotube immobilized membrane in direct contact membrane distillation, Sep. Purif. Technol., 136 (2014) 58-65.

[65] M. Bhadra, S. Roy, S. Mitra, Flux enhancement in direct contact membrane distillation by implementing carbon nanotube immobilized PTFE membrane, Sep. Purif. Technol., 161 (2016) 136-143.

[66] M. Bhadra, S. Roy, S. Mitra, A bilayered structure comprised of functionalized carbon nanotubes for desalination by membrane distillation, ACS Appl. Mater. Interfaces, 8 (2016) 19507-19513.

[67] A. Kyoungjin An, E.-J. Lee, J. Guo, S. Jeong, J.-G. Lee, N. Ghaffour, Enhanced vapor transport in membrane distillation via functionalized carbon nanotubes anchored into electrospun nanofibres, Scientific Rep., 7 (2017) 41562.

[68] M. Bhadra, S. Roy, S. Mitra, Nanodiamond immobilized membranes for enhanced desalination via membrane distillation, Desalination, 341 (2014) 115-119.

[69] M. Bhadra, S. Roy, S. Mitra, Desalination across a graphene oxide membrane via direct contact membrane distillation, Desalination, 378 (2016) 37-43.

[70] K.W. Lawson, D.R. Lloyd, Membrane distillation, J. Membr. Sci., 124 (1997) 1-25.

[71] E. Curcio, E. Drioli, Membrane distillation and related operations - A review, Sep. Purif. Rev., 34 (2005) 35-86.

[72] D. Singh, P. Prakash, K.K. Sirkar, Deoiled produced water treatment using direct-contact membrane distillation, Ind. Eng. Chem. Res., 52 (2013) 13439-13448.

[73] F. Macedonio, A. Ali, T. Poerio, E. El-Sayed, E. Drioli, M. Abdel-Jawad, Direct contact membrane distillation for treatment of oilfield produced water, Sep. Purif. Technol., 126 (2014) 69-81.

[74] M.S. El-Bourawi, Z. Ding, R. Ma, M. Khayet, A framework for better understanding membrane distillation separation process, J. Membr. Sci., 285 (2006) 4-29.

[75] M. Khayet, T. Matsuura, J.I. Mengual, Porous hydrophobic/hydrophilic composite membranes: Estimation of the hydrophobic-layer thickness, J. Membr. Sci., 266 (2005) 68-79.

[76] K.W. Lawson, D.R. Lloyd, Membrane distillation. I. Module design and performance evaluation using vacuum membrane distillation, J. Membr. Sci., 120 (1996) 111-121.

[77] F.A. Banat, J. Simandl, Theoretical and experimental study in membrane distillation, Desalination, 95 (1994) 39-52.

[78] B. Li, K.K. Sirkar, Novel membrane and device for vacuum membrane distillation-based desalination process, J. Membr. Sci., 257 (2005) 60-75.

[79] P.A. Hogan, Sudjito, A.G. Fane, G.L. Morrison, Desalination by solar heated membrane distillation, Desalination, 81 (1991) 81-90.

[80] J.P. Mericq, S. Laborie, C. Cabassud, Evaluation of systems coupling vacuum membrane distillation and solar energy for seawater desalination, Chem. Eng. J., 166 (2011) 596-606.

[81] S. Gunko, S. Verbych, M. Bryk, N. Hilal, Concentration of apple juice using direct contact membrane distillation, Desalination, 190 (2006) 117-124.

[82] S. Kimura, S.-I. Nakao, Transport phenomena in membrane distillation, J. Membr. Sci., 33 (1986) 285-298.

[83] V. Calabro, B.L. Jiao, E. Drioli, Theoretical and experimental study on membrane distillation in the concentration of orange juice, Industrial Eng. Chem. Res., 33 (1994) 1803-1808.

[84] S. Nene, S. Kaur, K. Sumod, B. Joshi, K.S.M.S. Raghavarao, Membrane distillation for the concentration of raw cane-sugar syrup and membrane clarified sugarcane juice, Desalination, 147 (2002) 157-160.

[85] K. Christensen, R. Andresen, I. Tandskov, B. Norddahl, P.J.H. du, Using direct contact membrane distillation for whey protein concentration, Desalination, 200 (2006) 523-525.

[86] N. Chlubek, M. Tomaszewska, Concentration of dairy wastes by membrane distillation, Environ. Protection Eng., 13 (1987) 17-24.

[87] A. Hausmann, P. Sanciolo, T. Vasiljevic, E. Ponnampalam, N. Quispe-Chavez, M. Weeks, M. Duke, Direct contact membrane distillation of dairy process streams, Membr. , 1 (2011) 48-58.

[88] A. Hausmann, P. Sanciolo, T. Vasiljevic, M. Weeks, K. Schroen, S. Gray, M. Duke, Fouling of dairy components on hydrophobic polytetrafluoroethylene (PTFE) membranes for membrane distillation, J. Membr. Sci., 442 (2013) 149-159.

[89] A. Cassano, C. Conidi, R. Timpone, M. D'Avella, E. Drioli, A membrane-based process for the clarification and the concentration of the cactus pear juice, J. Food Eng., 80 (2007) 914-921.

[90] V. Calabro, E. Drioli, F. Matera, Membrane distillation in the textile wastewater treatment, Desalination, 83 (1991) 209-224.

[91] A. Criscuoli, J. Zhong, A. Figoli, M.C. Carnevale, R. Huang, E. Drioli, Treatment of dye solutions by vacuum membrane distillation, Water Res., 42 (2008) 5031-5037.

[92] M. Tomaszewska, Concentration of the extraction fluid from sulfuric acid treatment of phosphogypsum by membrane distillation, J. Membr. Sci., 78 (1993) 277-282.

[93] B. Wu, X. Tan, W.K. Teo, K. Li, Removal of benzene/toluene from water by vacuum membrane distillation in a PVDF hollow fiber membrane module, Sep. Sci. Technol., 40 (2005) 2679-2695.

[94] B. Wu, X. Tan, K. Li, W.K. Teo, Removal of 1,1,1-trichloroethane from water using a polyvinylidene fluoride hollow fiber membrane module: Vacuum membrane distillation operation, Sep. Purif. Technol., 52 (2006) 301-309.

[95] M.M.A. Shirazi, A. Kargari, M. Tabatabaei, A.F. Ismail, T. Matsuura, Concentration of glycerol from dilute glycerol wastewater using sweeping gas membrane distillation, Chem. Eng. Process.: Process Intensification, 78 (2014) 58-66.

[96] M. Madhumala, D. Madhavi, T. Sankarshana, S. Sridhar, Recovery of hydrochloric acid and glycerol from aqueous solutions in chloralkali and chemical process industries by membrane distillation technique, J. Taiwan Inst. Chem. Eng., 45 (2014) 1249-1259.

[97] F.A. Banat, J. Simandl, Membrane distillation for dilute ethanol: Separation from aqueous streams, J. Membr. Sci., 163 (1999) 333-348.

[98] M. Gryta, The fermentation process integrated with membrane distillation, Sep. Purif. Technol., 24 (2001) 283-296.

[99] G. Lewandowicz, W. Bialas, B. Marczewski, D. Szymanowska, Application of membrane distillation for ethanol recovery during fuel ethanol production, J. Membr. Sci., 375 (2011) 212-219.

[100] M. Takht Ravanchi, T. Kaghazchi, A. Kargari, Application of membrane separation processes in petrochemical industry: a review, Desalination, 235 (2009) 199-244.

[101] I. Pinnau, L.G. Toy, Solid polymer electrolyte composite membranes for olefin/paraffin separation, J. Membr. Sci., 184 (2001) 39-48.

[102] T.-H. Khaing, J. Li, Y. Li, N. Wai, F.-s. Wong, Feasibility study on petrochemical wastewater treatment and reuse using a novel submerged membrane distillation bioreactor, Sep. Purif. Technol., (2010).

[103] K. Wang, S. Liu, Q. Zhang, Y. He, Pharmaceutical wastewater treatment by internal micro-electrolysis-coagulation, biological treatment and activated carbon adsorption, Environ. Technol., 30 (2009) 1469-1474.

[104] Z. Ding, L. Liu, Z. Liu, R. Ma, Fouling resistance in concentrating TCM extract by direct contact membrane distillation, J. Membr. Sci., 362 (2010) 317-325.

[105] K. Gethard, S. Mitra, Membrane distillation as an online concentration technique: Application to the determination of pharmaceutical residues in natural waters, Analytical Bioanalytical Chem., 400 (2011) 571-575.

[106] M.N. Chernyshov, G.W. Meindersma, A.B. de Haan, Modelling temperature and salt concentration distribution in membrane distillation feed channel, Desalination, 157 (2003) 315-324.

[107] M. Gryta, Fouling in direct contact membrane distillation process, J. Membr. Sci., 325 (2008) 383-394.

[108] D.Y. Cheng, S.J. Wiersma, Composite membrane for a membrane distillation system, in, Google Patents, 1983.

[109] S. Srisurichan, R. Jiraratananon, A.G. Fane, Humic acid fouling in the membrane distillation process, Desalination, 174 (2005) 63-72.

[110] Z. Amjad, Reverse osmosis, membrane technology, water chemistry and industrial application, Van Nostrand Reinhold, New York, USA, 1992.

[111] T. Nguyen, F.A. Roddick, L. Fan, Biofouling of water treatment membranes: A review of the underlying causes, monitoring techniques and control measures, Membranes, 2(4) (2012) 804-840.

[112] J.W. Chew, W.B. Krantz, A.G. Fane, Effect of a macromolecular- or bio-fouling layer on membrane distillation, J. Membr. Sci., 456 (2014) 66-76.

[113] M. Gryta, The assessment of microorganism growth in the membrane distillation system, Desalination, 142 (2002) 79-88.

[114] A.M. Alklaibi, N. Lior, Membrane-distillation desalination: Status and potential, Desalination, 171 (2005) 111-131.

[115] A. El-Abbassi, A. Hafidi, M. Khayet, M.C. Garcia-Payo, Integrated direct contact membrane distillation for olive mill wastewater treatment, Desalination, 323 (2013) 31-38.

[116] K. Karakulski, M. Gryta, Water demineralisation by NF/MD integrated processes, Desalination, 177 (2005) 109-119.

[117] M. Gryta, Desalination of thermally softened water by membrane distillation process, Desalination, 257 (2010) 30-35.

[118] J. Wang, D. Qu, M. Tie, H. Ren, X. Peng, Z. Luan, Effect of coagulation pretreatment on membrane distillation process for desalination of recirculating cooling water, Sep. Purif. Technol., 64 (2008) 108-115.

[119] L.D. Nghiem, T. Cath, A scaling mitigation approach during direct contact membrane distillation, Sep. Purif. Technol., 80 (2011) 315-322.

[120] F. He, J. Gilron, H. Lee, L. Song, K.K. Sirkar, Potential for scaling by sparingly soluble salts in crossflow DCMD, J. Membr. Sci., 311 (2008) 68-80.

[121] X. Yang, R. Wang, A.G. Fane, Novel designs for improving the performance of hollow fiber membrane distillation modules, J. Membr. Sci., 384 (2011) 52-62.

[122] G. Chen, X. Yang, R. Wang, A.G. Fane, Performance enhancement and scaling control with gas bubbling in direct contact membrane distillation, Desalination, 308 (2013) 47-55.

[123] Z.F. Cui, S. Chang, A.G. Fane, The use of gas bubbling to enhance membrane processes, J. Membr. Sci., 221 (2003) 1-35.

[124] Z. Ding, L. Liu, Z. Liu, R. Ma, The use of intermittent gas bubbling to control membrane fouling in concentrating TCM extract by membrane distillation, J. Membr. Sci., 372 (2011) 172-181.

[125] K.L. Hickenbottom, T.Y. Cath, Sustainable operation of membrane distillation for enhancement of mineral recovery from hypersaline solutions, J. Membr. Sci., 454 (2014) 426-435.

[126] E. Drioli, Y. Wu, Membrane distillation: An experimental study, Desalination, 53 (1985) 339-346.

[127] E. Drioli, Y. Wu, V. Calabro, Membrane distillation in the treatment of aqueous solutions, J. Membr. Sci., 33 (1986) 277-284.

[128] L.F. Dumee, K. Sears, J. Schutz, N. Finn, H. Chi, S. Hawkins, M. Duke, S. Gray, Characterization and evaluation of carbon nanotube Bucky-Paper membranes for direct contact membrane distillation, J. Membr. Sci., 351 (2010) 36-43.

[129] L. Dumee, V. Germain, K. Sears, J. Schutz, N. Finn, M. Duke, S. Cerneaux, D. Cornu, S. Gray, Enhanced durability and hydrophobicity of carbon nanotube bucky paper membranes in membrane distillation, J. Membr. Sci., 376 (2011) 241-246.

[130] L.F. Dumee, S. Gray, M. Duke, K. Sears, J. Schutz, N. Finn, The role of membrane surface energy on direct contact membrane distillation performance, Desalination, 323 (2013) 22-30.

[131] Y. Liao, R. Wang, A.G. Fane, Engineering superhydrophobic surface on poly(vinylidene fluoride) nanofiber membranes for direct contact membrane distillation, J. Membr. Sci., 440 (2013) 77-87.

[132] B. Bhushan, Y.C. Jung, Natural and biomimetic artificial surfaces for superhydrophobicity, self-cleaning, low adhesion, and drag reduction, Prog. Mater. Sci., 56 (2010) 1-108.

[133] A. Razmjou, E. Arifin, G. Dong, J. Mansouri, V. Chen, Superhydrophobic modification of TiO2 nanocomposite PVDF membranes for applications in membrane distillation, J. Membr. Sci., 415-416 (2012) 850-863.

[134] Z.-Q. Dong, X.-h. Ma, Z.-L. Xu, W.-T. You, F.-b. Li, Superhydrophobic PVDF-PTFE electrospun nanofibrous membranes for desalination by vacuum membrane distillation, Desalination, 347 (2014) 175-183.

[135] J. Zhang, Z. Song, B. Li, Q. Wang, S. Wang, Fabrication and characterization of superhydrophobic poly (vinylidene fluoride) membrane for direct contact membrane distillation, Desalination, 324 (2013) 1-9.

[136] C. Yang, X.-M. Li, J. Gilron, D.-f. Kong, Y. Yin, Y. Oren, C. Linder, T. He, CF4 plasma-modified superhydrophobic PVDF membranes for direct contact membrane distillation, J. Membr. Sci., 456 (2014) 155-161.

[137] S. Bonyadi, T.S. Chung, Flux enhancement in membrane distillation by fabrication of dual layer hydrophilic-hydrophobic hollow fiber membranes, J. Membr. Sci., 306 (2007) 134-146.

[138] M. Qtaishat, D. Rana, M. Khayet, T. Matsuura, Preparation and characterization of novel hydrophobic/hydrophilic polyetherimide composite membranes for desalination by direct contact membrane distillation, J. Membr. Sci., 327 (2009) 264-273.

[139] M. Qtaishat, M. Khayet, T. Matsuura, Novel porous composite hydrophobic/hydrophilic polysulfone membranes for desalination by direct contact membrane distillation, J. Membr. Sci., 341 (2009) 139-148.

[140] P. Peng, A.G. Fane, X. Li, Desalination by membrane distillation adopting a hydrophilic membrane, Desalination, 173 (2005) 45-54.

[141] Z. Wang, J. Jin, D. Hou, S. Lin, Tailoring surface charge and wetting property for robust oil-fouling mitigation in membrane distillation, J. Membr. Sci., 516 (2016) 113-122.

[142] J.A. Prince, V. Anbharasi, T.S. Shanmugasundaram, G. Singh, Preparation and characterization of novel triple layer hydrophilic- hydrophobic composite membrane for desalination using air gap membrane distillation, Sep. Purif. Technol., 118 (2013) 598-603.

[143] M. Khayet, T. Matsuura, Application of surface modifying macromolecules for the preparation of membranes for membrane distillation, Desalination, 158 (2003) 51-56.

[144] S. Lin, S. Nejati, C. Boo, Y. Hu, C.O. Osuji, M. Elimelech, Omniphobic membrane for robust membrane distillation, Environ. Sci. Technol. Lett., 1 (2014) 443-447.

[145] Z. Wang, S. Lin, Membrane fouling and wetting in membrane distillation and their mitigation by novel membranes with special wettability, Water Res., 112 (2017) 38-47.

[146] Y. Wu, S. Iglauer, P. Shuler, Y. Tang, W.A. Goddard, Alkyl Polyglycoside-Sorbitan Ester Formulations for Improved Oil Recovery, Tenside Surfactants Deterg., 47 (2010) 280-287.

[147] P.M. Kruglyakov, Hydrophile-lipophile balance of surfactants and solid particles: Physicochemical aspects and applications, Elsevier Science, 2000.

[148] Z.E. Proverbio, S.M. Bardavid, E.L. Arancibia, P.C. Schulz, Hydrophile-lipophile balance and solubility parameter of cationic surfactants, Colloids Surf. A: Physicochemical Eng. Aspects, 214 (2003) 167-171.

[149] H.M. Park, W.M. Lee, Helmholtz-Smoluchowski velocity for viscoelastic electroosmotic flows, J. Colloid Interface Sci., 317 (2008) 631-636.

[150] L.L. Schramm, Surfactants: Fundamentals and applications in the petroleum industry, The Press Syndicate of the University of Cambridge, United Kingdom, 2000.

[151] B. Kronberg, K. Holmberg, B. Lindman, Surface Chemistry of Surfactants and Polymers, John Wiley & Sons, United Kingdom, 2014.

[152] D. Lu, T. Zhang, J. Ma, Ceramic membrane fouling during ultrafiltration of oil/water emulsions: Roles played by stabilization surfactants of oil droplets, Environ. Sci. Technol., 49 (2015) 4235-4244.

[153] A.C.M. Franken, J.A.M. Nolten, M.H.V. Mulder, D. Bargeman, C.A. Smolders, WETTING CRITERIA FOR THE APPLICABILITY OF MEMBRANE DISTILLATION, Journal of Membrane Science, 33 (1986) 315-328.

[154] C. Boo, J. Lee, M. Elimelech, Omniphobic Polyvinylidene Fluoride (PVDF) Membrane for Desalination of Shale Gas Produced Water by Membrane Distillation, Environmental Science and Technology, 50 (2016) 12275-12282.

[155] C. Boo, J. Lee, M. Elimelech, Engineering Surface Energy and Nanostructure of Microporous Films for Expanded Membrane Distillation Applications, Environmental Science and Technology, 50 (2016) 8112-8119.

[156] L.D. Tijing, Y.C. Woo, J.-S. Choi, S. Lee, S.-H. Kim, H.K. Shon, Fouling and its control in membrane distillation—A review, Journal of Membrane Science, 475 (2015) 215-244.

[157] P. Walstra, Physical chemistry of foods, Marcel Dekker, Inc., New York, 2001.

[158] P.-J. Lin, M.-C. Yang, Y.-L. Li, J.-H. Chen, Prevention of surfactant wetting with agarose hydrogel layer for direct contact membrane distillation used in dyeing wastewater treatment, Journal of Membrane Science, 475 (2015) 511-520.

[159] F. Tiberg, J. Brinck, L. Grant, Adsorption and surface-induced self-assembly of surfactants at the solid–aqueous interface, Curr. Opin. Colloid Interface Sci., 4 (1999) 411-419.

[160] C. Zhang, Y. Ou, W.-X. Lei, L.-S. Wan, J. Ji, Z.-K. Xu, CuSO4/H2O2-Induced Rapid Deposition of Polydopamine Coatings with High Uniformity and Enhanced Stability, Angewandte Chemie - Intl. Edition, 55 (2016) 3054-3057.

[161] Z.-X. Wang, C.-H. Lau, N.-Q. Zhang, Y.-P. Bai, L. Shao, Mussel-inspired tailoring of membrane wettability for harsh water treatment, J. Mater. Chem. A., 3 (2015) 2650-2657.

[162] H.-C. Yang, K.-J. Liao, H. Huang, Q.-Y. Wu, L.-S. Wan, Z.-K. Xu, Mussel-inspired modification of a polymer membrane for ultra-high water permeability and oil-in-water emulsion separation, J. Mater. Chem. A., 2 (2014) 10225-10230.

[163] H.-C. Yang, J.-K. Pi, K.-J. Liao, H. Huang, Q.-Y. Wu, X.-J. Huang, Z.-K. Xu, Silica-decorated polypropylene microfiltration membranes with a mussel-inspired intermediate layer for oil-in-water emulsion separation, ACS Appl. Mater. Interfaces, 6 (2014) 12566-12572.

[164] H. Ma, P. Gao, Y. Zhang, D. Fan, G. Li, B. Du, Q. Wei, Engineering microstructured porous films for multiple applications via mussel-inspired surface coating, RSC Advances, 3 (2013) 25291-25295.

[165] Z. Wang, X. Jiang, X. Cheng, C.H. Lau, L. Shao, Mussel-inspired hybrid coatings that transform membrane hydrophobicity into high hydrophilicity and underwater superoleophobicity for oil-in-water emulsion separation, ACS Appl. Mater. Interfaces, 7 (2015) 9534-9545.

[166] W.-Z. Qiu, H.-C. Yang, L.-S. Wan, Z.-K. Xu, Co-deposition of catechol/polyethyleneimine on porous membranes for efficient decolorization of dye water, J. Mater. Chem. A., 3 (2015) 14438-14444.

[167] Y.-S. Choi, H. Kang, D.-G. Kim, S.-H. Cha, J.-C. Lee, Mussel-inspired dopamine- and plant-based cardanol-containing polymer coatings for multifunctional filtration membranes, ACS Appl. Mater. Interfaces, 6 (2014) 21297-21307.

[168] C. Cheng, S. Li, W. Zhao, Q. Wei, S. Nie, S. Sun, C. Zhao, The hydrodynamic permeability and surface property of polyethersulfone ultrafiltration membranes with mussel-inspired polydopamine coatings, J. Membr. Sci., 417-418 (2012) 228-236.

[169] Y. Lv, H.-C. Yang, H.-Q. Liang, L.-S. Wan, Z.-K. Xu, Nanofiltration membranes via co-deposition of polydopamine/polyethylenimine followed by cross-linking, J. Membr. Sci., 476 (2015) 50-58.

[170] G. Han, S. Zhang, X. Li, N. Widjojo, T.-S. Chung, Thin film composite forward osmosis membranes based on polydopamine modified polysulfone substrates with enhancements in both water flux and salt rejection, Chem. Eng. Sci., 80 (2012) 219-231.

[171] F. Li, Q. Cheng, Q. Tian, B. Yang, Q. Chen, Biofouling behavior and performance of forward osmosis membranes with bioinspired surface modification in osmotic membrane bioreactor, Bioresource Technol., 211 (2016) 751-758.

[172] H.C. Yang, J. Hou, V. Chen, Z.K. Xu, Janus membranes: Exploring duality for advanced separation, Angewandte Chemie 55 (2016) 13398-13407.

[173] H. Li, L. Peng, Y. Luo, P. Yu, Enhancement in membrane performances of a commercial polyamide reverse osmosis membrane via surface coating of polydopamine followed by the grafting of polyethylenimine, RSC Advances, 5 (2015) 98566-98575.

[174] H. Shi, L. Xue, A. Gao, Y. Fu, Q. Zhou, L. Zhu, Fouling-resistant and adhesion-resistant surface modification of dual layer PVDF hollow fiber membrane by dopamine and quaternary polyethyleneimine, J. Membr. Sci., 498 (2016) 39-47.

[175] R.N. Wenzel, Resistance of solid surfaces to wetting by water, Ind. Eng. Chem., 28 (1936) 988-994.

[176] L. Wang, F. Fang, Y. Liu, J. Li, X. Huang, Facile preparation of heparinized polysulfone membrane assisted by polydopamine/polyethyleneimine co-deposition for simultaneous LDL selectivity and biocompatibility, Appl. Surf. Sci., 385 (2016) 308-317.

[177] E. Herlinger, R.F. Jameson, W. Linert, Spontaneous autoxidation of dopamine, J. Chem. Soc. Perkin Transactions 2, (1995) 259-263.

[178] N.F. Della Vecchia, R. Avolio, M. Alfe, M.E. Errico, A. Napolitano, M. D'Ischia, Building-block diversity in polydopamine underpins a multifunctional eumelanin-type platform tunable through a quinone control point, Advanced Functional Mater., 23 (2013) 1331-1340.

[179] J. Liebscher, R. Mrowczynski, H.A. Scheidt, C. Filip, N.D. Haidade, R. Turcu, A. Bende, S. Beck, Structure of polydopamine: A never-ending story?, Langmuir, 29 (2013) 10539-10548.

[180] S. Saidin, P. Chevallier, M.R. Abdul Kadir, H. Hermawan, D. Mantovani, Polydopamine as an intermediate layer for silver and hydroxyapatite immobilisation on metallic biomaterials surface, Mater. Sci. Eng., C, Mater. Biol. Appl. , 33 (2013) 4715-4724.

[181] H.-C. Yang, W. Xu, Y. Du, J. Wu, Z.-K. Xu, Composite free-standing films of polydopamine/polyethyleneimine grown at the air/water interface, RSC Advances, 4 (2014) 45415-45418.

[182] A.N. Pham, T.D. Waite, Cu(II)-catalyzed oxidation of dopamine in aqueous solutions: Mechanism and kinetics, J. Inorg. Biochemistry, 137 (2014) 74-84.

[183] D.B. Knorr, N.T. Tran, K.J. Gaskell, J.A. Orlicki, J.C. Woicik, C. Jaye, D.A. Fischer, J.L. Lenhart, Synthesis and characterization of aminopropyltriethoxysilane-polydopamine coatings, Langmuir, 32 (2016) 4370-4381.

[184] R. Meszaros, L. Thompson, M. Bos, I. Varga, T. Gilanyi, Interaction of sodium dodecyl sulfate with polyethyleneimine: Surfactant-induced polymer solution colloid dispersion transition, Langmuir, 19 (2003) 609-615.

[185] H. Wang, Y. Wang, H. Yan, J. Zhang, R.K. Thomas, Binding of sodium dodecyl sulfate with linear and branched polyethyleneimines in aqueous solution at different pH values, Langmuir, 22 (2006) 1526-1533.

[186] S. Chen, L. Li, C. Zhao, J. Zheng, Surface hydration: Principles and applications toward low-fouling/nonfouling biomaterials, Polym., 51 (2010) 5283-5293.

[187] S. Chen, F. Yu, Q. Yu, Y. He, S. Jiang, Strong resistance of a thin crystalline layer of balanced charged groups to protein adsorption, Langmuir, 22 (2006) 8186-8191.

[188] X. Lu, Y. Peng, L. Ge, R. Lin, Z. Zhu, S. Liu, Amphiphobic PVDF composite membranes for anti-fouling direct contact membrane distillation, J. Membr. Sci., 505 (2016) 61-69.

[189] W. Qiang, Z. Fulong, L. Jie, L. Beijia, Z. Changsheng, Oxidant-induced dopamine polymerization for multifunctional coatings, Polym. Chem., 1 (2010) 1430-1433.

[190] C. Zhang, Y. Ou, W.-X. Lei, L.-S. Wan, J. Ji, Z.-K. Xu, CuSO4/H2O2-Induced Rapid Deposition of Polydopamine Coatings with High Uniformity and Enhanced Stability, Angew. Chem., Int. Ed., 55 (2016) 3054-3057.

[191] F. Ponzio, J. Barthes, J. Bour, M. Michel, P. Bertani, J. Hemmerle, M. D'Ischia, V. Ball, Oxidant control of polydopamine surface chemistry in acids: A mechanism-based entry to superhydrophilic-superoleophobic coatings, Chem. Mater., 28 (2016) 4697-4705.

[192] B. Wu, F. Hochstrasser, E. Akhondi, N. Ambauen, L. Tschirren, M. Burkhardt, A.G. Fane, W. Pronk, Optimization of gravity-driven membrane (GDM) filtration process for seawater pretreatment, Water Research, 93 (2016) 133-140.

[193] J. Drelich, E. Chibowski, Superhydrophilic and superwetting surfaces: Definition and mechanisms of control, Langmuir, 26 (2010) 18621-18623.

[194] N.J. Shirtcliffe, G. McHale, S. Atherton, M.I. Newton, An introduction to superhydrophobicity, Adv. Colloid Interface Sci., 161 (2010) 124-138.

[195] M. Jin, J. Wang, X. Yao, M. Liao, Y. Zhao, L. Jiang, Underwater oil capture by a three-dimensional network architectured organosilane surface, Adv. Mater., 23 (2011) 2861-2864.

[196] C. Luo, Q. Liu, Oxidant-Induced High-Efficient Mussel-Inspired Modification on PVDF Membrane with Superhydrophilicity and Underwater Superoleophobicity Characteristics for Oil/Water Separation, ACS Appl. Mater. Interfaces, 9 (2017) 8297-8307.

[197] S.W. Weidman, E.T. Kaiser, The mechanism of the periodate oxidation of aromatic systems. III: A kinetic study of the periodate oxidation of catechol, J. Am. Chem. Soc, 88 (1966) 5820-5827.

[198] H. Lee, S.M. Dellatore, W.M. Miller, P.B. Messersmith, Mussel-inspired surface chemistry for multifunctional coatings, Science, 318 (2007) 426-430.

[199] D. Breite, M. Went, A. Prager, A. Schulze, Tailoring Membrane Surface Charges: A Novel Study on Electrostatic Interactions during Membrane Fouling, Polymers, 7 (2015) 1497.

[200] M. Vaselbehagh, H. Karkhanechi, S. Mulyati, R. Takagi, H. Matsuyama, Improved antifouling of anion-exchange membrane by polydopamine coating in electrodialysis process, Desalination, 332 (2014) 126-133.

[201] S. Kasemset, Z. He, D.J. Miller, B.D. Freeman, M.M. Sharma, Effect of polydopamine deposition conditions on polysulfone ultrafiltration membrane properties and threshold flux during oil/water emulsion filtration, Polymer (United Kingdom), 97 (2016) 247-257.

[202] A.B.D. Cassie, S. Baxter, Wettability of porous surfaces, Trans. Faraday Soc., 40 (1944) 546-551.

[203] C.J. van Oss, M.K. Chaudhury, R.J. Good, Monopolar Surfaces, Adv. Colloid Interface Sci., 28 (1987) 35-64.

[204] C.J. van Oss, W. Wu, A. Docoslis, R.F. Giese, The interfacial tensions with water and the Lewis acid-base surface tension parameters of polar organic liquids derived from their aqueous solubilities, Colloids Surfaces B (Biointerfaces), 20 (2001) 87-91.

[205] A.M. Dokter, S. Woutersen, H.J. Bakker, Anomalous slowing down of the vibrational relaxation of liquid water upon nanoscale confinement, Phys. Rev. Lett., 94 (2005) 178301-178301.

[206] A. Tiraferri, Y. Kang, E.P. Giannelis, M. Elimelech, Superhydrophilic thin-film composite forward osmosis membranes for organic fouling control: Fouling behavior and antifouling mechanisms, Environ. Sci. Technol., 46 (2012) 11135-11144.